INVESTIGATIONS OF CARBON FIBRES AND THEIR PRECURSOR MATERIALS BY E.S.R. AND RELATED TECHNIQUES

by

Ernest Geoffrey Cooper B.A.

A thesis submitted to the University of Keele for the Degree of Doctor of Philosophy

Department of Physics,
University of Keele,
Keele, Staffordshire.

August , 1977.

To my mother Catherine

ABSTRACT

The desirable mechanical properties that have lead to the manufacture of carbon fibre laminates for aerospace applications are developed in fibre heat treated in excess of 1000°C. The research group at Keele made an exhaustive study of these high temperature fibres by electron spin resonance (ESR) and other electronic techniques. However, we report here a similar investigation of the electronic processes in carbon fibre heat treated below 1000°C as established by ESR, electrical conductivity and thermoelectric power (TEP) measurements.

We established that the g-value of the ESR spectrum was anisotropic indicating that even in the early stages of heat treatment the free spins are associated with layer planes which are preferentially aligned along the fibre axis. The results tend to indicate that excessive preoxidation hinders the structural development within these fibres.

The electrical conduction takes place by a process of 'electron hopping' between localized sites beyond the nearest neighbour separation. This process of conduction implies a disordered structure, however we find that the result is not inconsistent with our model as the hopping appears to take place along two dimensional layer planes.

The spin-lattice relaxation processes were also determined and it is evident that the spin system is not efficiently coupled to the lattice.

In addition to the study of the thermal degradation of the precursor materials we also applied the ESR technique to a study of the free radicals produced in the precursors by mechanical degradation and by irradiation damage. Tentative assignment of the free radicals produced by irradiation damage was made.

ACKNOWLEDGMENTS.

I would like to thank the following for their contributions:

Professors D.J.E. Ingram and W. Fuller for their use of research facilities.

Dr. D.E. Dugdale for superivising the research program.

Dr. D. Robson and Dr. F.Y.I. Assabghy for their invaluable introduction to the carbon field and to Dr. Assabghy for his permission to use the illustration of Fig. 6.9.

Dr. D.E. Dugdale and Dr. J. Beswick for the use of their pulse saturation equipment and in particular to Dr. Beswick for his assistance in the measurement of the spin lattice relaxation times using the equipment.

Dr. B. Henderson for the use of his Varian 'Q' and 'X' band spectrometers.

Dr. E.F. Slade, Dr. G. Lancaster, Dr. C.E.C. May and other members of the Physics Department for their assistance.

The technical staff for their assistance in particular Mr. G. Dudley and Mr. W. Brearley.

Mr. P. Collis of the computer centre for writing a 'macro' for use with the program referred to on page 105.

The Science Research Council for their financial support.

Rolls-Royce Ltd., for the use of their facilities during a visit to their Research Establishment at Old Hall, Derby. Particular thanks are extended to Dr. J. Johnson and Dr. P. Rose for their assistance. The author would also like to thank Dr. Johnson for the illustrations that comprise Fig. 3.3.

Dr. Eburt of the Paterson Laboratories at the Christie Hospital and Holt Radium Institute, Manchester for electron irradiating our precursor fibres.

Finally, I am indebted to members of my family for their support. I would particularly like to thank my brother Gerald for his careful drawing of a number of the diagrams contained in this thesis. I am also indebted to my sister Kathleen for putting in long back breaking hours of dedication in typing this thesis.

LIST OF FIGURES AND TABLES

CONTENTS

CHAPTER 1

INTRODUCTION

Carbon is a vital engineering material and has for many years been the subject of considerable research. In recent years carbon fibres were produced by controlled pyrolysis of high molecular weight textile fibres. Laminated sheets of carbon fibre, bound in an epoxy resin, can be produced and used in the manufacture of high strength, low density components. For several years now carbon fibre has been heralded as the material that would revolutionise engineering structures. However prohibitive development costs have limited their application to the aerospace industry.

In recent years many of the properties of carbon fibre have been investigated. Assabghy and Robson carried out a study of the electronic processes in carbon fibre heat treated above 1000°C by making ESR, electrical conductivity, thermoelectric power and magnetoresistance measurements.

The fibres chosen for our study were derived from Courtelle (acrylonitrile + 7% methyl acrylate copolymer) fibre. The samples were preoxidized in air to a temperature of 400°C after which they were heat treated in an inert atmosphere to various temperatures up to 1000°C. These fibres were prepared while on a months visit to the Rolls-Royce research laboratories. At Keele ESR, electrical conductivity, and thermoelectric power measurements were made on this series.

Chapter 2 contains a brief account of the basic theory of ESR. During the initial stages of pyrolysis spin centres are formed which readily saturate using the available microwave powers. This indicates that the coupling between the spin system and the lattice is not very efficient. A discussion of the various spin-lattice relaxation processes is also included.

Because of their importance the various form of carbon have been subjected to an intensive program of research. Included in Chapter 3 is an account of the available ESR and electronic models that have been proposed. For completeness a summary is given of the results obtained by Assabghy and Robson, together with a brief comparison of these results with the existing models. Also included is a current account of the structure of carbon fibres.

It was found necessary to record measurements at liquid helium temperatures and a discussion of the low temperature techniques used and of the ESR spectrometer is included in Chapter 4.

Chapter 5 contains an account of the ESR and spin-lattice relaxation results. These results are discussed in some detail at the rear of Chapter 5.

Chapter 6 contains a brief account of the expected conduction behaviour in disordered materials and our conductivity and thermoelectric power results were analysed for evidence of disorder.

Chapter 7 contains an account of the theory of ESR as applied to free radicals and includes a brief review of the production and trapping of free radicals in polymeric materials by mechanical degradation and by irradiation damage. Chapter 8 contains a study of the free radicals produced in our acrylic precursors by these techniques.

Chapter 9 contains a few concluding remarks.

ZEEMAN ENERGY LEVELS

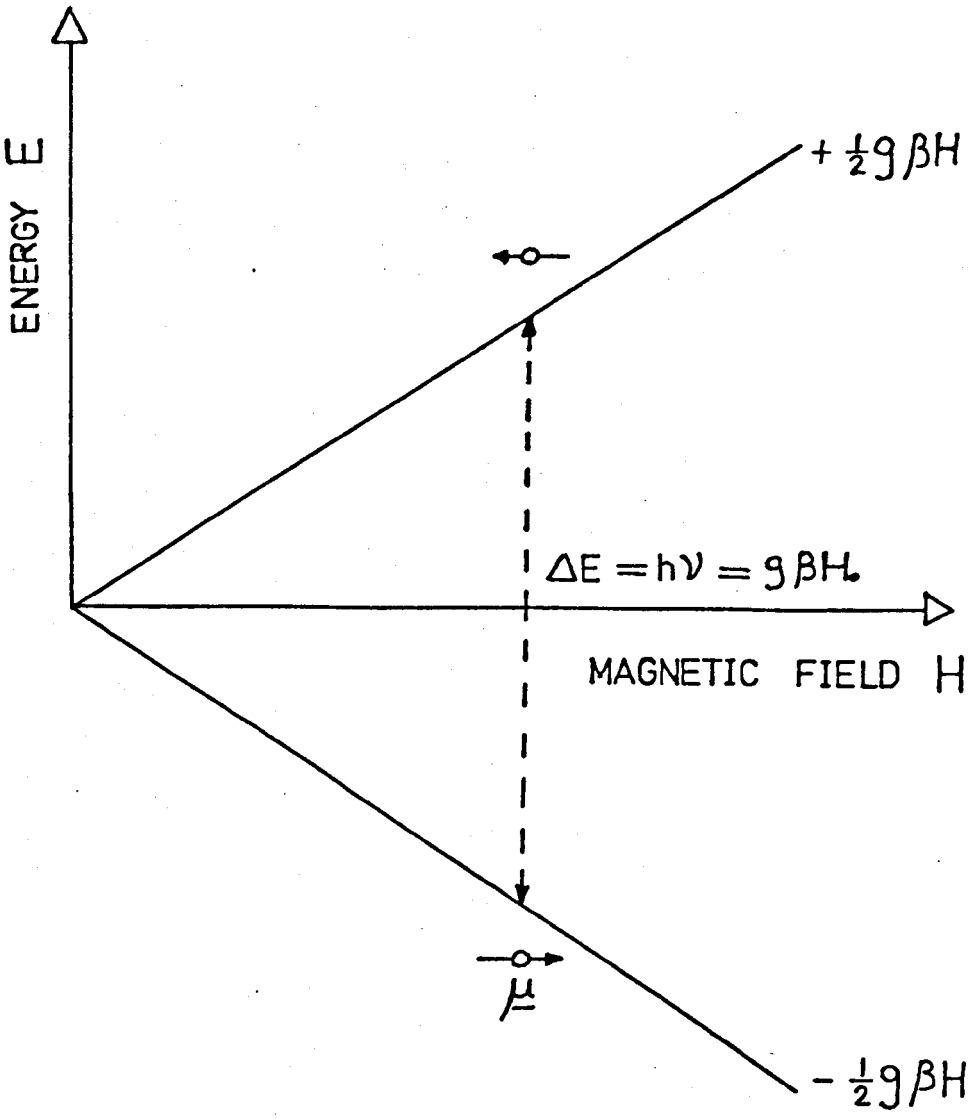

FIGURE 2.1

CHAPTER 2

THE BASIC THEORY OF ESR

2.1 Introduction

There is a wealth of evidence, both theoretical and experimental to show that an electron possesses an intrinsic angular momentum which is known as its spin. Because the electron is an electrically charged particle rotating about its internal axis, it also possesses a magnetic moment. The energy of interaction of a magnetic moment μ in the presence of an applied static magnetic field $\underline{H}_o$ is

$$E = - \mu . \underline{H}_o \qquad (2.1)$$

Quantum mechanically the magnetic moment is quantized with respect to the direction of the applied static field. For a free electron two orientations are possible, parallel or antiparallel, corresponding to two discrete Zeeman energy levels. The former is the low energy state and the latter the high energy state corresponding to spin quantum numbers $M_s = - \frac{1}{2}$ and $M_s = + \frac{1}{2}$ respectively.

The magnetic moment of a free spin quantized with respect to the direction of the magnetic field H_o is

$$\mu_w = - g\beta M_s \qquad (2.2)$$

where 'g' is a number called the g-factor

where β is the Bohr magneton

with energy $E_{M_s} = g\beta M_s H_o \qquad (2.3)$

so that $E + \frac{1}{2} = + \frac{1}{2} g\beta H_o \qquad (2.4)$

$$E - \tfrac{1}{2} = - \tfrac{1}{2} g\beta H_o \qquad (2.5)$$

The energy separation of these levels is hence

$$\Delta E = g\beta H_o \qquad (2.6)$$

as illustrated in Fig. 2.1

We can see that the numerical factor g or g-factor as it is called in paramagnetic resonance is a measure of the rate of divergence of the Zeeman levels with increasing field. The application of an oscillating field polarized in a plane perpendicular to the static field induces transitions or 'spin flips' from the low to the high spin state providing that the frequency of oscillation ν of the radiation field is such that

$$h\nu = \Delta E = g\beta H_o \qquad (2.7)$$

The selection rule for such spin transitions is $\Delta M_s = \pm 1$

The free spin g-factor has been shown to have the value[1] 2.002319 $\pm$ 0.000001 and for a magnetic field of some 10 K Gauss the resonance condition corresponds to a frequency in the microwave region. The two principal microwave frequencies employed in paramagnetic resonance experiments are of order 10 G H_z and 34 G H_z corresponding to wavelengths of about 3 cms, known as X - band, and 8 mm, known as Q - band. For the free spin case the corresponding resonant field strengths are about 3.5 K Gauss and 12 K Gauss.

2.2 The free ion

Generally for an atom or an ion the electrons possess orbital angular momentum, and under conditions for which the Russell- Saunders coupling scheme applies, the spin angular momentum $\underline{S}$ and the orbital angular momentum $\underline{L}$ combine to give a resultant total angular momentum $\underline{J}$.

$$\underline{J} = \underline{L} + \underline{S} \qquad (2.8)$$

Associated with this resultant angular momentum we have a resultant magnetic moment μ

where $$\underline{\mu} = \underline{\mu}_S + \underline{\mu}_L \tag{2.9}$$

and $$\underline{\mu}_S = -2\beta \underline{S} \tag{2.10}$$

and $$\underline{\mu}_L = -\beta \underline{L} \tag{2.11}$$

- and with the result that $\underline{\mu}$ precesses uniformly about $\underline{J}$.

In the absence of a magnetic field the terms formed by Russell-Saunders coupling are each 2J + 1 fold degenerate, but in a magnetic field H_o the energy of each state is

$$g_L \beta H_o M_J \tag{2.12}$$

where M_J is the magnetic quantum number and takes the values J, J-1, ... - J where g_L is a number depending on the values of J, L and S and is called the Lande spectroscopic splitting factor.

$$g_L = \frac{3}{2} + \frac{S(S+1) - L(L+1)}{2J(J+1)} \tag{2.13}$$

Magnetic resonance transition are induced according to the selection rule $\Delta M_J = \pm 1$

The resonance condition analogous to that for the free spin becomes

$$h\nu = g_L \beta H_o (M_J + 1) - M_J = g_L \beta H_o \tag{2.14}$$

For a Cr^{3+} ion having a $3d^3$ configuration we obtain the following terms:

$$^2P,\ ^2D\ (2),\ ^2F,\ ^2G,\ ^2H,\ ^4P,\ ^4F$$

FREE ION ENERGY LEVELS OF A $3d^3$ CONFIGURATION

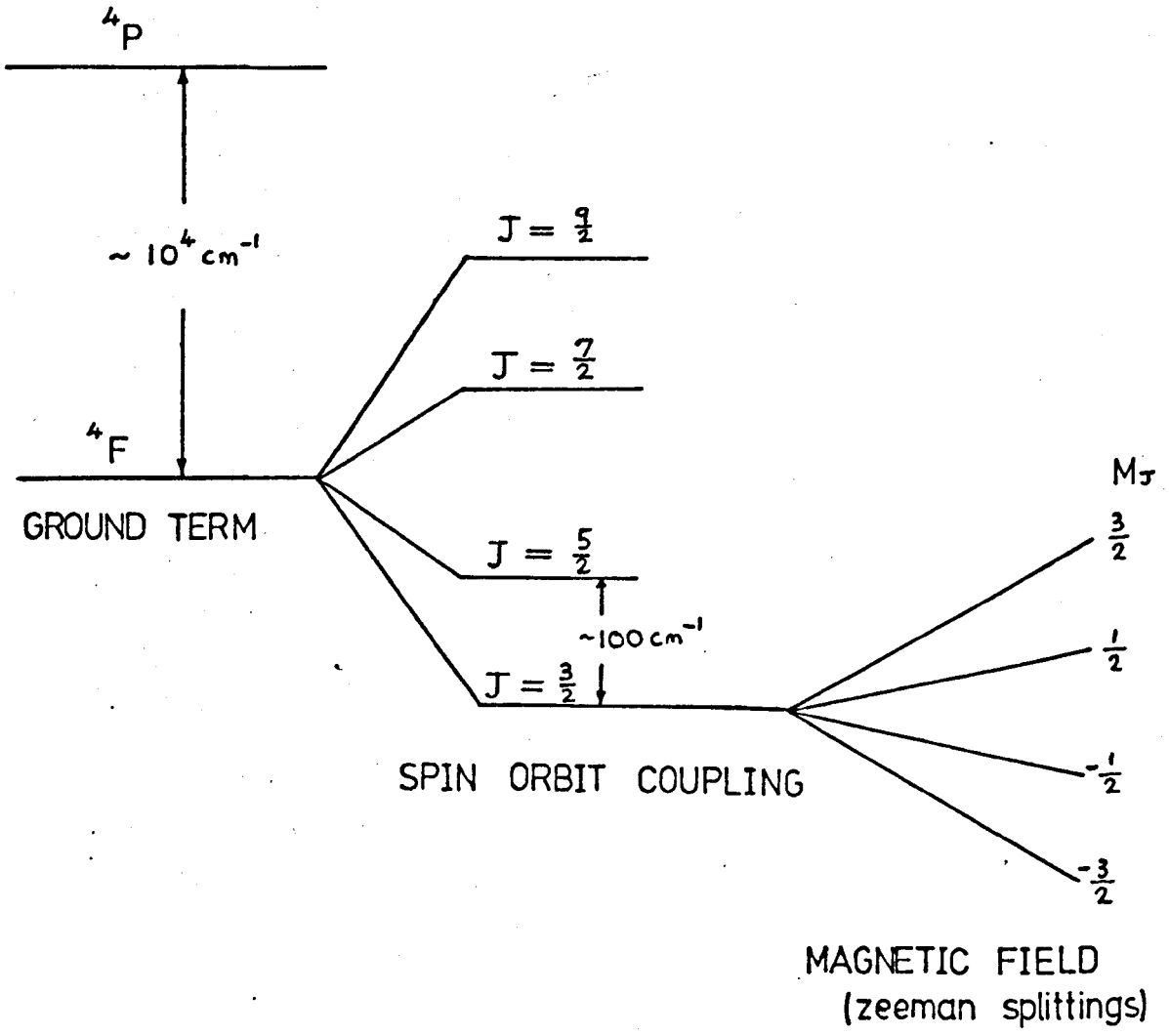

FIGURE 2.2

By applying Hund's rules the ground term is seen to be ^4F for which $L = 3$ and $S = \frac{3}{2}$ giving $J = \frac{9}{2}, \frac{7}{2}, \frac{5}{2}, \frac{3}{2}$ as illustrated in Fig. 2.2

2.3 Ions in crystals

Many paramagnetic ions have successfully been studied in various crystalline environments, and a general Hamiltonian can be formed to express the interactions affecting the electronic energy levels in an operator form.

$$\mathcal{H} = \mathcal{H}_E + \mathcal{H}_{LS} + \mathcal{H}_{SI} + \mathcal{H}_Q + \mathcal{H}_M + \mathcal{H}_{IH} + \mathcal{H}_V \qquad (2.15)$$

Where $\mathcal{H}_E$ is an operator representing the total kinetic energy of the electrons, and the coulombic interaction of the electrons with the nucleus and with each other.

$$\mathcal{H}_E = \sum_i \left(\frac{\underline{p}_i^2}{2m} - \frac{Ze^2}{\underline{r}_i} \right) + \sum_{j<i} \frac{e^2}{\underline{r}ij} \qquad (2.16)$$

where $\underline{p}_i$ is the momentum of the i^{th} electron and $\underline{r}_i$ its displacement from the nucleus.

$\underline{r}ij$ is the separation between the i^{th} and j^{th} electron

Z is the nuclear charge.

The energy separations between electronic levels are large and of order 10^5 cms.$^{-1}$

$\mathcal{H}_{LS} = \lambda \underline{L}.\underline{S}$ is an operator representing the spin orbit coupling and can be thought of as the magnetic interaction between the spin and orbital moments; λ being the spin-orbit coupling constant. This energy represents an interaction of between 10^2 and 10^3 cm $^{-1}$.

$\mathcal{H}_M$ is the operator describing the interaction of the orbital and the spin magnetic moments with the external magnetic field $\underline{H}_o$

THE 'd' ELECTRON ORBITALS IN AN OCTAHEDRAL ARRANGEMENT OF POINT CHARGES

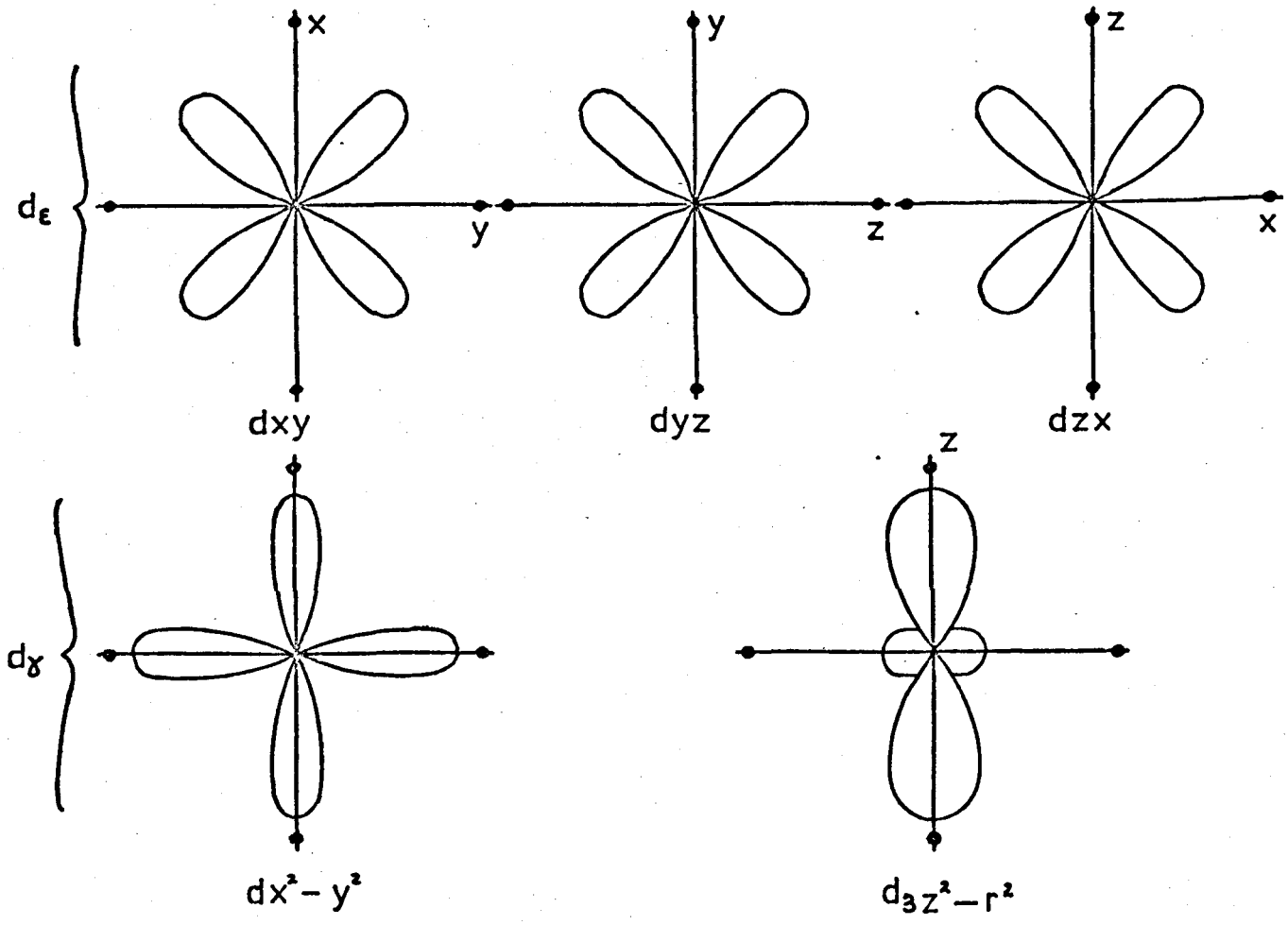

FIGURE 2.3

since $$-\underline{\mu}_L \cdot \underline{H}_o = \beta \underline{L} \cdot \underline{H}_o \qquad (2.17)$$

and $$-\underline{\mu}_s \cdot \underline{H}_o = 2\beta \underline{S} \cdot \underline{H}_o \qquad (2.18)$$

$$\mathcal{H}_M = \beta \underline{H}_o \cdot (\underline{L} + 2\underline{S}) \qquad (2.19)$$

$\mathcal{H}_{SI} = a\ \underline{I} \cdot \underline{S}$ is the hyperfine interaction and represents the interaction of the nuclear spin moments with the electron spin moments and will be discussed more fully later (see section 7.1)

$\mathcal{H}_Q$ represents the nuclear quadripole operator and $\mathcal{H}_{IH}$ represents the interaction of the nuclear angular momentum with the external field. Both terms are small representing interactions of order 10^{-4} cm.$^{-1}$

$\mathcal{H}_V$ is the crystal field operator[2]

$$\mathcal{H}_V = e\,V(r) \qquad (2.20)$$

where V (r) is the electrostatic potential produced at the site of the paramagnetic ion by the surrounding electrons and nuclei. The electric field produced at the paramagnetic ion can, depending on the strength, cause a considerable distortion of the electronic orbitals centred on the ion. In its simplest approximation the crystal field[3] is considered as that due to a group of point charges distributed in some regular way around the paramagnetic ion.

As an illustrative example of the effect of the crystal field we can consider an octahedral field of negative point charges acting on the strongly directional 'd' orbitals see Fig. 2.3. Under an octahedral field it is clear that the three orbitals represented by the functions dxy, dyz and dzx labelled $d\varepsilon$ have the same energy. Also it is found that the two

SPLITTING OF THE 5'd' ORBITALS IN OCTAHEDRAL AND TETRAGONAL SYMMETRY

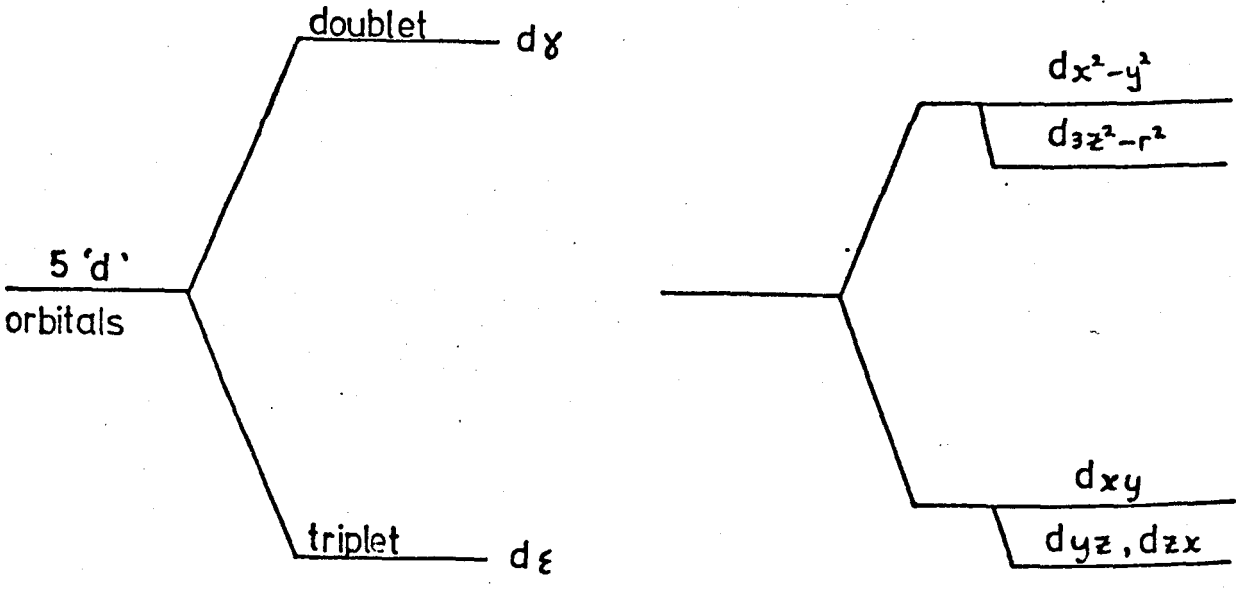

FIGURE 2.4

other orbitals, labelled $d\gamma$, have the same energy. Since the surrounding negative point charges lie along the co-ordinate axis the two $d\gamma$ orbitals experience a greater repulsive interaction with the surrounding point charges, than do the $d\varepsilon$ orbitals, as a result the d orbital energy levels become split as indicated in Fig 2.4 (a). If we add a tetragonal distortion to the system, obtained by increasing the separation of the neighbouring ions that lie along the Z axis, a further splitting results as shown in Fig 2.4 (b). This arises because the $d_{x^2-y^2}$ and dxy orbitals will be relatively uninfluenced by this further distortion, whereas the repulsive interaction between the $d_{3z^2-r^2}$, dyz and the dzx orbitals and the neighbouring ions will be considerably lessened and the splitting results.

In reconsideration of the Cr^{3+} ion in an octahedral field the 3d electrons can be distributed among the $d\varepsilon$ and $d\gamma$ orbitals in the following manner:

(i) The three electrons can be placed in the $d\varepsilon$ orbitals in only one way, this singlet corresponds to the lowest total energy.

(ii) One electron can be placed in the $d\varepsilon$ orbital and two in the $d\gamma$ orbitals in three ways giving a triply degenerate state.

(iii) Two electrons can be placed in the $d\varepsilon$ orbital together with one in the $d\gamma$ orbital in six ways, however it is found that these six levels split into two sets of triplets. This can be understood by considering the repulsive interactions between the electrons in the various orbital states. When one electron is in the $d_{3z^2-r^2}$ state the repulsive interaction is large for the dyz and dzx orbitals and small for a dxy orbital. Similarly if one electron is in the $d_{x^2-y^2}$ orbital the repulsive interaction will be large for a dxy orbital and small for a dyz or dzx orbital. The results of these initial splittings are illustrated in Fig. 2.5.

Cr^{3+} ION IN AN AXIAL FIELD

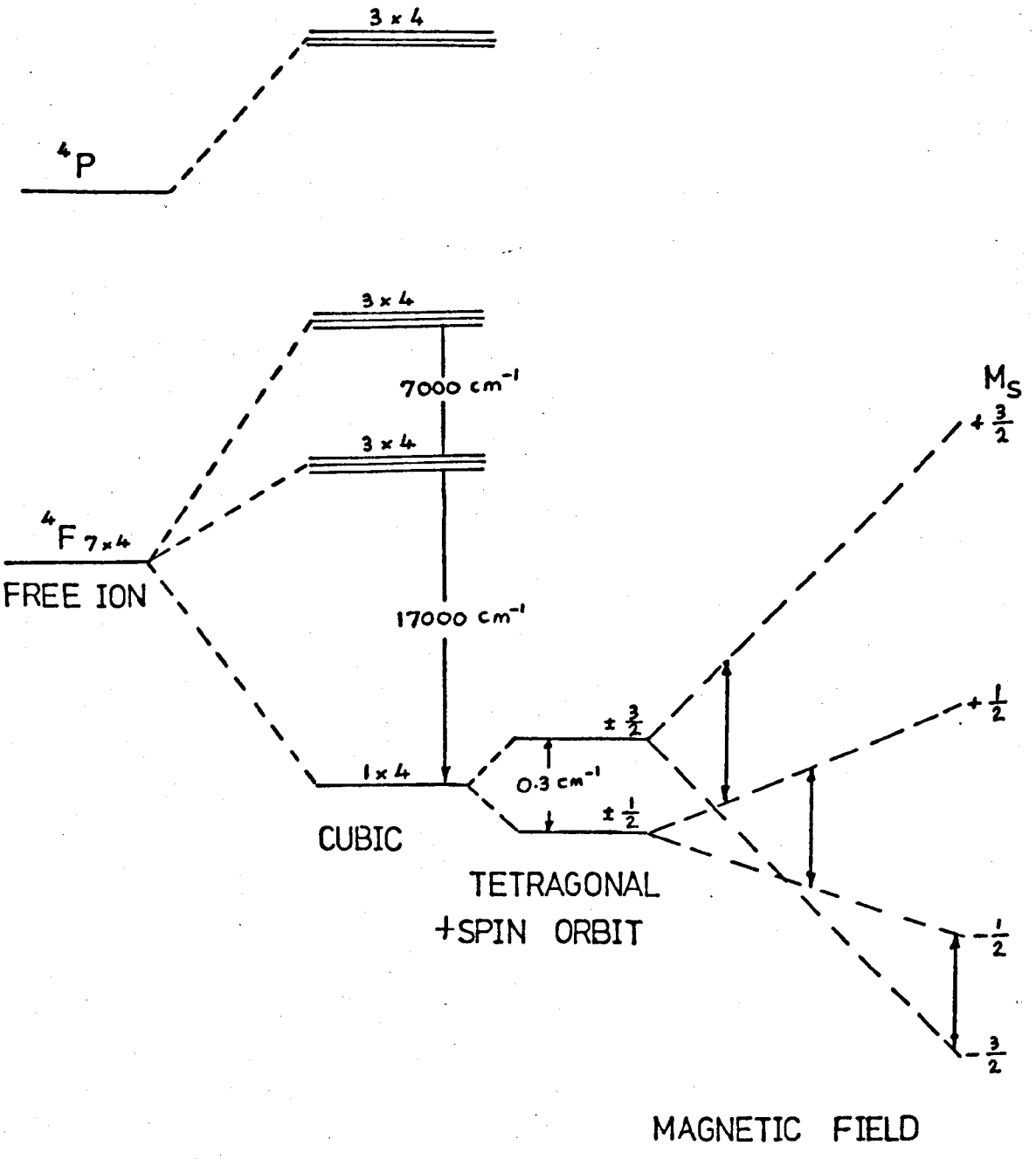

FIGURE 2.5

The crystal field tends to remove as much orbital degeneracy as possible and in the above example the ground state is an orbital singlet so that all the orbital angular momentum has been removed and we say that the state is 'quenched'. There are two important theorems connected with the removal of degeneracy by a crystal field.

(i) That due to Kramer's which states that for a system containing an odd number of electrons a crystal field cannot lift the degeneracy of each level below two.

(ii) That due to Jahn and Teller which states that a non-linear molecule which has a degenerate ground state tends to distort sufficiently to remove the degeneracy.

Even when the ground state is an orbital singlet some orbital angular momentum is added into the system as a result of the mixing of the excited states with the ground state. As a consequence the g-factor is found to differ from that of the free spin by an amount which is related to the ratio of the spin-orbit coupling constant to the separation of the orbital energy levels.[3] However if the crystal field effect is small the Russell-Saunders coupling holds and the g-factor approximates to the Lande splitting factor. The crystal field approximation does not formally apply to the strong field case because the bonding is covalent and hence involves a not inconsiderable overlap of the orbitals of the paramagnetic ion with those of the surrounding ions.

2.4 The spin Hamiltonian.

If the ground state is an orbital singlet we define an effective spin $\underline{S}$ obtained by equating the number of levels in the ground state to $(2S + 1)$ each level having a quantum number M_s. The interaction between the effective spin $\underline{S}$ and the applied magnetic field $\underline{H}$ is :

$$\mathcal{H}_M = \beta \underline{H} \cdot \underline{g} \cdot \underline{S} = \beta\left[H_x g_x S_x + H_y g_y S_y + H_z g_z S_z\right] \qquad (2.21)$$

where the components are along the (x,y,z) crystal axes.

For an axial crystal field $g_x = g_y = g_\perp$ and $g_z = g_\parallel$ taking the Z axis as the tetragonal axis and if the magnetic field is applied at θ to the Z axis in the X Z plane:-

$$\mathcal{H}_M = \beta H\left[g_\perp S_x \sin\theta + g_\parallel S_z \cos\theta\right] \qquad (2.22)$$

where $g_\perp$ is the g-value with the magnetic field perpendicular to the Z axis.

where $g_\parallel$ is the g-value with the magnetic field parallel to the Z axis.

For the Cr^{3+} ion in a cubic field, the orbital singlet ground state may be described by an effective spin $S = \frac{3}{2}$. The spin Hamiltonian reduces to $g\beta H S_z$ and the energy levels are $g\beta H M_s$ with $M_s = +\frac{3}{2}, +\frac{1}{2}, -\frac{1}{2}, -\frac{3}{2}$.

If however the site symmetry is trigonal, the crystal field interacts with spin through the spin orbit coupling and gives a zero field splitting. This is illustrated in Fig. 2.5 for the Cr^{3+} ion. The crystal field separates the two doublets $M_S = \pm\frac{1}{2}$ and $M_S = \pm\frac{3}{2}$ and it is necessary to introduce a new term into the spin Hamiltonian to take account of this.

$$\mathcal{H}_M = \beta H\left[g_\perp S_x \sin\theta + g_\parallel S_z \cos\theta\right] + D\left[S_z^2 - \tfrac{1}{3}S(S+1)\right] \qquad (2.23)$$

A sufficiently general Hamiltonian can be written in the form:

$$\mathcal{H}_M = \underbrace{\beta\left[g_x H_x S_x + g_y H_y S_y + g_z H_z S_z\right]}_{(1)} + \underbrace{D\left[S_z - \tfrac{1}{3}S(S+1)\right]}_{(2)} + \underbrace{E(S_x^2 - S_y^2)}_{(3)}$$

$$+ \underbrace{(A_x I_x S_x + A_y I_y S_y + A_z I_z S_z)}_{(4)} \qquad (2.24)$$

Where the term (1) represents the splitting of the (2 S + 1) multiplet by the magnetic field.

Where the term (2) represents the splitting by a crystalline field of tetragonal symmetry.

Where the term (3) represents the splitting by a crystalline field of lower symmetry.

Where the term (4) represents the hyperfine interaction.

2.5 Spin-spin interaction.

The magnetic dipole moment of each unpaired electron will sense a magnetic field that is the sum of the external field and that derived from the distribution of neighbouring dipoles; then for radiation of fixed frequency, resonance will occur over a range of magnetic field values resulting in a broadened line that is the sum of a number of individual lines. While the individual component lines might well be of Lorentzian line shape, the overall envelope will be Gaussian (See page 17 for a discussion of Lorentzian and Gaussian line shapes).

The contribution of all neighbouring spins 'i' to the dipolar field is

$$H_{\text{dipolar}} = \sum_i \frac{\mu_{iz}\ (1 - 3\cos^2\theta i)}{r_i^3} \qquad (2.25)$$

where r_i is the distance from a particular spin centre to its i^{th} neighbour where θ_i is the angle between the vector $\underline{r}_i$ and the external field H_z where μ_{iz} is the Z component of the i^{th} spin.

Such dipolar broadening effects are lessened considerably in magnetically dilute systems and especially so in solutions where the rapid tumbling motion averages the $(1 - 3\cos^2\theta i)$ term to zero in a time short compared with the inverse of the line width frequency. In solutions this

so called 'motional narrowing' results in very narrow lines.

2.6 Exchange Interactions

In a number of magnetically non - dilute systems line widths are observed that are considerably less than might be expected on the basis of dipolar broadening. This problem was taken to task [4] and shown to be due to a process similar to 'motional narrowing' and was called 'exchange narrowing'. As the paramagnetic ions or free radicals move close together the overlap of unpaired electrons leads to exchange of electrons between the molecules. In the solid state the exchange frequency is very high of the order of 10^{10} cycles/ sec.

A crystalline sample of diphenylpicrylhydrazyl (DPPH) affords a good example of exchange narrowing where a line width of some 100 gauss might be expected from the estimated interatomic distances whereas a line width of the order of 3 gauss is observed [2].

The exchange interaction is written

$$E_{ex} = - \sum_{i>j} 2 J_{ij} \underline{S}_i . \underline{S}_j \qquad (2.26)$$

J_{ij} is the exchange integral

Van Vleck[2] showed that the exchange interaction does not contribute to the expression for the second moment but increases the value of the fourth moment. The overall effect on the line is to narrow the centre and to extend the wings. Anderson and Weiss [5] suggest that an exchange narrowed line should be Lorentzian in character and this seems to be so from observations. Changes in lineshape from Gaussian to Lorentzian that are accompanied by narrowing indicate strongly that exchange is the responsible mechanism.

Pake [3] in his review of Van Vlecks fourth moment calculation shows that the full width at half power is:

$$\Delta w_{\frac{1}{2}} = \frac{1}{T_2} = \frac{\pi}{2}\left(\frac{Wd^2}{W_e}\right) \qquad (2.27)$$

where $W_d = \frac{E_d}{h}$ is the dipolar interaction in the absence of exchange and expressed in frequency units.

where $W_e = \frac{J}{h}$ is the exchange integral in the same units and is a type of hopping frequency.

A similar result is obtained for motional narrowing[6].

Dipolar interactions are line broadening mechanisms from within the spin system. These interactions together with other interactions that vary rapidly compared with the time for a spin transition contribute to a homogeneously broadened line, and clearly include exchange and motional narrowing. Inhomogeneously broadened lines however arise from interactions outside the spin system that vary slowly compared with the time for a spin transition, examples of which include unresolved hyperfine components, magnetic field inhomogeneities and g anisotropy broadening.

2.7 The Bloch phenomenological equations

In an attempt to explain the dynamic magnetic properties of an assemblage of paramagnetic particles Bloch[7] devised a series of equations, the so called Bloch phenomenological equations, in which attention was focussed not on the individual magnetic moments, but rather on their collection macroscopic property the bulk magnetization $\underline{M}$. If as a result of a small perturbation the magnetization has a component M_z along the direction of the static field then Bloch proposed that the magnetization would exponentially return to its thermal equilibrium value M_{oz} in a

characteristic time T_1. In effect some of the magnetic moments flop from the high to the low spin state to restore the thermal equilibrium value. As a result Zeeman energy is given up by the spins to the lattice and T_1 becomes known as the spin-lattice relaxation time or the longitudinal relaxation time. It is necessary to introduce a further relaxation time T_2 which is the time taken for these individual precessing dipoles to become out of phase. This loss of phase coherence arises from the dipole - dipole interactions (see section 2.5) where the different local fields sensed by the individual moments causes them to precess at slightly different frequencies. In terms of the macroscopic properties it is the time in which the transverse components M_x and M_y of the non-equilibrium magnetization decay to their zero equilibrium values. Bloch also proposed that the transverse components of the magnetization decay exponentially to zero. Since the transverse relaxation time T_2 involves only interactions within the spin system it was also known as the spin-spin relaxation time. Besides relaxing to the equilibrium value $M_o\hat{z}$ the magnetization will also precess about the magnetic field. The Bloch phenomenological equations for a system of paramagnetic particles having negative magnetic moments become in the (x,y,z) cartesian co-ordinate system:

$$\frac{dM_x}{dt} = \gamma(\underline{H} \times \underline{M})_x - \frac{M_x}{T_2} \qquad (2.28)$$

$$\frac{dM_y}{dt} = \gamma(\underline{H} \times \underline{M})_y - \frac{M_y}{T_2} \qquad (2.29)$$

$$\frac{dM_z}{dt} = \gamma(\underline{H} \times \underline{M})_z + \frac{M_o - M_z}{T_1} \qquad (2.30)$$

where γ is the magnetogyric ratio.

In paramagnetic resonance we also have an oscillating radiation field $\underline{H}_1$ so arranged to be plane polarized along the x axis. Providing $\underline{H}_1 \ll \underline{H}_o$ the above equations still apply. The radiation field takes the form $2H_1 \cos\omega t\ \underline{i}$ and this may be considered as the sum of two counter rotating fields; since only that field rotating in the same direction as the precessing spins is effective in producing the resonance motion and we obtain:

$$\underline{H} = H_1 \cos\omega t\ \underline{i} + H_1 \sin\omega t\ \underline{j} + H_o \underline{K} \tag{2.31}$$

It becomes advantageous to transform to a rotating co-ordinate system (x', y', z') in which the x' y' plane rotates with respect to the x y plane with an angular frequency vector $\underline{\omega}$ about the $z = z'$ axis using the operator

$$\left.\frac{d}{dt}\right]_{\text{rotating}} = \left.\frac{d}{dt}\right]_{\text{laboratory}} - \underline{\omega} \times \tag{2.32}$$

we have for the magnetization vector

$$\left.\frac{d\underline{M}}{dt}\right]_{\text{rotating}} = \left.\frac{d\underline{M}}{dt}\right]_{\text{laboratory}} - \underline{\omega} \times \underline{M} \tag{2.33}$$

and $$\left.\frac{d\underline{M}}{dt}\right]_{\text{laboratory}} = \gamma\left(\underline{H} \times \underline{M}\right) \tag{2.34}$$

therefore

$$\left.\frac{d\underline{M}}{dt}\right]_{\text{rotating}} = \gamma\left(\underline{H}_o - \frac{\omega}{\gamma} + \underline{H}_1\right) \times \underline{M} \tag{2.35}$$

therefore the effective field in the rotating co-ordinate system becomes:

$$\underline{H} = \left(H_o - \frac{\omega}{\gamma}\right)\underline{K}' + H_1 \underline{i}' \tag{2.36}$$

and $$M_x = M_{x'} \cos\omega t - M_{y'} \sin\omega t \tag{2.37}$$

and the Bloch equations in the rotating frame become:

$$\frac{dM_{x'}}{dt} = -\gamma M_{y'}\left(H_o - \frac{\omega}{\gamma}\right) - \frac{M_{x'}}{T_2} \tag{2.38}$$

$$\frac{dM_{y'}}{dt} = -\gamma\left[H_1 M_{z'} - M_{x'}\left(H_o - \frac{\omega}{\gamma}\right)\right] - \frac{M_{y'}}{T_2} \tag{2.39}$$

$$\frac{dM_{z'}}{dt} = \gamma H_1 M_{y'} + \frac{M_o - M_z}{T_1} \tag{2.40}$$

If we consider steady state solutions that is those for which the time spent in sweeping through the resonance is long compared to T_1 we obtain:

$$M_{y'} = \frac{-\chi_o \omega_o T_2 H_1}{1 + (\omega_o - \omega)^2 T_2^2 + \gamma^2 H_1^2 T_1 T_2}$$

$$M_{x'} = \frac{\chi_o \omega_o T_2 H_1 (\omega_o - \omega) T_2}{1 + (\omega_o - \omega)^2 T_2^2 + \gamma^2 H_1^2 T_1 T_2}$$

where $\omega_o = \gamma H_o$ is the Larmour precession frequency

where $\chi_o = M_o/H_o$ is the equilibrium susceptibility

If we write the susceptibility in the form $\chi = \chi' - i\chi''$ to allow for M_x having a component in phase as well as a component out of phase with H_x and if H_x is the real part of $2H_1 e^{i\omega t}$ then the magnetization is the real part of $2\chi H_1 e^{i\omega t}$

$$M_x = 2\chi' H_1 \cos\omega t + 2\chi'' H_1 \sin\omega t \tag{2.41}$$

and in comparing this equation with equation (2.37) we obtain

$$\chi' = \tfrac{1}{2}\chi_o \omega_o T_2 \left\{ \frac{T_2(\omega_o - \omega)}{1 + T_2^2(\omega_o - \omega)^2 + \gamma^2 H_1^2 T_1 T_2} \right\} \tag{2.42}$$

$$\chi'' = \tfrac{1}{2}\chi_o\omega_o T_2 \frac{1}{1 + T_2^2(\omega_o-\omega)^2+\gamma^2H_1^2T_1T_2} \qquad (2.43)$$

we find that this out of phase susceptibility produces energy absorption. It is often desirable that paramagnetic resonance experiments be carried out under conditions such that $\gamma^2H_1^2T_1T_2 \sim o$. Magnetic field scanning at a fixed frequency is employed and the out of phase susceptibility transforms as follows:

$$\chi''(H) = \left(\frac{\chi_o H_o}{\Delta H_{\frac{1}{2}}}\right) \frac{1}{\left[1 + \left(\frac{H - H_o}{\frac{1}{2}\Delta H_{\frac{1}{2}}}\right)^2\right]^2} \qquad (2.44)$$

where $H = \frac{\omega}{\gamma}$ is the magnetic field

where $H_o = \frac{\omega_o}{\gamma}$ is the resonance field

where $\Delta H_{\frac{1}{2}}$ is the full width at half the maximum height

Usually the first derivative presentation is obtained where -

$$\frac{d\chi''}{dH} = \left(\frac{4\chi_o H_o}{(\Delta H_{\frac{1}{2}})^2}\right) \frac{\left(\frac{H - H_o}{\frac{1}{2}\Delta H_{\frac{1}{2}}}\right)}{\left[1 + \left(\frac{H - H_o}{\frac{1}{2}\Delta H_{\frac{1}{2}}}\right)^2\right]^2} \qquad (2.45)$$

- is the first derivative lineshape for a Lorentzian line. The full width at half the maximum height is related to the derivative peak to peak width by

$$\Delta H_{\frac{1}{2}} = \sqrt{3}\Delta H_{pp} \qquad (2.46)$$

The normalised Lorentzian first derivative line shape can be written in terms of the peak to peak height Y_{pp} and the peak to peak width as follows:

$$\frac{d\chi'}{dH} = \frac{Y_{pp}(H - H_o)(\Delta H_{pp})^3}{\left[0.75(\Delta H_{pp})^2 + (H - H_o)^2\right]^2} \qquad (2.47)$$

LINE SHAPE FUNCTIONS

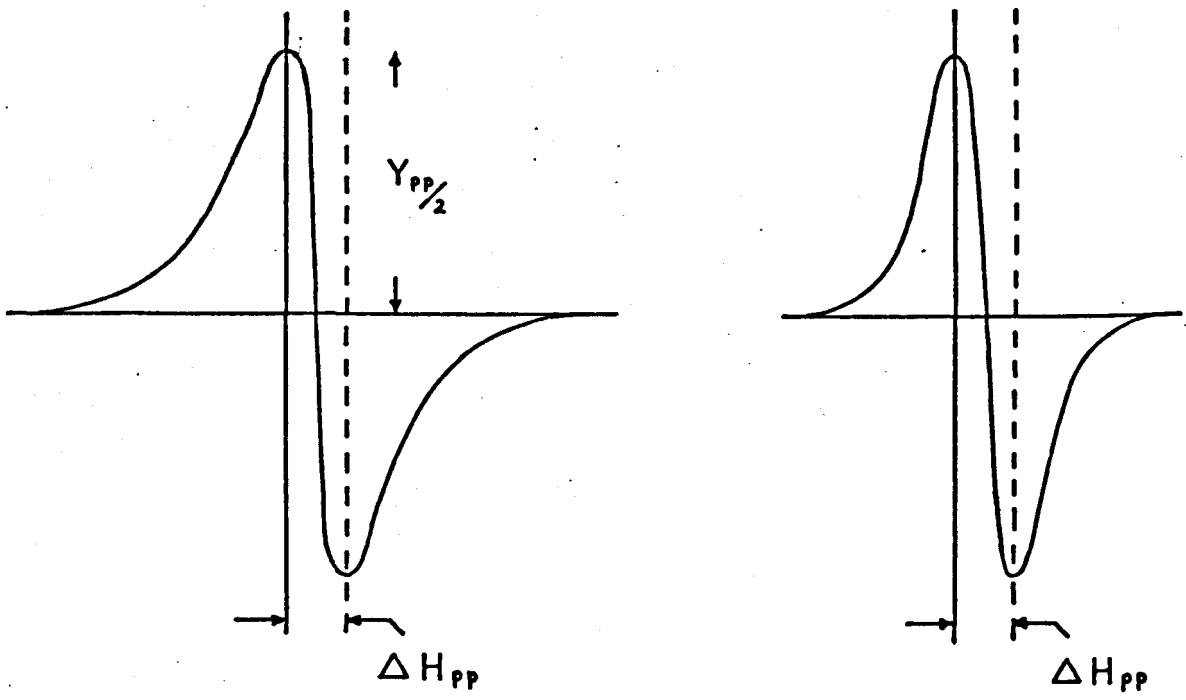

LORENTZIAN GAUSSIAN

FIGURE 2.6

The equivalent equation for the first derivative line shape for a Gaussian function is

$$\frac{d\overset{''}{X}}{dH} = \frac{2Y_{pp}(H - H_o)\exp - 2\left[(H - H_o)/\Delta H_{pp}\right]^2}{H_{pp}\exp(-0.5)} \qquad (2.48)$$

Fig. 2.6 illustrates the first derivative line shape for both functions. On successively increasing the power on the sample we may find, in the absence of efficient spin-lattice relaxation mechanisms, that the signal amplitude no longer continues to increase but in fact passes through a maximum. This arises because the saturation factor $\gamma^2 H_1^2 T_1 T_2$ no longer approximates to zero. Portis[8] used these ideas of saturation to distinguish between Homogeneous and Inhomogeneous line broadening; he argued that a Homogeneously broadened line would decrease in absorption at the centre of the line where the power is greatest before affecting the wings. The effect being to change the line shape and to broaden the line. For an Inhomogeneously broadened line each of the individual component lines saturate to the same extent and the effect is that the overall line shape is retained.

Spin lattice relaxation mechanisms manifest themselves as various processes which will now be discussed.

2.8 The direct process:

In which the spins exchange a whole quantum directly with a lattice vibration of the appropriate resonance frequency as illustrated in Fig. 2.7 (a) The temperature dependence of the relaxation time is given by [9]

$$T_1 \propto \frac{1}{T} \qquad (2.49)$$

SPIN LATTICE RELAXATION PROCESSES

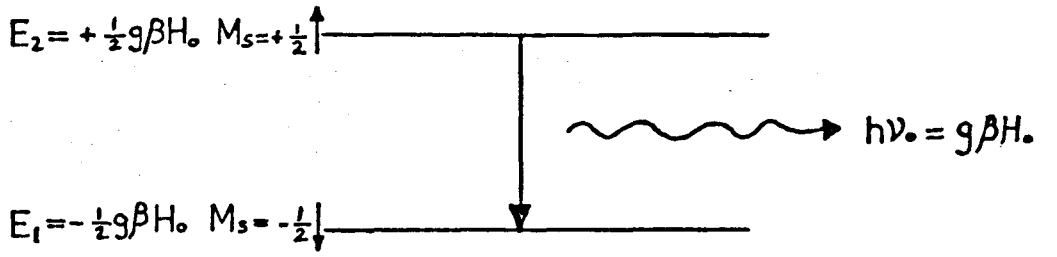

(a) THE DIRECT PROCESS

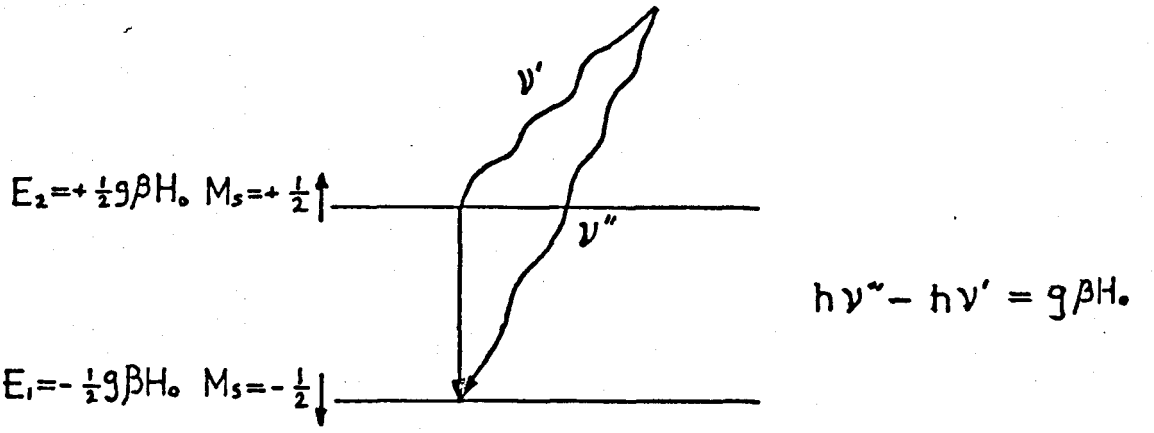

(b) THE RAMAN PROCESS

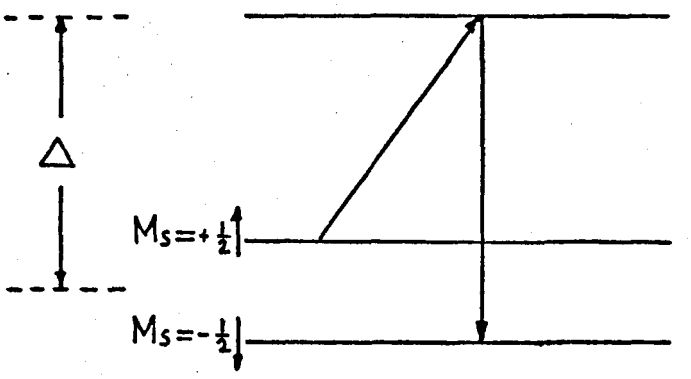

(c) THE ORBACH PROCESS

FIGURE 2.7

2.9 The Raman process:

In which two phonons are used whose frequency difference is equal to that of the magnetic resonance frequency and is illustrated in Fig. 2.7 (b). For such a process the spin-lattice relaxation time varies with absolute temperature as follows (9)

$$T_1 \propto \frac{1}{T^7} \tag{2.50}$$

$$\text{or} \quad T_1 \propto \frac{1}{T^9} \tag{2.51}$$

The direct process in contrast to the Raman process is a first order process and as such is more favourable, however it is essentially a resonant phenomena in which only a small percentage of the phonon spectrum can participate, whereas the use of two phonons in the Raman process utilises a much greater proportion of the available phonon spectrum. At low temperatures only the lowest phonon energy levels are appreciably occupied apart from the large population at the resonant frequency range. As a result the direct process tends to dominate at the lower temperatures whereas the Raman process dominates at the higher temperatures. One mechanism [10] by which the spin and the lattice interact is via the dipole-dipole interaction. Modulation of the dipolar field arises because the lattice vibrations themselves modulate the dipole-dipole separation. If the frequency of a phonon were to coincide with the precessional frequency of a dipole then there is a possibility that a spin transition will take place.

Both Kronig[11] and Van Vleck [12] suggested that the dominant relaxation mechanism arise from crystal field effects. The lattice vibrations modulate the orbital motion via variations in the crystalline electric fields. These changes in the orbital motion react on the spins through the spin - orbit interaction.

Spin-lattice relaxation may manifest itself in a further relaxation process, that of Orbach [9], which is essentially a two stage phonon process employing an intermediate energy level (see Fig 2.7 (c)). The temperature dependence of an Orbach process is

$$\frac{1}{T_1} \propto e^{-\Delta/KT} \tag{2.52}$$

where Δ is the energy separation between the first excited orbital state and the ground state. Orbach processes are readily applicable to rare earth paramagnetic resonance studies where as a result of the strong spin-orbit coupling the magnetic spin states are strongly coupled to the lattice through the orbit-lattice interaction resulting in very fast relaxation times.

2.10 Spin and lattice temperatures

A useful concept to introduce is that of the spin temperature T_{sp} which is defined by the instantaneous relative Boltzmann populations of the two spin levels:

$$\frac{\cap \text{upper}}{\cap \text{lower}} = e^{-g\beta H/KT_{sp}} \tag{2.53}$$

The lattice temperature is assumed to be that of the surroundings as the lattice can be considered to be an infinitely large heat capacity reservoir capable of absorbing large quantities of spin energy without rising in temperature. At resonance the spin temperature increases as the population difference decreases.

2.11 The phonon bottleneck.

We find that atliquid helium temperatures or lower the spin specific heat is much larger than that of the lattice and as such the lattice can no longer be thought of as an infinite sink. At this

THE SPIN , PHONON AND BATH SYSTEMS — THEIR RELAXATION TIMES AND TEMPERATURES

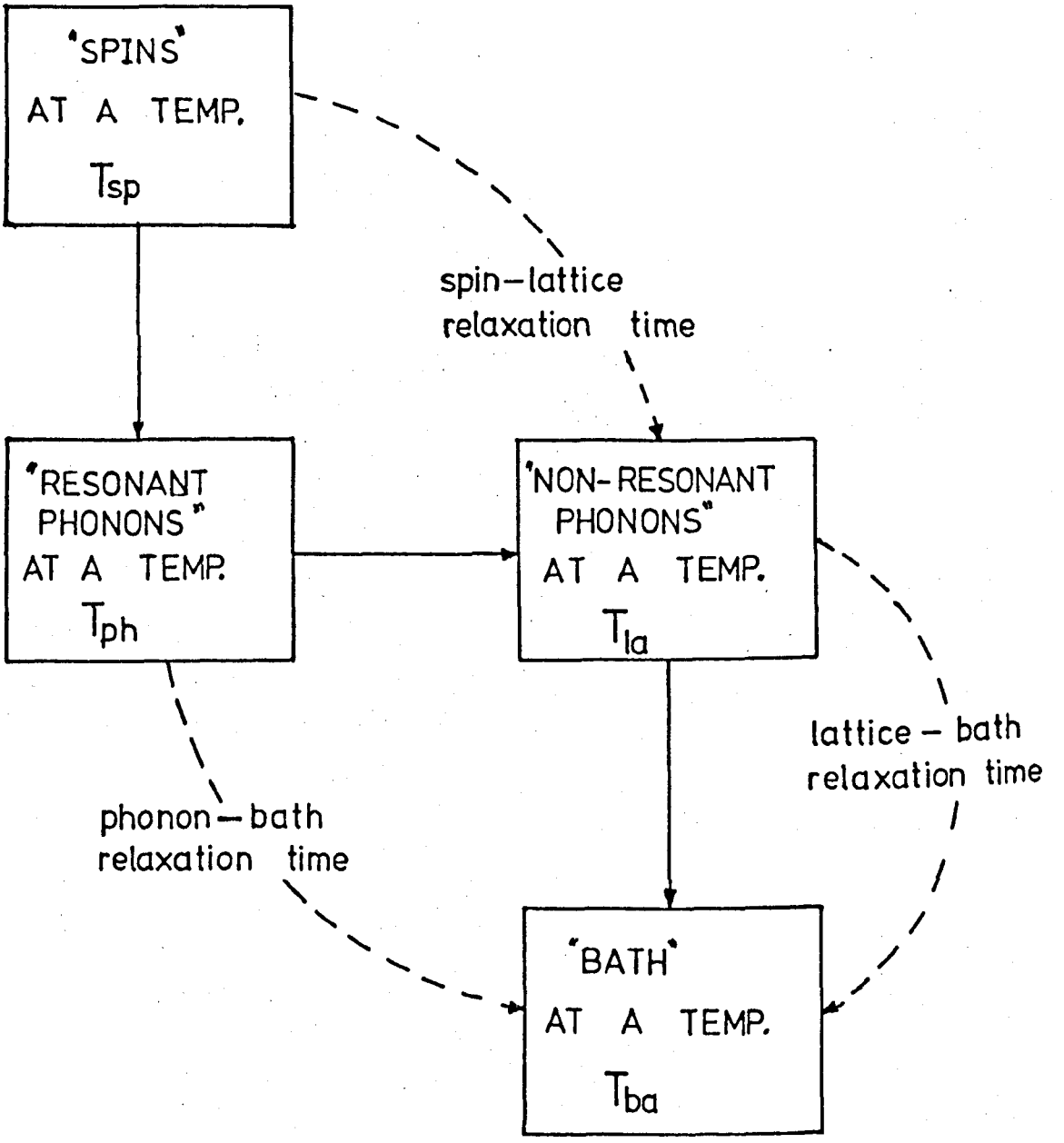

FIGURE 2.8

temperature the direct process dominates and energy is transferred to the lattice modes resonant with the spins; these phonons are raised to a high temperature $T_{ph.}$ A bottleneck [13] situation may arise because the lattice modes become saturated and can no longer accept energy from the spins, until some of these hot phonons have transferred their energy either directly to the bath or by energy transfer to the non-resonant lattice modes. The spin-lattice relaxation time becomes the time taken to transfer the spin energy to the bath. The slowest process and hence the relaxation rate determining process is the time taken to pass the hot phonon energy on to the bath. Fig 2.8 illustrates schematically the various relaxation times.

The basic criterion for a phonon bottleneck is given by

phonon-bath relaxation time > spin-phonon relaxation time

spin-lattice relaxation time > spin-phonon relaxation time

the severity of the bottleneck is determined by the size of these inequalities.

2.12 The exchange reservoir.

Bloembergen and Wang [14] have shown that the exchange system acts as an intermediate thermal reservoir (see Fig. 2. 9) provided that the spin exchange relaxation times and the exchange lattice relaxation time are sufficiently rapid to by-pass the more usual spin-lattice process. Since the spin-exchange interaction is a spin-spin relaxation effect one might predict that the measured relaxation time be independent of the measurement temperature, further since T_2 is a spin-spin relaxation time we expect $T_1 = T_2$

The criterion for an exchange dominating process is that

THE SPIN , EXCHANGE , PHONON AND BATH SYSTEMS-

THEIR RELAXATION TIMES AND TEMPERATURES

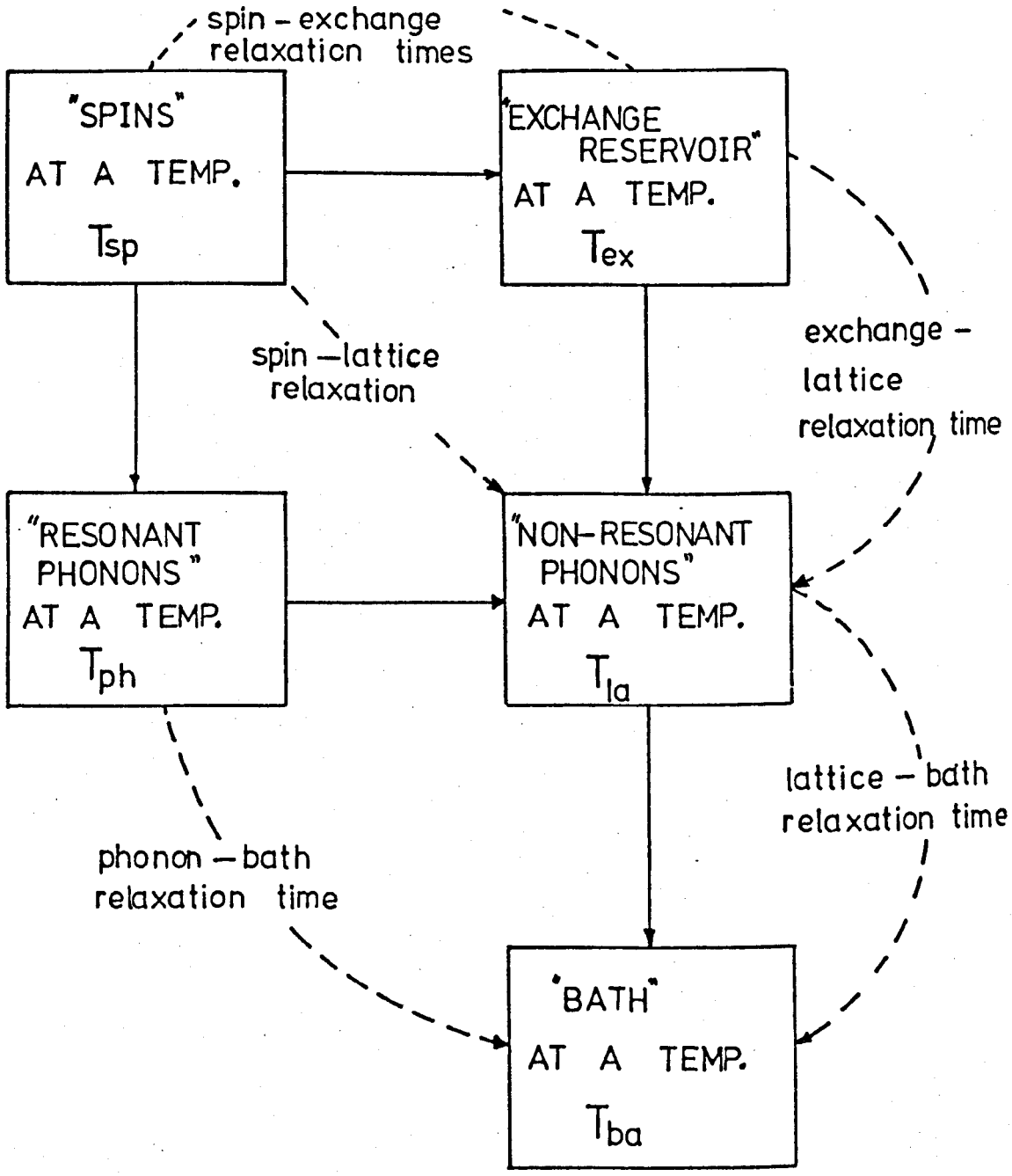

FIGURE 2.9

Spin-lattice relaxation time $>$ spin-exchange relaxation time

Spin-exchange relaxation time $>$ exchange-lattice relaxation time.

It is the strength of the exchange interaction together with the Neel temperature that will ultimately determine the low temperature relaxation mechanism.

HEXAGONAL STRUCTURE

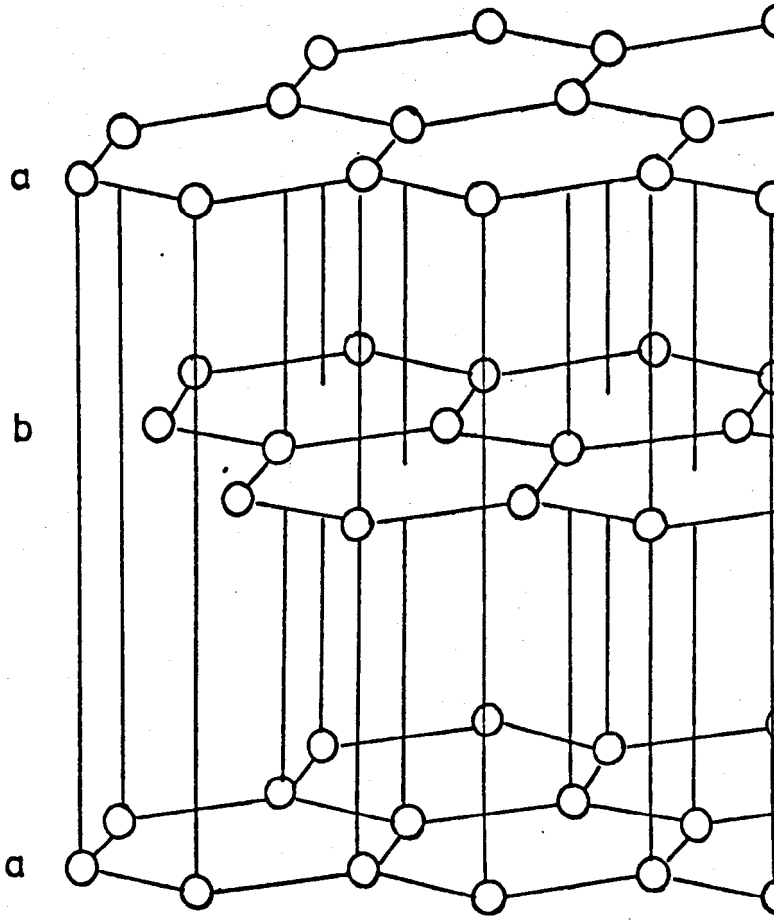

FIGURE 3.1

OF GRAPHITE

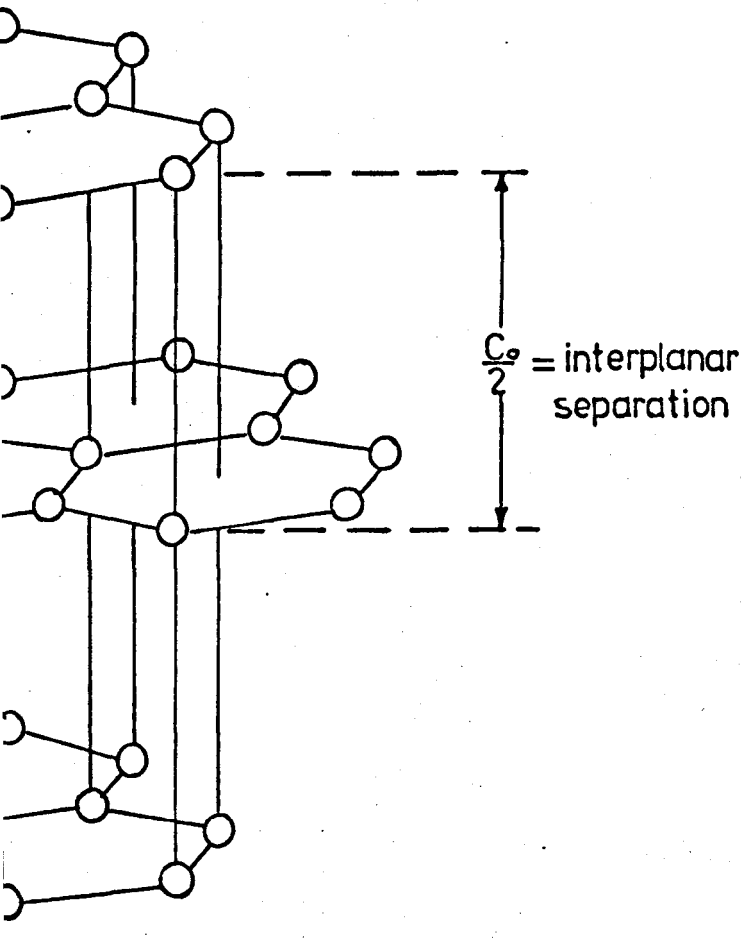

CHAPTER 3

INTRODUCTION TO CARBON

3.1 Graphite

For very many years considerable research has been devoted to an understanding of the properties of the various carbons obtained by heat treatment of organic materials. Much of the detailed consideration given to the properties of single crystal graphite has been reviewed in a book by Ubbelohde and Lewis [15].

The basic hexagonal layered structure of graphite is shown in Fig. 3.1 from which it can be seen that alternate layers lie perpendicularly above each other. Each atom in any layer lying above the mid point of the hexagon in the layer immediately below it.

Each atom has four valence electrons which are utilised in Sp^2 hybrid formation. The tight in-plane covalent bonding results in a carbon - carbon separation of some 1.42 A^o, this compares with a layer plane separation of 3.35 A^o. It is this anisotropic lattice structure that accounts for the highly anisotropic properties of graphite.

Wallace[16] in his initial consideration of the band structure of graphite used a two dimensional band model, neglecting the effect of interlayer interaction. He showed that at the corners of the first Brillouin zone the π bands touched, so that graphite can be considered metallic along certain directions. However both p type and n type samples can be obtained by the effect of impurity doping, since a forbidden gap exists along other directions.

One of the results of the three dimensional model of Slonczewski and Weiss [17] was that the π valence and conduction bands overlap along the zone edges. The three - dimensional model correctly predicts

approximately equal carrier densities and mobilities [18]. Directly as a consequence of its anisotropic lattice structure, graphite tends to be strongly anisotropic in its properties. Perhaps most significant in the electronic properties in the strikingly anisotropic electrical resistivity. The resistivity parallel to the direction of the c axis $\rho_{\parallel}$ is considerably greater than that perpendicular to the c axis $\rho_{\perp}$, indeed ratios of $\frac{\rho_{\parallel}}{\rho_{\perp}}$ have been reported as high as 10^4 [19].

Anisotropy is also observed in the mechanical properties of graphite, having an elastic modulus parallel to the direction of the c axis ~ 35 G N m^{-2} while that along the plane ~ 1015 G N m^{-2}. [20]

3.2 Carbon fibres.

In the search for a carbon material, of low density and having the highly desirable mechanical properties of graphite and which could be readily and cheaply manufactured, carbon fibre emerged. Carbon fibres are formed by controlled pyrolysis of high molecular weight textile fibres. Because of its all carbon back-bone polyacrylonitrile $(- C H_2 - C H (CN) -)_n$ based fibres were chosen for the initial studies. However Houtz [21], in an initial attempt to produce carbon fibre, pyrolysed Orlon* fibre (Acrylonitrile + methyl acrylate copolymer containing 10% methyl acrylate) in air to 200°C and formed a carbon with mechanical properties inferior to those of the original precursor fibre.

Shindo [22] undaunted by these results carried out a most comprehensive study of the mechanical, physical and structural properties of carbon fibres formed by controlled pyrolysis of polyacrylonitrile in an inert atmosphere up to heat treatment temperature (HTT) $\sim$ 3000°C. He found however, that improved mechanical properties were obtained by a first stage slow pyrolysis in air to about 300°C. He reported obtaining carbon fibres

* DUPONT ACRYLIC

INITIAL PYROLYSIS PRODUCTS

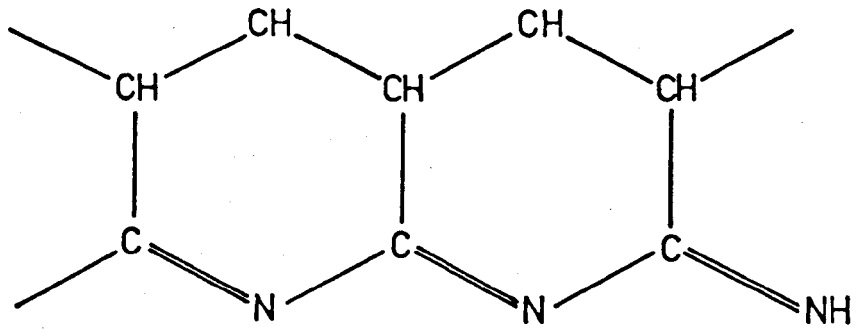

(a)

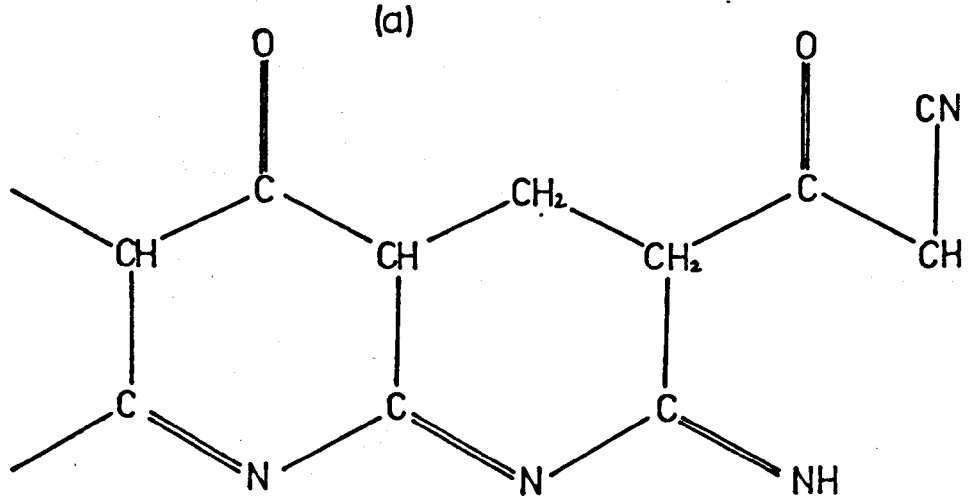

(b)

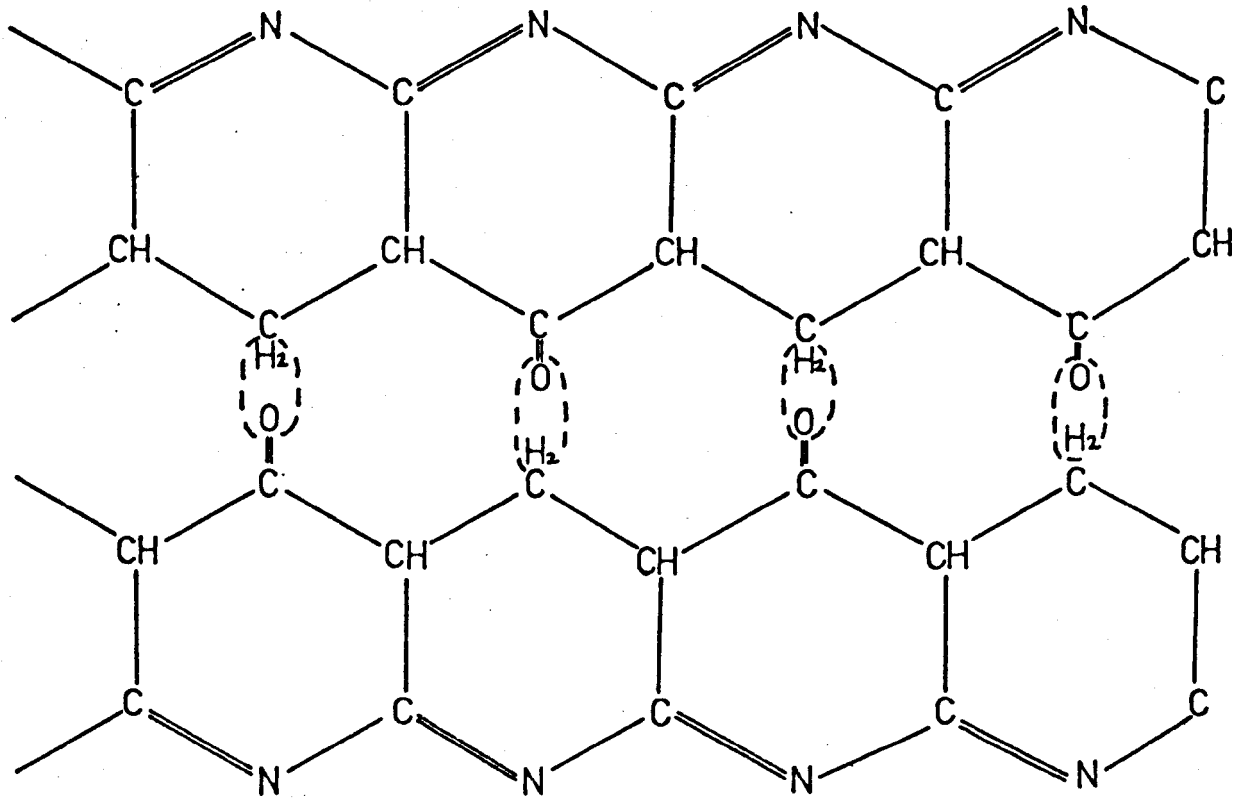

(c)

FIGURE 3.2

having highly promising mechanical properties, and with their hexagonal layer planes oriented about the fibre axis. The size of the crystallites and the elastic modulus were found to increase with increasing HTT as the structure developed, while the tensile strength reached a maximum around HTT ~ 1000°C.

It has been shown[23] that PAN forms a ladder polymer during the initial pyrolysis stage. On heating to 200 - 220°C in vacuo the polymer turns red brown as condensed hydrogenated naphthylpyridine ring structures are formed. Fig. 3.2 (a) shows the structure proposed after infra red studies had indicated a decrease in the nitrile ($C \equiv N$) absorption and an increase in the absorption due to - $(C = N)_n$ - conjugation. Support for this structure [24] has been obtained by an infra red spectral study of the pyrolyis of several model compounds.

Kennedy and Fontanna [25] have examined this initial stage of the vacuum pyrolysis, using the differential thermal analysis technique, and showed that an exotherm having a maximum at 265°C occurs. Turner and Johnson [26] carried out a similar study and showed that the exotherm extends between 190°C and 285°C and having a maximum at 262°C. The exotherm was shown to be associated with the formation of the ladder polymer together with a small amount of chain scission. Further heating results in a weight loss, ammonia and hydrogen cyanide being evolved, the loss of ammonia reaching a maximum around 280°C while the considerably greater loss of hydrogen cyanide reaches a peak around 360°C.

The polymer blackens when heat treated in air to 200°C. The conjugated ring structure is formed together with ketone formations along the ladder [27] (see Fig. 3.2. (b)). The empirical formula for these fibres [28] is fairly well fitted by this structure.

Further heat treatment in an inert atmosphere results in the elimination of water. Watt[27] suggested that this resulted from a linking up of the conjugated structures (see Fig. 3.2 (C)).

In the light of Shindo's [22] earlier efforts, workers at Rolls-Royce[29] and Royal Aircraft Establishment [30], independently reported research resulting in a very considerable improvement in the mechanical properties of PAN based carbon fibres.

Although Shindo [22] found that improved mechanical properties were obtained by using a preoxidation stage it has been shown that similar mechanical properties can be achieved by a slow pyrolysis in an inert atmosphere [31]. However a preoxidation stage is still preferred as it enables the carbonization and ultimate graphitization stages to be carried out more quickly. It should be realised however, that the rate of preoxidation should be sufficiently slow so as not to disrupt the original textile structure. Indeed rapid preoxidation has been shown to result in a fused core and eventually yielding a lamellar rather than a fibrillar structure on graphitizing [32].

A most important parameter determining the mechanical properties of the resulting carbon fibre is the tensioning in the fibre during the initial pyrolysis stage. The natural shrinkage of the polymer during the preoxidation stage should be restricted, and further improved properties will result if the fibre is stretched [33]. Moreton [34] showed that carbon fibres with high moduli could be obtained by pyrolysing acrylic fibres, that had been highly drawn in dry steam with stretch ratios of between 5 and 13. After preoxidation of these fibres at 220°C and carbonization at 1000°C followed by graphitization at 2500°C he was able to show that the modulus increased with stretch achieving a maximum modulus of 345 GN/m^2.

In using the term graphitization we are using the accepted nomenclature after Franklin [35] to describe the effect of heat treatment to temperatures between 1000°C and 3000°C. Carbon fibres produced from polyacrylonitrile based textiles are non-graphitizing in that the crystallite dimensions and order, do not develop to those of graphite. Carbonization is the process of heat treatment to 1000°C in an inert atmosphere during which considerable aromatic condensation takes place. Materials that do graphitize tend to have an excess of hydrogen in the polymer unit, and during carbonization the material passes through a fusion stage [36] which results in a reorientation of the aromatic layered structures. On graphitizing such a material the well oriented layered structures coalesce and crystallite development leading ultimately to a graphitic carbon takes place. On the other hand Franklin [35] has shown that non-graphitizing carbons tend to form rigid cross-linked aromatic structures during the carbonization stage and generally do not fuse. It is thought that on graphitizing such materials the cross linking tends to resist coalescence and ultimately the carbons fail to graphitize.

It has been reported, after extensive X-ray diffraction and electron microscopy studies, that the fine structure of carbon fibre made from polyacrylonitrile consists of a fibrillar character [37,38,39]. The fibres are polycrystalline and consist of small crystallites stacked end to end and although well oriented they have no ordered packing sequence, that is they are 'turbostratic'. The thickness of the fibrils L_c extends over at least 12 layer planes and averages 50 Å while the overall length L_a seems to be limited by lattice defects to lie in the range 60 - 120 Å, although individual layers may be very much longer. Fibrillar branching, bending and twisting would seem to be responsible for the high strength and modulus of carbon fibres. Sharp edge microvoids of width 10-20 Å are contained in the structure.

CARBON FIBRES OBSERVED AFTER FRACTURE

1μ

X 10,500

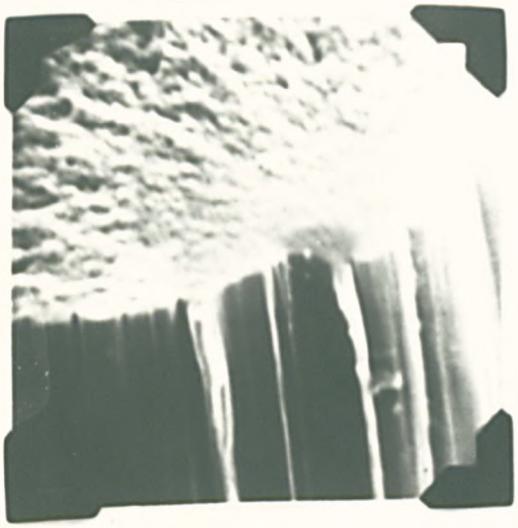

SURFACE FLAW OF INDETERMINABLE ORIGIN

(a)

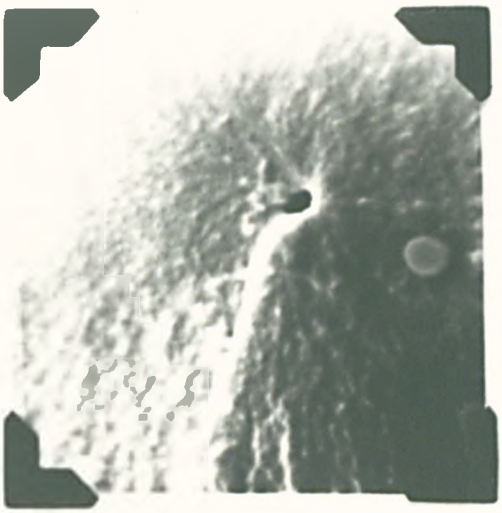

FIBRE PREOXIDIZED IN AIR TO 375°C TYPICAL INTERNAL FLAW

(b)

GRAPHITIZED COURTELLE

X 3,780

(c)

CARBON COMPOSITE UNDER BRITTLE FRACTURE

(d)

FIGURE 3.3

Bacon et al.[39] and others [40,41] have shown that the properties of the initial precursor are reflected in the properties of the resulting carbon. Indeed the preferred orientation together with any defects and voids present in the parent fibre are carried over into the carbon fibre. Further the fibrous nature of the fine structure of carbon fibres closely relates to that of the fine texture of the precursor fibre. Defects in carbon fibres tend to limit the strength of the fibres and removal of such flaws result in an improvement of the mean tensile strength [42]. Fig. 3.3 (a) and (b) show typical flaws in carbon fibres. Fig. 3.3 (c) gives an indication of the fibrillar structure while Fig. 3.3 (d) shows the brittle fracture of a carbon composite.

The modulus of carbon fibres increases with increasing heat treatment temperature as the crystallite order is improved. The tensile strength however passes through a maximum at HTT 1500°C and the mean tensile strength ~ 2 GN/m^2.

X-ray diffraction studies show that when the modulus is of order 103 GN/m^2 the basal planes of the crystallites are lying within $\pm$ 35° of the fibre axis and at 413 GN/m^2 the angle has been reduced to $\pm$ 13° [43]. If then the angle could be further reduced the fibre modulus could be substantially increased. Johnson[44] reported a most remarkable increase in the layer plane alignment by doping to 1% with boron; Allen et al.[45] found the modulus of these fibres to be greatly increased ~ 545 GN/m^2. One way in which this angle could be further reduced is by hot stretching at high temperatures. A 29% stretch at 2800° yields a modulus of some 655 GN/m^2 [43]. Interestingly a 400% stretch in cellulose fibres is required to attain a comparable modulus.

The work of the group at Keele has been the subject of several publications [46,47,48,49] including a thesis[50] presented by Assabghy

CLASSIFICATION OF CARBONACEOUS MATERIALS
BY THEIR ELECTRONIC PROPERTIES

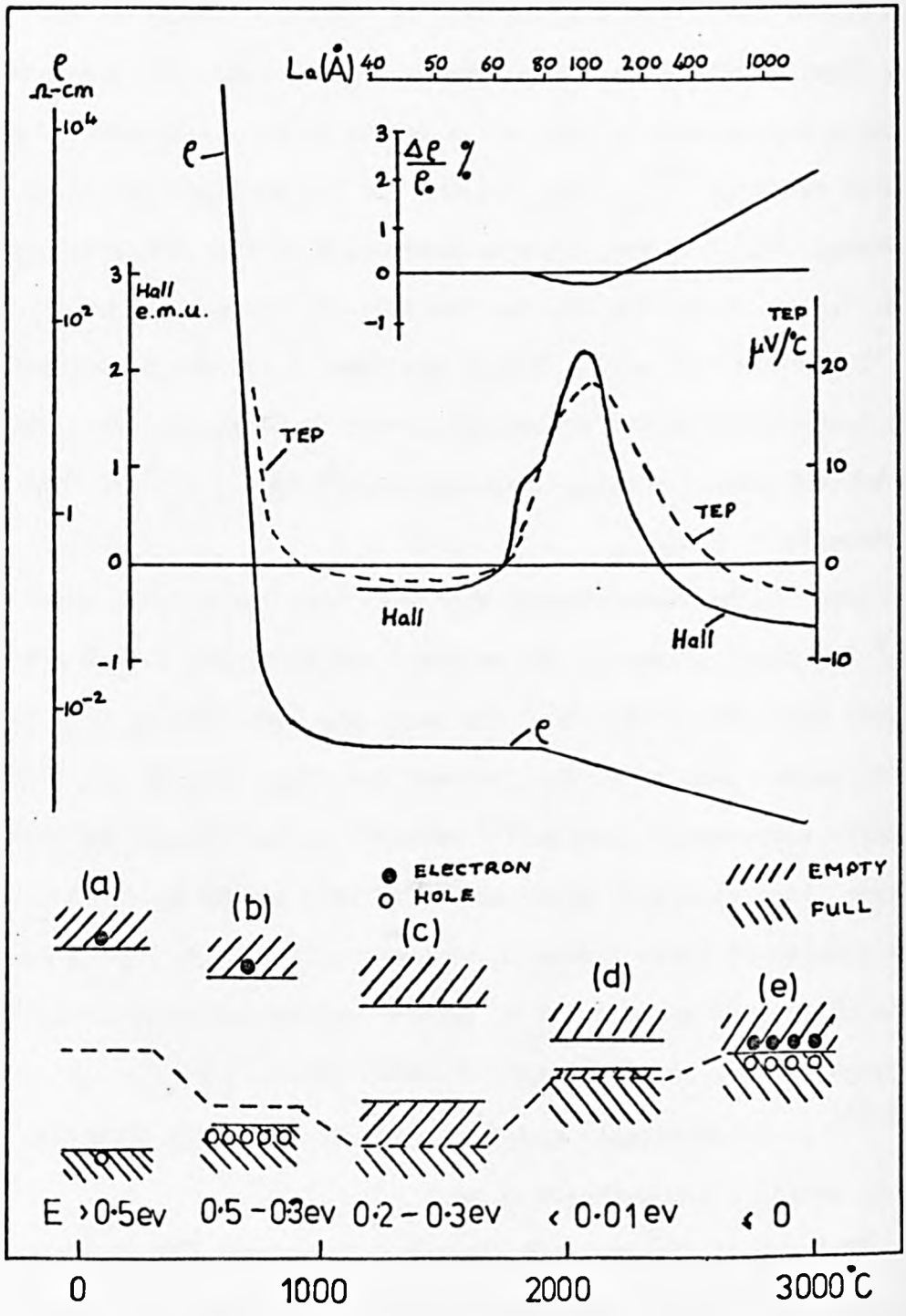

FIGURE 3.4

for the degree of PhD. Studies were made of the ESR and other electronic properties of fibres heat treated to temperatures between 1000°C and 3000°C, and yielded valuable information as to the structure of carbon fibres. The results were compared with those obtained by a study of carbonaceous materials and a brief account of the existing models and of the comparison will be given.

3.3 The electronic properties of carbon materials.

Fig. 3.4 shows the model presented by Mrozowski and co-workers[51,52,53] illustrating the development of the electronic properties with progressive heat treatment for samples that readily graphitize. The model is interpreted in terms of a progressive narrowing of the band gap between the valence and conduction π bands with special emphasis given to the position of the Fermi level. The band gap for any particular heat treatment temperature being estimated from plots of log resistivity against the reciprocal absolute temperature.

For HTT'S is the range 0 - 600°C the resistivity is extremely high and at 600°C the resistivity would probably exceed 10^7 Ω - cm. In excess of this temperature cross linking, dehydrogenation and imperfect condensation of the aromatic layers is thought to expose free valencies that act as electron traps creating holes in the valence band. This tends to be confirmed by the positive TEP below HTT 1000°C. On further heat treatment the concentration of traps increases and the valence band is progressively depleted. These ideas are reflected in a sharp fall in the TEP and resistivity.

The TEP and Hall coefficient become negative at about 1000°C. This is thought to occur because the valence band becomes so depleted that the Fermi level falls below the inflection in the energy (E) versus wave number ($\underline{K}$) contour resulting in a change of sign of the effective mass. Above 1400°C the structure is repaired somewhat as the crystallites

CLASSIFICATION OF CARBONACEOUS MATERIALS
BY THEIR ESR PROPERTIES

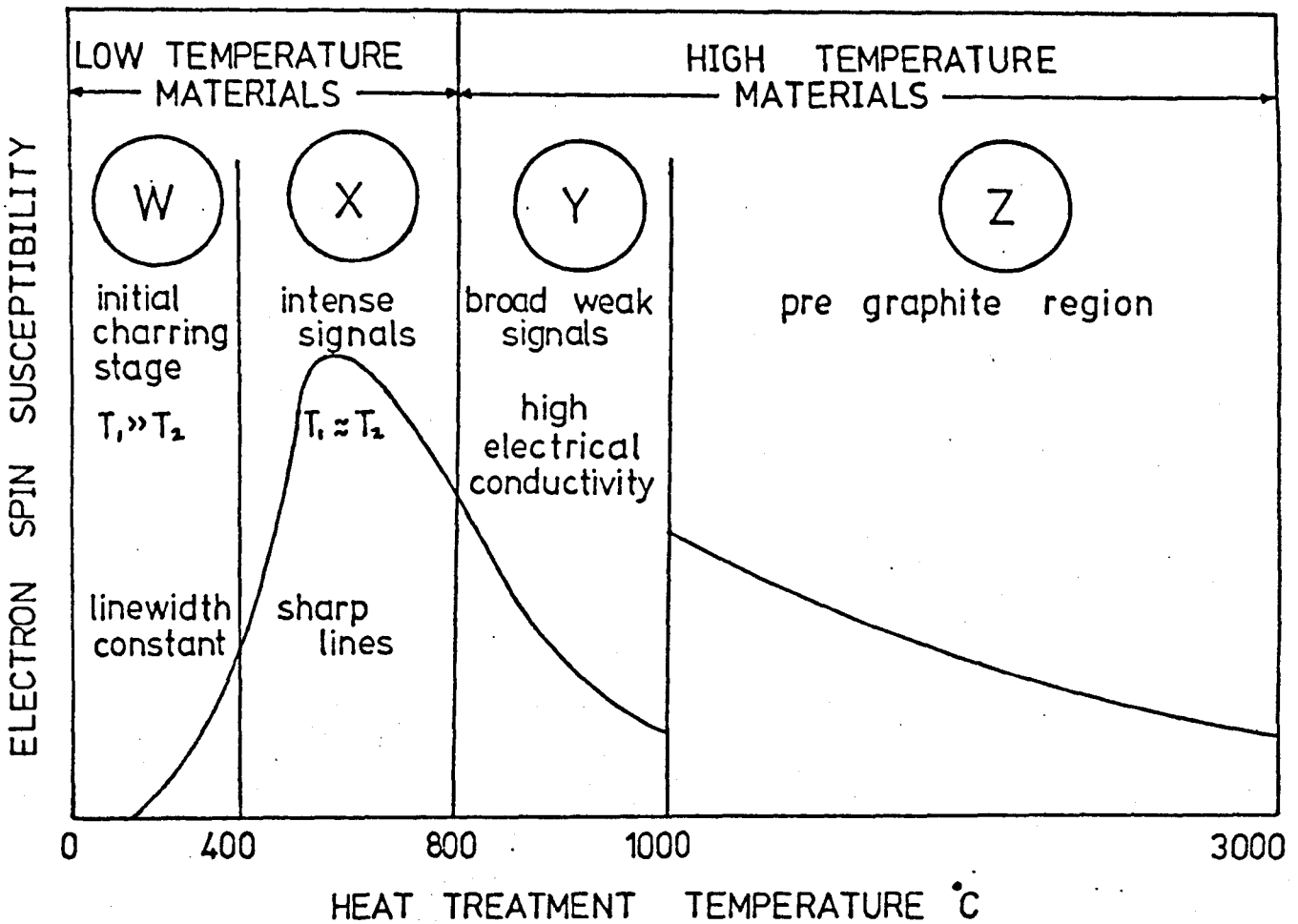

FIGURE 3.5

develop . As a result the concentration of holes is reduced and at about 1750°C the TEP once again becomes positive and increases rapidly. The energy gap narrows as crystallite development takes place, and the peak in the TEP curve at HTT-2000°C is thought to arise from the competing influence of a decreasing hole concentration and an increasing electrical conductivity by thermal excitation.

Over the range 1000 - 2000°C the resistivity does not vary greatly this is because although the scattering will be reduced as the crystallite order is increased the carrier concentration is also reduced. On heat treating above 2000°C a pyrographite sample is produced with an energy gap which is < 0.01ev and which may even disappear. The Hall coefficient and the TEP become negative due to the slightly increased mobility of the electrons.

No explanation of the magnetoresistance has been provided although it has been suggested that a relation should exist between the magnetoresistance and the sign of the carriers[50].

3.4 The ESR properties of carbon materials.

Fig. 3.5 illustrates the broad classification of carbonaceous materials by means of their ESR properties according to Singer [54].

In the initial stage of pyrolysis W the ESR lines like those of most free radicals readily power saturate. The spin-lattice relaxation time T_1 is rather longer than the spin-spin relaxation time T_2. Pastor and Hoskins [55] using a pulse technique measured T_1 at 77K, 4.2K and 1.4K for a dextrose sample heat treated to 250°C and obtained the values 2.0, 40 and 400m sec respectively.

The nature and origin of the free spin species has proven difficult to identify. Much of the difficulty has centred on the problem of trying, probably mistakenly, to determine a unique model applicable to

all materials. Generally broad ~ 10 gauss asymmetrical lines are observed which do not have any resolved hyperfine structure. Hyperfine structure would not be expected if the electron spin is associated with large conjugated structures. It has been reported that on heat treating acenaphthylene [56] to 270°C signals are observed even though the char has the same elemental composition as the starting material. This observation tends to suggest that volatiles need not be formed in order to produce a high spin concentration.

Singer and Lewis [57, 58, 59] carried out an 'in situ' programmed pyrolysis of aromatic hydrocarbons in stable inert liquids and generally observed well resolved hyperfine spectra in the early stages of pyrolysis. Positive identification of free radical intermediates having been made in a number of cases, and the studies show that thermal bond dissociation takes place at the most reactive sites of the molecule. Furthermore, it was shown that nuclear hyperfine interaction is the main line broadening mechanism in low temperature chars [57]. For the hydrocarbons studied a tentative correlation appears to have been obtained between the planarity of the free radical intermediates and the resulting order on graphitizing. They also reported that only a few aromatic rings are needed for stabilization of the spin.

In the region X the spin concentration reaches a maximum and the samples contain at least 80% carbon. The maximum spin concentration generally occurs at the same heat treatment temperature as the minimum ESR line width.

The lines are usually of Lorentzian shape and the spin-lattice relaxation time T_1 is observed both to become independent of the measurement temperature and to become approximately equal to the spin-spin relaxation time T_2. For a sucrose sample heat treated to 600°C Singer et al.[60] showed, using the C W - saturation technique that $T_1 \approx T_2 \sim 10^{-7}$ secs.

Hoskins and Pastor [61] made similar measurements at 300, 77 and 4.2 K on a carbon sample prepared from a dextrose sample charred at 560°C and showed that at each of these temperatures $T_1 \approx T_2 \sim 2 \times 10^{-7}$ sec.

Since the lines are Lorentzian and since the spin-lattice relaxation time becomes independent of the measurement temperature then it is evident that exchange is the mechanism responsible for the sharp narrowing. Exchange narrowing being thought to occur because of an increase of like spins within the samples.

Gaseous oxygen has been observed to have a pronounced effect on certain of the ESR characteristics of samples heat treated over a narrow range of temperature centred about the temperature where the exchange narrowing occurs. The line width is broadened and the interaction is observed to shorten the spin-lattice relaxation time. The total spin concentration and the line shape generally remain constant during oxygen penetration, and the ESR properties are restored by removing the oxygen, showing that the effect is purely physical.

Further condensation of the aromatic layers takes place in the upper part of region X and the ESR lines are observed to broaden. This is usually explained as a shortening of the spin lattice relaxation time T_1 by interaction with conduction electrons. It is interesting to note, however, that the carbons obtained when acenaphthylene is heat treated to between 650 and 750°C show large deviations from Curie behaviour. The line shapes are complicated by skin depth problems indicating that the chars exhibit appreciable conductivity even in the exchange narrowed region.

In the other two regions Y and Z the carbons are characterised by their electrical properties. For a sample of single crystal graphite Wagoner [62] recognised the ESR spectra to be similar in character to that observed during a study of the conduction spins in alkali metals [63]. It would seem therefore that the character of the unpaired electron is changing

from the Curie type of localized magnetic centre to the Pauli delocalized magnetic centre associated with conduction electrons.

Mrozowski[64] has made a study of the temperature dependence of the spin resonance intensity in doped and in neutron irradiated polycrystalline carbon samples. He reported that both Pauli and Curie spin centres contribute to the spin resonance intensity. The temperature dependence of the intensity being separated into a Curie part with $I = C/T$, and a conduction part which is nearly temperature independent, and of the form $I_{CON} = A + BT$. By measuring the ratio of the intensity at liquid nitrogen to that at room temperature he was able to estimate a value for the fraction (X) of the conduction spinsat room temperature. These results have been largely substantiated by experiment[65,66,67,68,69].

Interpretation of the temperature dependence of the g-factor suggested that the resonance line results from a mixing effect between the g-factor of the conduction spin centres g_c and that of the localized spin centres g_L. Each spin contributes an amount proportional to the intensity so that we have

$$g_{observed} = Xg_c + (1 - X)\, g_L \qquad (3.1)$$

More recently Delhaes et al.[70] have established, over the temperature range 300 - 4.2 K, that a similar additive relation exists for the line width.

The ESR and the electronic models presented are capable of explaining a multitude of experimental results, including with certain reservations, those of Robson et al. A brief account of these results and of the comparison with the existing models will be given.

3.5 The electronic properties of carbon fibres.

The resistivity of carbon fibres was observed to fall from

$\sim 3000\,\mu\Omega$ - cm at HTT 1000°C to $\sim 800\,\mu\Omega$ - cm at HTT $\sim$ 2800°C in a similar manner to that reported by Shindo[22] and Yamaguchi[71]. The resistivity appears to be smaller in magnitude than that for graphitizing carbons, probably because of preferred alignment of the crystallites within the fibre. Reduced scattering is further assisted by the end to end stacking of the crystallites within the fibrils. However, at higher HTT'S $\sim$ 2600°C the graphitizing carbon resistivity falls below that of the carbon fibre as graphitization and thermal excitation set in. The thermoelectric power follows the model presented by Mrozowski for graphitizing carbons except for HTT'S greater than 2000°C. At HTT $\sim$ 1750°C the TEP becomes positive, however, unlike the results for graphitizing carbons the TEP reaches a plateau at $\sim$ 2500°C having the magnitude $12.0\,\mu V\,°C^{-1}$. The absence of a fall in the magnitude of the TEP at higher heat treatment temperatures is taken to indicate that there still exists a considerable bandgap preventing an increase in carrier concentration by thermal excitation. Between HTT'S 1000 and 1750°C the magnetoresistance is small and positive but at 1750°C becomes negative and increasingly so with increased heat treatment.

Fujita[72] in his explanation of negative magnetoresistance assumed the carriers to be diffusely scattered at the crystallite boundaries, and suggested that under these circumstances the application of a magnetic field increases the mean free path. Above 1750°C the negative magnetoresistance increases with increasing heat treatment and this was explained by Fujita as being due to an increase in the mean free path as the crystallite size increases.

Below HTT 1750°C a positive magnetoresistance would not be expected as X-ray diffraction studies indicate the prescence of small crystallites. It is argued that boundary scattering is no longer the

dominant scattering process; stress in the fibre creates random scattering leading to a positive magnetoresistance.

It is known that major structural changes take place at HTT ~ 1750°C which lead to an annealing of stresses in the fibre. Discontinuous changes in the X-ray diffraction parameters[73] and the observation that this is the temperature at which the carbon-carbon bond can be thermally broken [74,15] are in accord with this proposition. It is also noted that hot stretching can take place only at temperatures in excess of 1750°C.

The ESR properties of carbon fibres heat treated above 1000°C agree well with those obtained by previous workers for carbonaceous materials. The appearance of the g-shift at HTT 1750°C occurs at a c-spacing of 3.49 Å when the interlayer interaction is large enough to produce a g-shift.

In all of the properties associated with the degree of graphitization, the g-value anisotropy, the electrical resistivity ρ_{300K}, the resistivity ratio ρ_{77K}/ρ_{300K}, the thermoelectric power and the magnetoresistance it has been established that the fibres are non-graphitizing.

The effect of hot stretching of the fibres is to change these properties in the direction of increased graphitization. A linear relationship was found to exist between these properties.

A term the 'relative graphitic order' was defined as the resistivity ratio, in order to indicate the structural order with the fibres more effectively than did the heat treatment temperature [49].

BLOCK DIAGRAM OF THE ESR SPECTROMETER

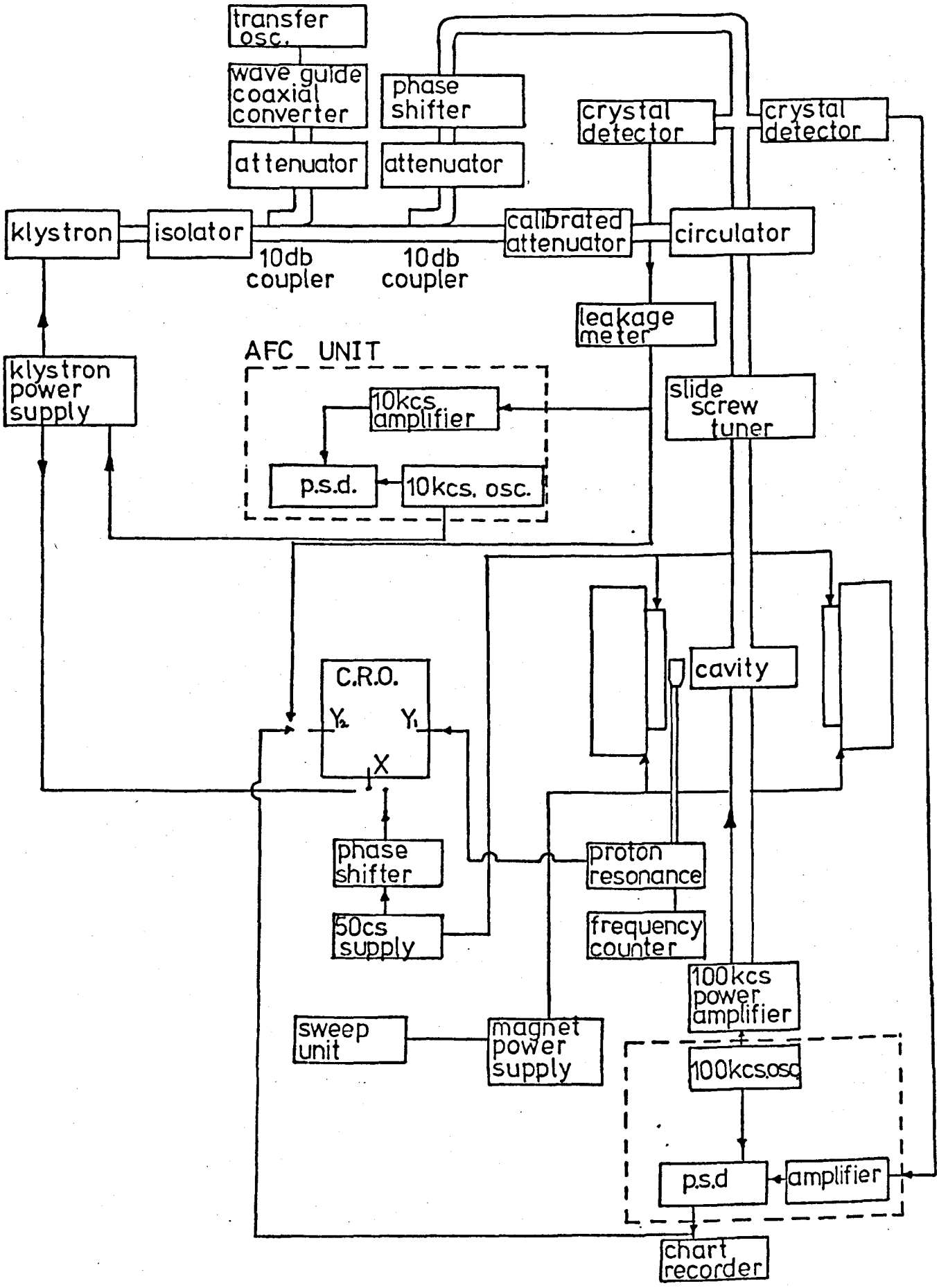

FIGURE 4.1

CHAPTER 4

THE ESR SPECTROMETER AND LOW TEMPERATURE TECHNIQUES.

4.1 The spectrometer

The majority of ESR measurements were made on a conventional X-band spectrometer employing magnetic field modulation and phase sensitive detection at 100 KH_z. An automatic frequency control (AFC) system used to lock the klystron frequency to that of the cavity operated in a similar way by modulation of the klystron reflector voltage and phase sensitive detection at 10 KH_z. Liquid helium facilities were later developed employing audio frequency (a.f.) 400 H_z magnetic field modulation.

Fig. 4.1. shows the spectrometer in block diagram form and it can be seen that a microwave bucking system was used. The X-band klystron comprised a valve insert (EMI/VARIAN 9696 A) in a cavity (EMI/VARIAN 25257). The klystron had a maximum power output of 230 m watt and was manually tunable over the range 7.0 - 10.3 GH_z and was powered by a Hewlett Packard klystron power supply (HP 7163).

Microwaves transmitted along the waveguid pass unattenuated through an isolator, however, microwaves reflected back towards the klystron are absorbed. Power can be coupled from the main line by each of the two 10dB couplers. The first is used to accurately measure the microwave frequency; the microwaves are attenuated and by means of a waveguide to coaxial converter a signal is passed into a Hewlett Packard transfer oscillator (HP 5257A) and frequency counter. At the second 10dB coupler the microwaves are attenuated, phase shifted and passed on to the two detecting crystals via a magic tee. This power supplies the crystals with the necessary bias to produce an operating crystal current of $\frac{1}{2}$ m A, required for a maximum sensitivity of detection. Along the main waveguide the

microwaves pass through a calibrated attenuator to be directed by a circulator into the resonance cavity. Power is critically coupled into the cavity by an adjustable coupling screw so that no power reaches the detecting crystals. At resonance power reflected from the cavity is directed by the circulator through the magic tee and on the detecting crystals.

The output from one of the crystals is fed into an AFC unit where the 10 KH_z signal is phase sensitive detected and if necessary an error signal will be applied to the klystron reflector to lock the klystron frequency to that of the cavity.

The output from the other crystal is pre-amplified (Brookdeal LA350) in a low noise amplifier before being fed into a lock-in amplifier for phase sensitive detection. The output of which is a first derivative presentation of the absorption line and can be displayed on an oscilloscope screen or be traced out on a pen recorder.

4.2 The microwave cavity

The initial experiments were carried out in a cylindrical cavity (Microspin W932) operating in the H011 mode. The 100 KH_z magnetic field modulation was fed onto four rods placed vertically within the cavity. The rods being connected externally to the cavity to form a Helmholtz coil system. By means of a switch the modulating field could be changed by 90^o enabling ESR studies to be carried out as a function of the orientation of the magnetic field. Later a H011 cylindrical cavity was made using a similar design so that it could be used with its axis either horizontal or vertical. In the horizontal position it was used in a study of stretched acrylic fibres. (See section 8.2)

4.3 The magnetic field

The magnetic field was obtained using a Newport type E, 7 inch, air cooled electromagnet fed by its associated power supply type D104. The magnet was mounted on a platform so that a 360° rotation could be made. A sweep unit (Newport SSU) was used to sweep through the ESR resonance. Coils were available on which an a.f. modulation of the d.c. magnetic field could be applied.

A proton resonance unit (Newport PMK II) was used to measure the magnetic field. The r.f. coil in the head of the probe contains a sample rich in protons and the whole arrangement forms a series resonant circuit. For a particular magnetic field the procedure is to adjust a capacitor in the r.f. head until resonance is induced in the sample. By means of a 50 H_z modulation of the d.c. magnetic field the resonance can be displayed on a scope and the frequency measured using an electronic counter (MARCONI TM5951 - $1417/_2$)

4.4 Low temperature techniques.

Using the H011 cylindrical cavity measurements were made at 77K by immersing the sample in liquid nitrogen contained in a quartz finger dewar, the tail of which extended into the cavity. Measurements between 77K and room temperature were obtained by using a flow system. Nitrogen gas from a storage cylinder is passed into coiled copper tubing immersed in liquid nitrogen. The cold gas is then passed over the sample contained in a vacuum insulated double walled quartz flow dewar. The temperature is varied by adjusting the rate of flow of gas from the storage cylinder and is measured by a thermocouple. A most satisfactory thermocouple, well calibrated over the range 300K to 4.2K, is the Oxford Instruments Fe-Au/Chromel thermocouple consisting of a wire sample of spectroscopically fine gold

containing 0.03 atomic percent of iron, and one of chromel. For these experiments to prevent water droplets from entering the cavity dry nitrogen gas should be flushed through the cavity.

For temperatures below 77K an Oxford Instruments stainless steel cryostat (MD4) was used. The inner can of which is surrounded by a copper radiation shield connected to a liquid nitrogen bath, while the whole outer jacket is evacuated.

Very stable and specific temperatures down to the triple point of nitrogen 61.5K can be obtained by controlled pumping of a small quantity of liquid nitrogen placed in the inner tail. However, caution should be exercised as excessive pumping of a large volume will give temperatures well below the triple point, as a solid crust is formed on the surface.

Liquid helium is transferred into the tail of the cryostat from a storage container using a vacuum insulated double walled stainless steel transfer tube. By controlling the rate of flow of liquid helium into the tail, temperatures, stable for a few minutes, can be obtained.

Ideally about $\frac{1}{2}$ litre of liquid helium is collected in the tail of the cryostat and temperatures as low as 1.6K can be reached by pumping on the liquid helium. By pumping through a cartesian manostat, in a controlled manner, very stable temperatures in the range 4.2 - 1.6K can be obtained. The temperature is monitored by measuring the vapour pressure above the surface of the helium. One end of a stainless steel tube is passed down into the cryostat, the other end is attached by incompressible rubber tubing to the arm of a mercury manometer the other arm of which is evacuated.

For measurements of temperature above 4.2K a mesh cage is fixed around the cavity and filled with activated charcoal granules. Activated charcoal is a sample of carbon having a large porous surface area. Carbon resistance thermometers are attached to the side of the cavity with varnish, and to prevent shorting of the contacts with the activated charcoal it is necessary to insert the cavity in a latex sheath. The activated charcoal readily saturates with liquid helium and these absorbed molecules are retained long after the surrounding liquid helium has boiled away. Pumping results in a more rapid desorption of the helium molecules, the heat of desorption being extracted from the cavity. By controlled pumping therefore it is possible to maintain steady temperatures for a few minutes. The method is effective up to about 18K. Above 35K the rate of rise of temperature slows considerably enabling ESR measurements to be made.

Two potted Allen Bradley carbon resistance thermometers CCC 159 and CCC 160, purchased from Cryogenic Calibrations, were used. These thermometers are well calibrated over the range 100K - 2K and correspond to respective resistance values of 200 Ω and 1000 Ω . The resistance of each thermometer was measured on a bridge using a Keithley 150B microvolt ammeter as a null detector.

CHAPTER 5

ESR STUDIES.

Previous workers have shown that the properties of the starting acrylic are reflected in the properties of the high heat treatment temperature carbon fibres.[39,40,41] Assabghy[50] showed a g-anisotropy to occur in acrylics heat treated above 1750°C and explored the possibility of using the g-shift as an indication of crystallite order. We have attempted a study of fibres heat treated to less than 1000°C to obtain an indication of order within the fibres.

5.1 The samples.

The fibres chosen for this study were derived from Courtelle fibres (acrylonitrile + 7% methyl acrylate copolymer) containing 10,000 1½ denier *filaments to each tow. To prevent shrinkage in the preoxidation stage the fibres were wound on steel frames. The fibres were then pyrolised to 400°C at a rate of 1°C min^{-1} in a stream of air. Due to the excessively high preoxidation temperature, the fibres invariably fractured during this stage. The oxidized fibres were then placed in a graphite crucible and carbonized at a rate of 12°C min^{-1} in an Argon atmosphere, to provide a series of samples heat treated to temperatures between 400 and 1000°C, at approximately 50°C intervals.

Each of the carbonized samples were monitored for contraction in length and weight loss (corrected for absorbed water content) in comparison with the length and weight of the 400°C oxidized sample.

The weight loss on carbonizing to 1000°C was ~ 50% while the contraction in length measured some 8%.

Strength and modulus measurements were carried out on each of 10 monofilament fibres taken from the sample carbonized to 1000°C, using

* 1 denier is the weight in grammes of 9,000 metres (monofilament).

LINE SHAPE – SPECIMEN IN AIR

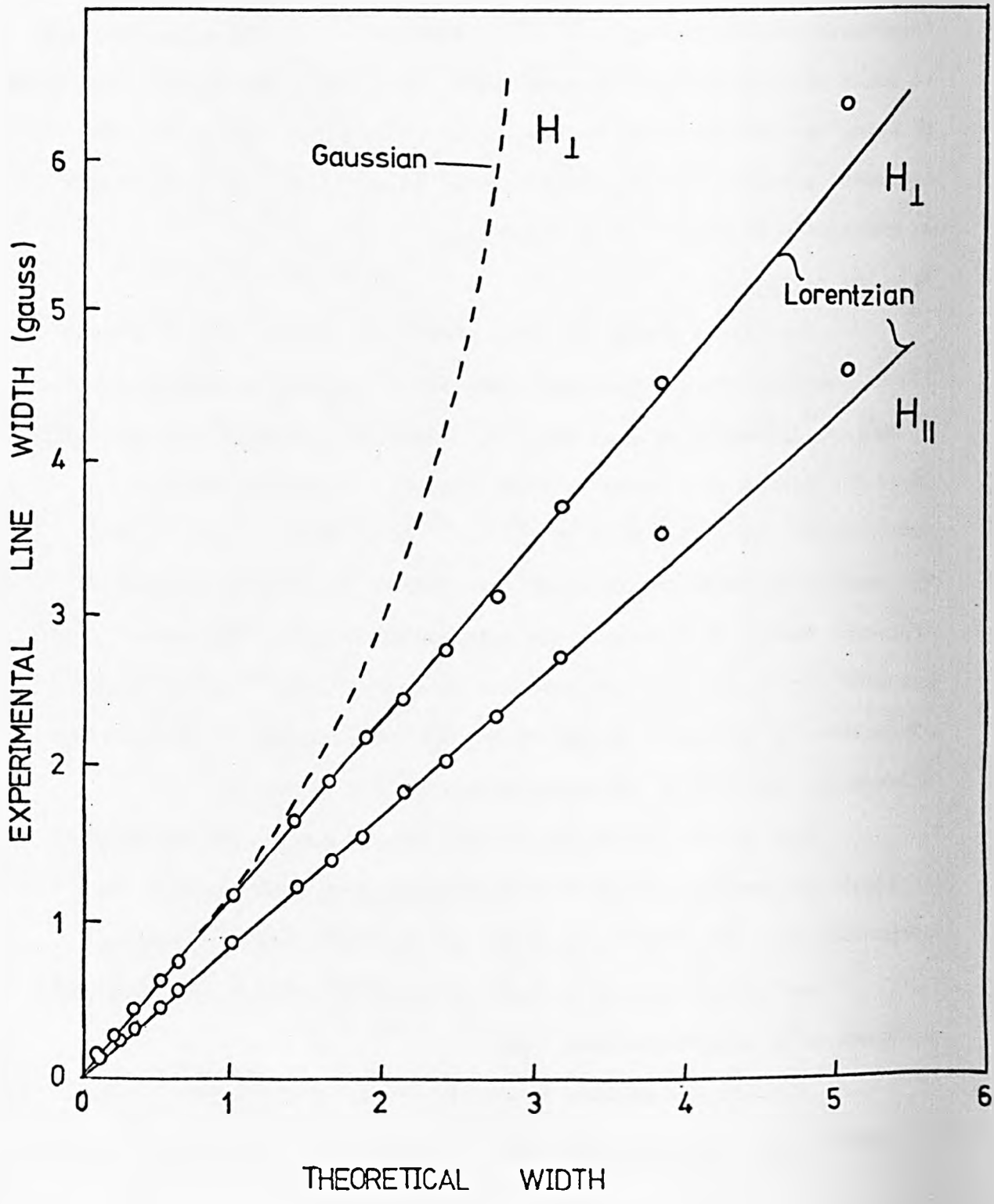

FIGURE 5.1

LINE SHAPE — SPECIMEN UNDER VACUUM

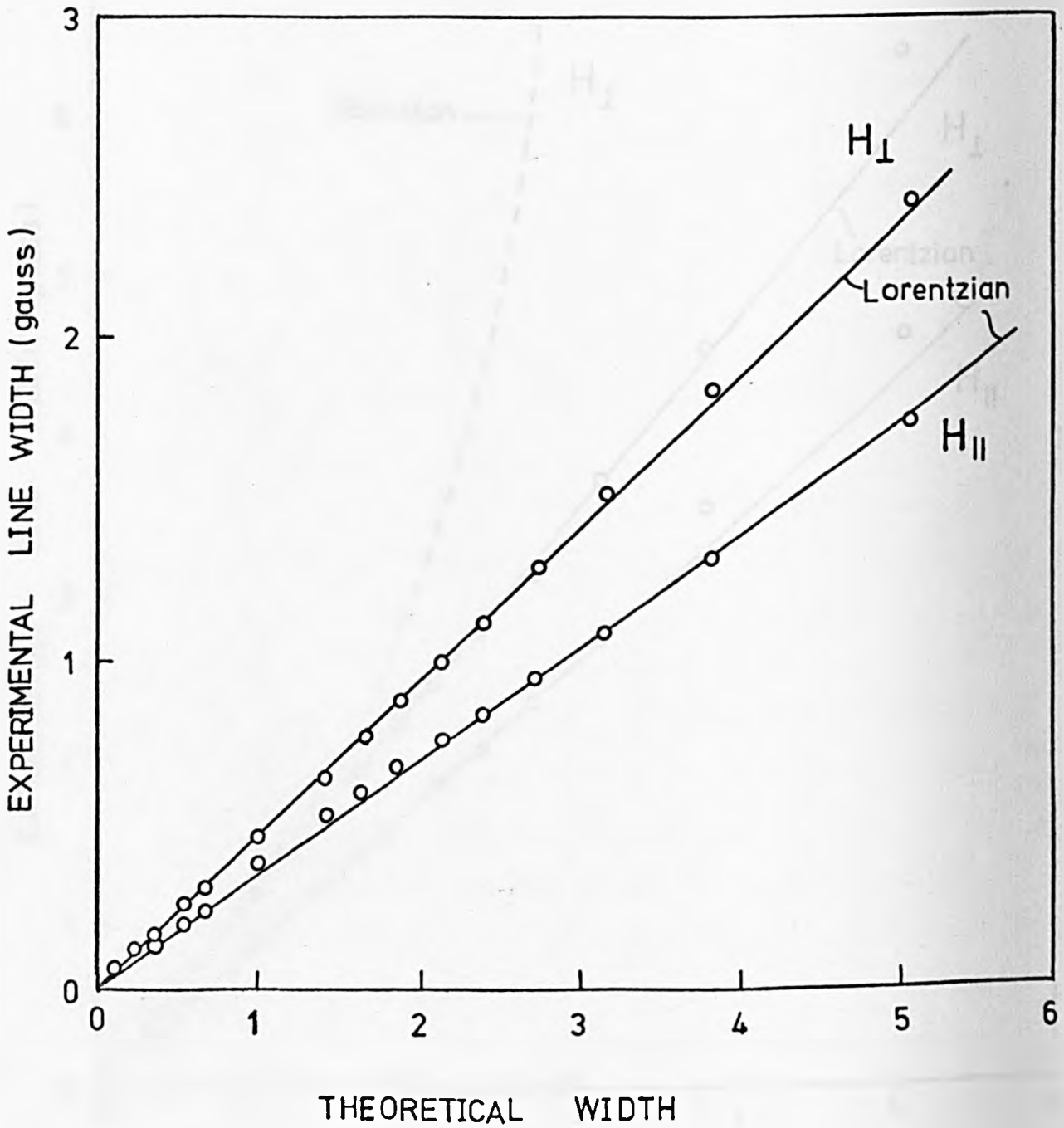

FIGURE 5.2

an Instrom tensile testing machine having a 0-50 gm load cell. The fibre dimensions were then measured by means of a travelling microscope with a calibrated eyepiece. The modulus obtained was $\sim$ 151 $\pm$ 6 GN/m^2 and the breaking stress $\sim$ 1.28 $\pm$ 0.05 GN/m^2 which compare unfavourably with those obtained by preoxidizing at 220°C before carbonizing at 1000°C viz modulus $\sim$ 245 GN/m^2 and breaking stress $\sim$ 1.7 GN/m^2.

5.2 The ESR study

Methods of mounting the fibres for ESR have previously been developed by Assabghy[50]. Small bundles of fibres, some 2 - 3 mm long, were mounted with their axes parallel between strips of cellotape. Several strips were placed in a spectrosil tube and inserted in the cavity so that ESR studies could be performed with the magnetic field either perpendicular or parallel to the fibre axis.

The six line hyperfine spectrum of Mn^{2+}, observed in a crushed sample of magnesium oxide doped with manganese, was used as a monitor for Q changes, during temperature dependence studies of the ESR parameters. The Mn^{2+} resonance was observed to have a Curie temperature dependence between room temperature and liquid nitrogen, and its g-value was calibrated against a powdered polycrystalline sample of dipheryl-picryl-hydrazyl (DPPH) having a g-value of 2.0036.

At 9.2 GHz the 87 gauss isotropic hyperfine separation centred about g=2.0066 enabled accurate g-value measurement of the carbon fibre resonance without interference from the very narrow $\sim$ 1 Gauss Mn^{2+} lines.

5.3 The line shape

In section 2.7 we sketched the origin of the Lorentzian and Gaussian line shape functions for a first derivative presentation. Using these functions it is possible to calculate the width of the lines at

Q BAND SPECTRUM OF
INERT TREATED COURTELLE (378°C)

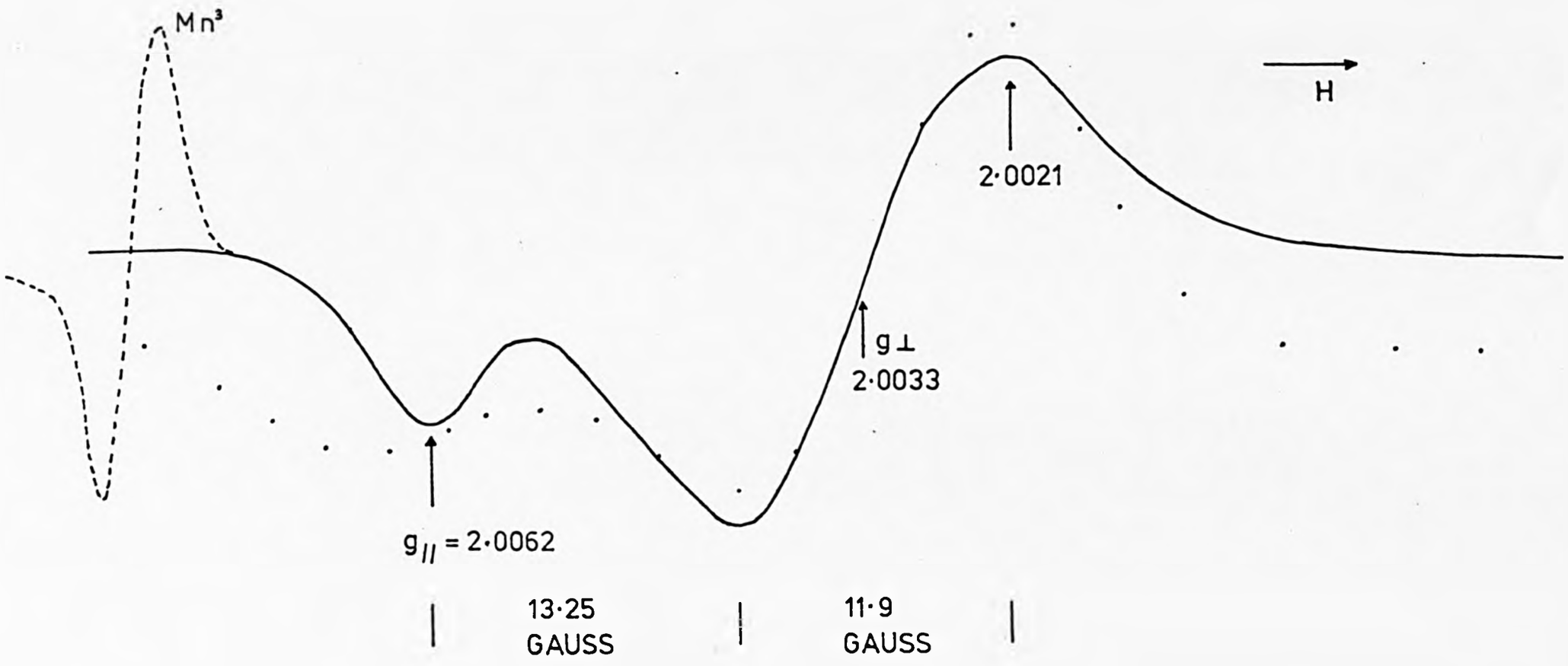

FIGURE 5.3

various fractional heights, and by plotting these calculated widths against those of the experimental curve, measured at the same fractional height, it is readily observed whether the experimental line shape approximates to either function.

With two exceptions the line shapes were Lorentzian to at least five line widths. For the series heat treated above 660°C the line shape remained Lorentzian for all measurement temperatures down to 2K. Fig's. 5.1 and 5.2 illustrate typical line shape analysis of the spectra obtained for sample G6 (HTT 710°C). It is evident that oxygen penetration broadens the line width but leaves the line shape unaltered.

The ESR spectra recorded for samples that had either been pyrolysed up to 200°C in air, or up to 378°C in an inert atmosphere, were not of Lorentzian shape. At X-band a single asymmetrical line of some 9-10 gauss width is observed while at Q-band the ESR line "splits". Fig. 5.3 illustrates the ESR spectrum obtained for a sample inert treated to 378°C.

Singer et al.[60] observed asymmetrical line shapes for low temperature sucrose chars and proposed that the shape arose from unresolved hyperfine structure. However, the spectrum illustrated in Fig. 5.3 could quite possibly be a powder spectrum - the sample having axially symmetric spin sites and g-values as indicated. A computer program based on the approach of Boas et al.[75] was written to investigate this possibility. Spectra were computed using both Gaussian and Lorentzian line shape functions, however, neither provided a good fit to the experimental curve. The Gaussian function provided the better fit and it is included in Fig. 5.3 for completeness.

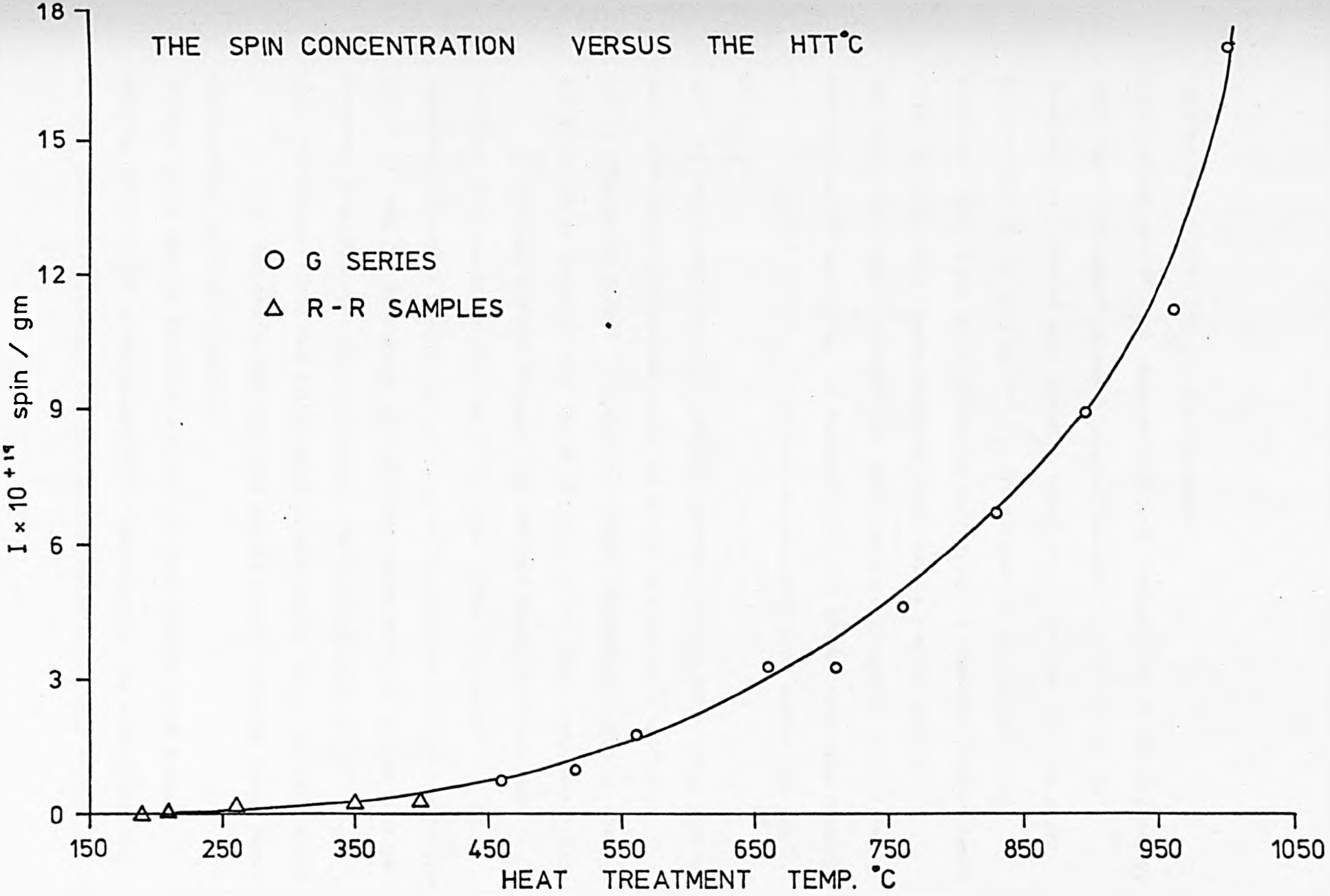
THE SPIN CONCENTRATION VERSUS THE HTT°C
O G SERIES
Δ R-R SAMPLES
I x 10+19 spin / gm
18
15
12
9
6
3
0
150
250
350
450
550
650
750
850
950
1050
HEAT TREATMENT TEMP. °C

FIGURE 5.4

5.4 The ESR intensity.

The spin concentration of each sample was determined by comparison with a known weight of a high heat treatment temperature carbon sample (H 1750°C), which had previously been calibrated[50] against a powdered carbon dispersed in chalk. The Mn^{2+} reference was used in each experiment to carefully monitor any Q changes. Equal lengths of fibre and standard, contained in identical quartz capillary tubes, were used to ensure that the filling factor was constant during each experiment.

The second integrated area under the derivative curve is then proportional to the intensity. Because we were comparing lines of the same shape (Lorentzian) then the second integrated area was evaluated using $S_F^2 D$, where S_F is the peak to peak line width and D is the peak to peak derivative height. The suitability of this method was checked by writing a numerical integration program employing a Runge Kutte Quartic routine; agreement to within 5% was achieved.

Fig. 5.4 shows a plot of the spin concentration against the heat treatment temperature and it is immediately obvious that the spin concentration increases continuously up to HTT 1000°C. This behaviour contrasts sharply with that usually observed in low temperature chars; a maximum in the spin concentration usually occurs in the HTT region 600 - 800°C.

Absorbed molecular oxygen causes line broadening for samples prepared in the temperature range 660 to 830°C. However, we found that the spin concentration was unaffected to within the 5% experimental error. Interestingly both the evacuated and unevacuated samples give Lorentzian line shapes, and the line width was always reproducible on evacuating to less than 10^{-5} mm Hg. It would appear that the oxygen penetration was homogeneous.

SAMPLE	HEAT TREATMENT TEMPERATURE	PERCENTAGE OF CONDUCTION CARRIERS	PERCENTAGE OF LOCALIZED CARRIERS
G 1	1000 C	40	60
G 2	960 C	32	68
G 3	895 C	21	79
G 4	830 C	–	–
G 5	760 C	0	100

TABLE 5.1

	HTT °C	'X' BAND room temp. (gauss)		'X' BAND room temp. evacuated		'X' BAND liquid nitrogen		'X' BAND liquid helium		'Q' BAND room temp.	
		$\Delta H_{\parallel}$	$\Delta H_{\perp}$	$\Delta H_{\parallel}$	$\Delta H_{\perp}$	$\Delta H_{\parallel}$	$\Delta H_{\perp}$	$\Delta H_{\parallel}$	$\Delta H_{\perp}$	$\Delta H_{\parallel}$	$\Delta H_{\perp}$
G1	1000	36				33		22		37·4	
G2	960	20				14		6·5		20·3	
G3	895	10				3·58	3·70	1·37	1·43	9·9	
G4	830	~10		3·30	3·38	1·10	1·22	0·95	1·04	~ 7·7	
G5	760	~ 4·0		1·01	1·04	0·80	1·10	1·36	1·69	~ 6·0	
G6	710	~1·71	~ 2·36	0·71	0·90	1·58	2·32	2·10	2·80	~1·88	~ 2·47
G7	660	~1·84	~ 2·49	0·83	1·03	2·69	3·52	3·10	3·76	~2·35	~ 2·88
G8	562	4·12	4·65			4·54	5·03			4·8	7·2
G9	515	4·72	5·33			4·96	5·58			5·7	7·4
G10	460	5·00	5·50			5·20	5·75			7·3	10·0
RR	400	4·35	4·80							8·5	
	350	4·56	5·00							8·0	
	260	4·95	5·20							7·5	
	210	7·70	7·90							11·2	
IT	378	9·30	9·50							12·0	
G6	EVACUATED AT LIQUID NITROGEN $\Delta H_{\parallel}$ 1·40 gauss $\Delta H_{\perp}$ 1·94 gauss										

TABLE 5.2

5.5 The temperature dependence of the spin concentration

The temperature dependence of the spin concentration was determined relative to the Mn^{2+} standard. Curie temperature dependence was established for samples heat treated up to 760°C. However, above this temperature departures from Curie behaviour were observed. Using Mrozowski's analysis (See sections 3.4) we estimated the percentage of the Localized spin sites and hence of the conduction spin sites contained within the samples at room temperature (See Table 5.1).

It was not possible to make this analysis for sample G4 because of a sensitivity difficulty, this arose because the ESR signal narrowed sharply as the measurement temperature was lowered to 77K. Hence ESR spectra could not be recorded, using the same depth of magnetic field modulation, at room temperature and at liquid nitrogen without overmodulating the latter spectrum.

It is significant that for samples heat treated to 1000°C we found a 40% conduction spin concentration while Assabghy[50] reported an 80% conduction spin concentration.

5.6 The line widths

Line widths measurements were made on spectra recorded at both X and Q band (See Table 5.2). We have already noted (see section 5.3) that the ESR signal obtained from very low heat treatment temperature chars is asymmetrical, and of constant line width and shape. However, samples preoxidized above 210°C are symmetrical, of Lorentzian shape and are of order 5 gauss line width. The ESR signals begin to narrow at HTT 660°C before broadening is initiated at HTT 760°C. Over the range of HTT 710°C - 1000°C the line width increases from approximately 1 gauss to 36 gauss.

ESR SPECTRA - SAMPLE G6

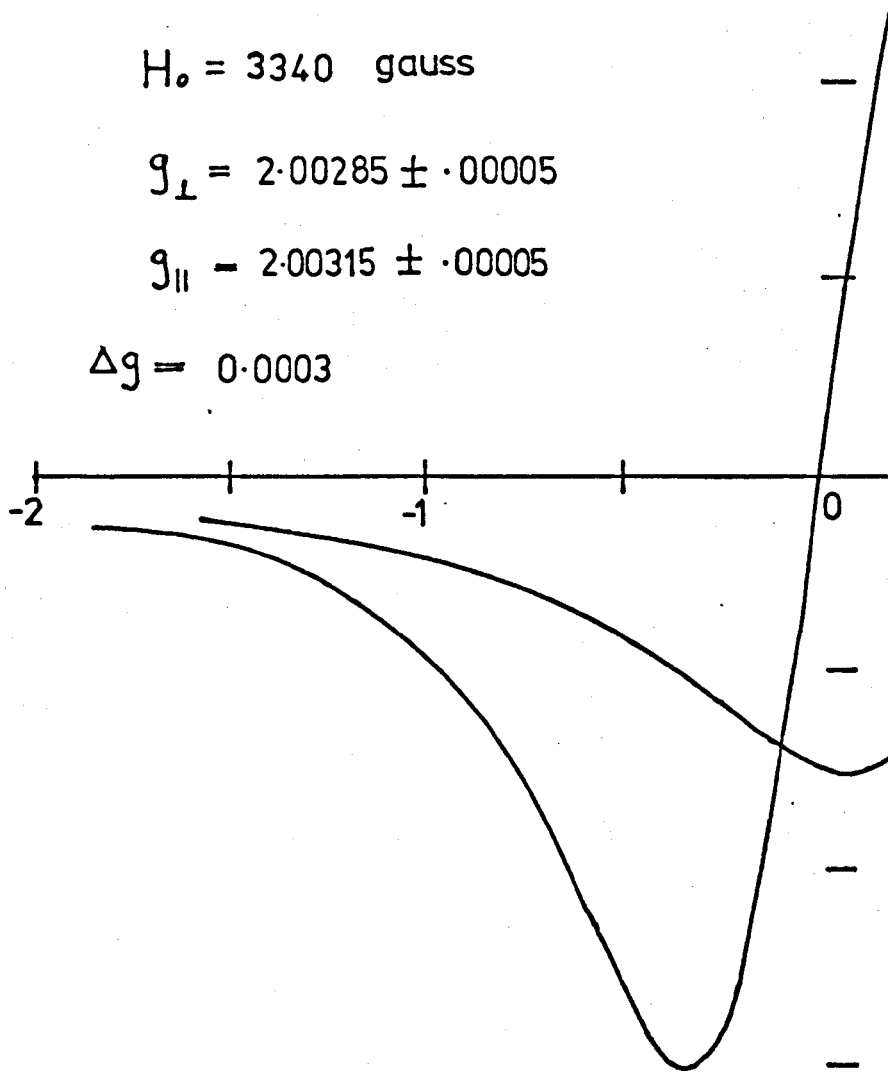

FIGURE

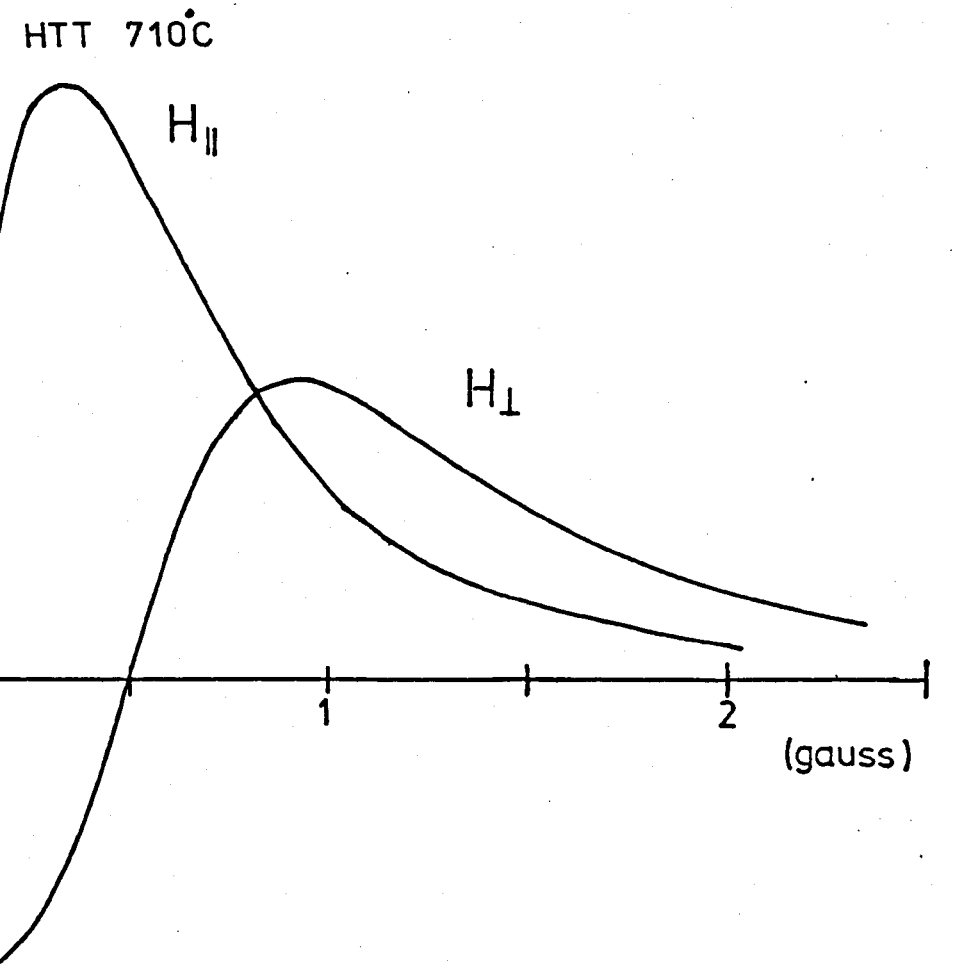
HTT 710°C
H∥
H⊥
1
2
(gauss)

Air produces considerable broadening of the line width for samples heat treated in the range 660°C to 830°C, and it was necessary to evacuate these sample to less than 10^{-5}cm.Hg to obtain reproducible line widths.

The fibres exhibit a symmetrical resonance which for samples heat treated up to 760°C is clearly anisotropic with $\Delta H_{\perp}$ being greater than $\Delta H_{\parallel}$ by some 40%. In this case $\parallel$ (parallel) and $\perp$ (perpendicular) denote orientations of the magnetic field with respect to the fibre axis. Air appears to have little affect on the anisotropy ratio.

The line width anisotropy is accompanied by an anisotropy in the peak to peak height sufficient to maintain the spin intensity constant for both orientations of the magnetic field. Fig. 5.5 is a scale drawing illustrating the anisotropic features of the resonance obtained for sample G 6 (HTT 710°C) including the line width, peak to peak height and g-value.

Anistropy of the line width terminates with the onset of broadening although small anisotropic effects would be difficult to observe in resonances of some 10 gauss width. Indeed sample G 4 (HTT 830°C) has a line width of 10 gauss when measured in air with no observable anisotropy, however, on evacuating, the line width measured $\sim$ 3 gauss and a 2% anisotropy of line width was measured.

For sample G 6 it was found that the line widths ($\Delta H_{\parallel}$ and $\Delta H_{\perp}$) when measured at liquid nitrogen were approximately independent of whether the sample was evacuated.

The resonances obtained for samples G 5, G 6 and G 7 all showed some evidence of broadening as the temperature was lowered from 77K to 4.2K. However, the spectra obtained from those samples heat treated above 830°C

narrowed quite markedly from their broad room temperature values as the temperature was lowered to 4.2K. For sample G 3 HTT 895°C the resonance had a line width of order 10 gauss at room temperature and only of order 1.4 gauss at 4.2K. Coupled with this narrowing we found for samples G 3 and G 4 some evidence of anisotropy in the line width as the temperature was lowered.

For samples heat treated below 562°C the spectra broaden when measured at Q band. The effect is to increase the line width anisotropy, this is because the line width with the magnetic field perpendicular to the sample ($\Delta H_{\perp}$) is increased slightly more so than with the magnetic field parallel to the sample ($\Delta H_{\parallel}$). For samples G 6 and G 7 there is little increase in line width anisotropy in comparison with the X band results. The line widths for samples G1 to G 4 inclusively seem relatively unaffected by measurement at Q band.

5.7 The g-anisotropy

The g-value of the resonance when measured for orientations the magnetic field both parallel (defined as $g_{\parallel}$) and perpendicular (defined as $g_{\perp}$) to the fibre axis show some interesting anisotropic effects with $g_{\parallel}$ greater than $g_{\perp}$.

Fig. 5.5 shows the spectra obtained by evacuating sample G 6 (HTT 710°C) to less than 10^{-5}cm.Hg. The line width is of order 1 gauss and g-value measurements accurate to $\pm$ 0.00005 were possible. The resonance is symmetrical, of Lorentzian shape with $g_{\parallel}$ = 2.00315 and $g_{\perp}$ = 2.00285 and as Fig. 5.5 illustrates the shift in position on rotating the magnetic field is somewhat greater than the line width.

The g-anisotropy was found to be unaffected by the presence of air, however, to obtain maximum sensitivity it was necessary to evacuate those samples whose line widths were broadened by the presence of air.

SAMPLE	HTT°C		$g_{\parallel}$	$g_{\perp}$	$\Delta g = g_{\parallel} - g_{\perp}$
G3	895	EVACUATED	2·00303	2·00268	0·00035
G4	830	"	2·00297	2·00269	0·00028
G5	760	"	2·00307	2·00273	0·00034
G6	710	"	2·00315	2·00285	0·00030
G7	660	"	2·00329	2·00294	0·00035
G8	562		2·00329	2·00315	0·00014
G9	515		2·00337	2·00327	0·00010
G10	460		2·00339	2·00327	0·00012

TABLE 5.3

It is difficult to establish the presence of a g-shift at low measurement temperatures due to the lack of a suitable reference. Sample G 4 has a line width of order 1 gauss at 4.2K and strips of fibre were mounted between cellotape and placed on top of each other so that the fibre axis in alternate layers were perpendicular. ESR measurements were made at 4.2K and it was found that with the magnetic field perpendicular to the sample a symmetrical line was obtained, however, with the magnetic field in the mixed parallel and perpendicular orientation a distorted line shape was observed.

At 77K a g-shift was readily established using the Mn^{2+} reference.

We note from table 5.3 that both $g_{\parallel}$ and $g_{\perp}$ tend to decrease with increasing HTT.

5.8 The spin-lattice relaxation times

The amplitude of the absorption signal is proportional to the instantaneous population difference between the two spin levels. The spin-lattice relaxation time can be measured either by the pulse method or the saturation method.

In the pulse method the transition is saturated with short calibrated pulses of very high, resonant, microwave power and a low power continuous microwave sensing signal is used to monitor the recovery of the population difference to their equilibrium values.

In the continuous wave saturation method[6] relatively high microwave powers are fed onto the sample to saturate the transition.

For the saturation method the experimental procedure consists in searching for the power level at which the signal level is a maximum. The spin-lattice relaxation time may then be calculated from changes in the signal amplitude, or line width, near the saturation value; the method

yields the value of the product T_1T_2.

The determination of T_1 requires that Bloch's equations hold (Section 2.7) and that the spin interactions be homogeneous, enabling the spin-spin relaxation time T_2 to be related to the line width recorded at low power, viz

$$T_2 = \frac{2}{\sqrt{3}\gamma\Delta H_{p-p}} \qquad 5.1$$

$$T_2 = (1{\cdot}52 \times 10^7 \Delta H_{p-p})^{-1} \text{ sec} \qquad 5.2$$

ΔH_{p-p} is the peak to peak line width in gauss.

Although the line width obtained at low power is independent of the power, above saturation the line width increases and the signal amplitude decreases with increasing power.

In section 2.7 we introduced, via the Bloch equations, the saturation term $H_1^2 \gamma^2 T_1 T_2$. At low microwave powers i.e. off saturation, this term tends to zero. More usually the effects of saturation are considered by use of the saturation factor S.

$$S = \frac{1}{1 + \gamma^2 H_1^2 T_1 T_2} \qquad 5.3$$

By expressing the equation for the first derivative signal amplitude in terms of S, it can be shown[76] that the maximum of the first derivative peak to peak amplitude with respect to the power level occurs when

$$S = {}^2/_3 \qquad 5.4$$

$$\text{so that} \quad \gamma^2 H_1^2 T_1 T_2 = \tfrac{1}{2} \qquad 5.5$$

$2H_1$ is the amplitude of the r.f. magnetic field for which the signal amplitude is a maximum and thus H_1^2 is directly proportional to the

SATURATION BEHAVIOUR

– IN VACUUM

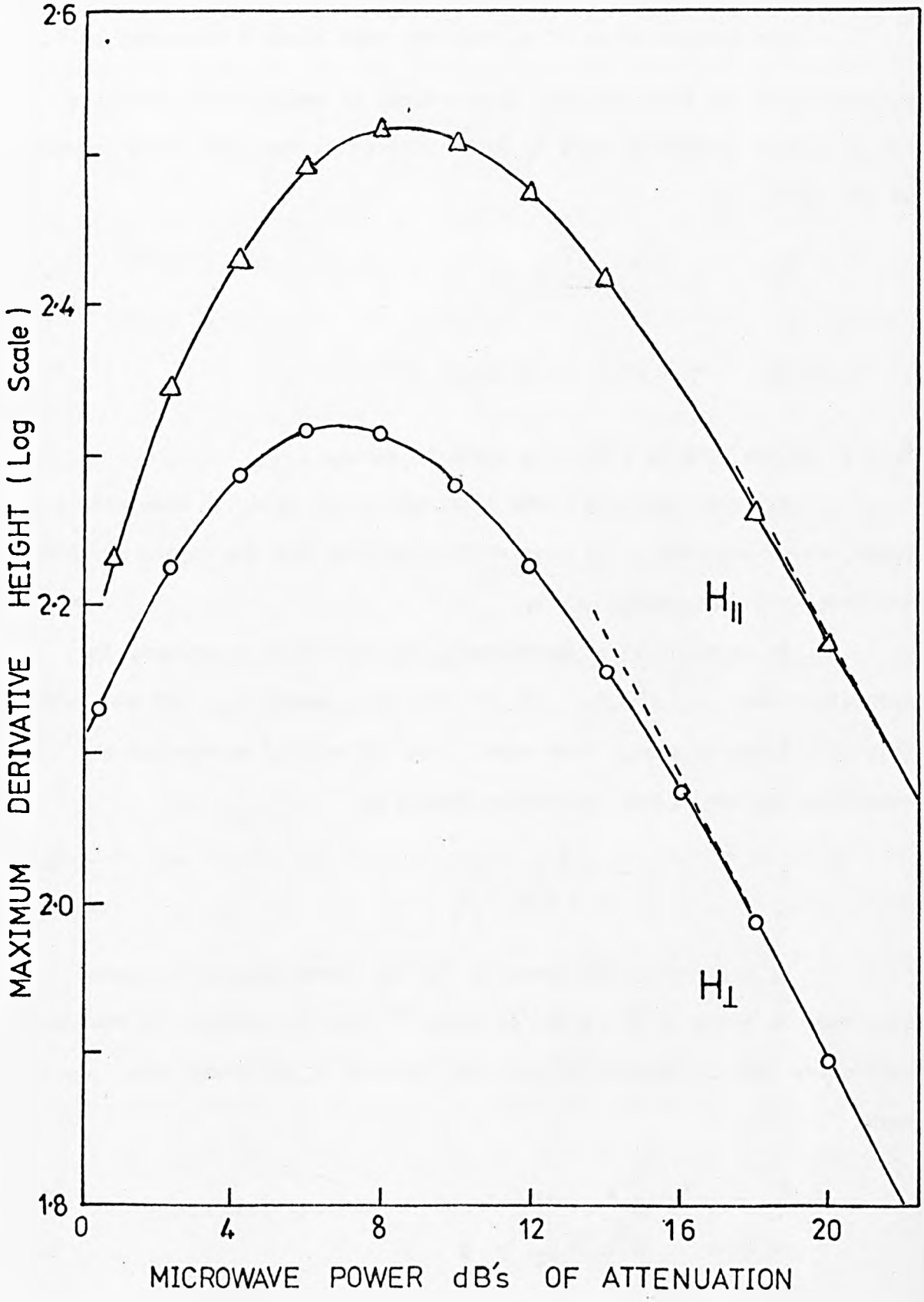

FIGURE 5.6

SATURATION BEHAVIOUR

– IN AIR

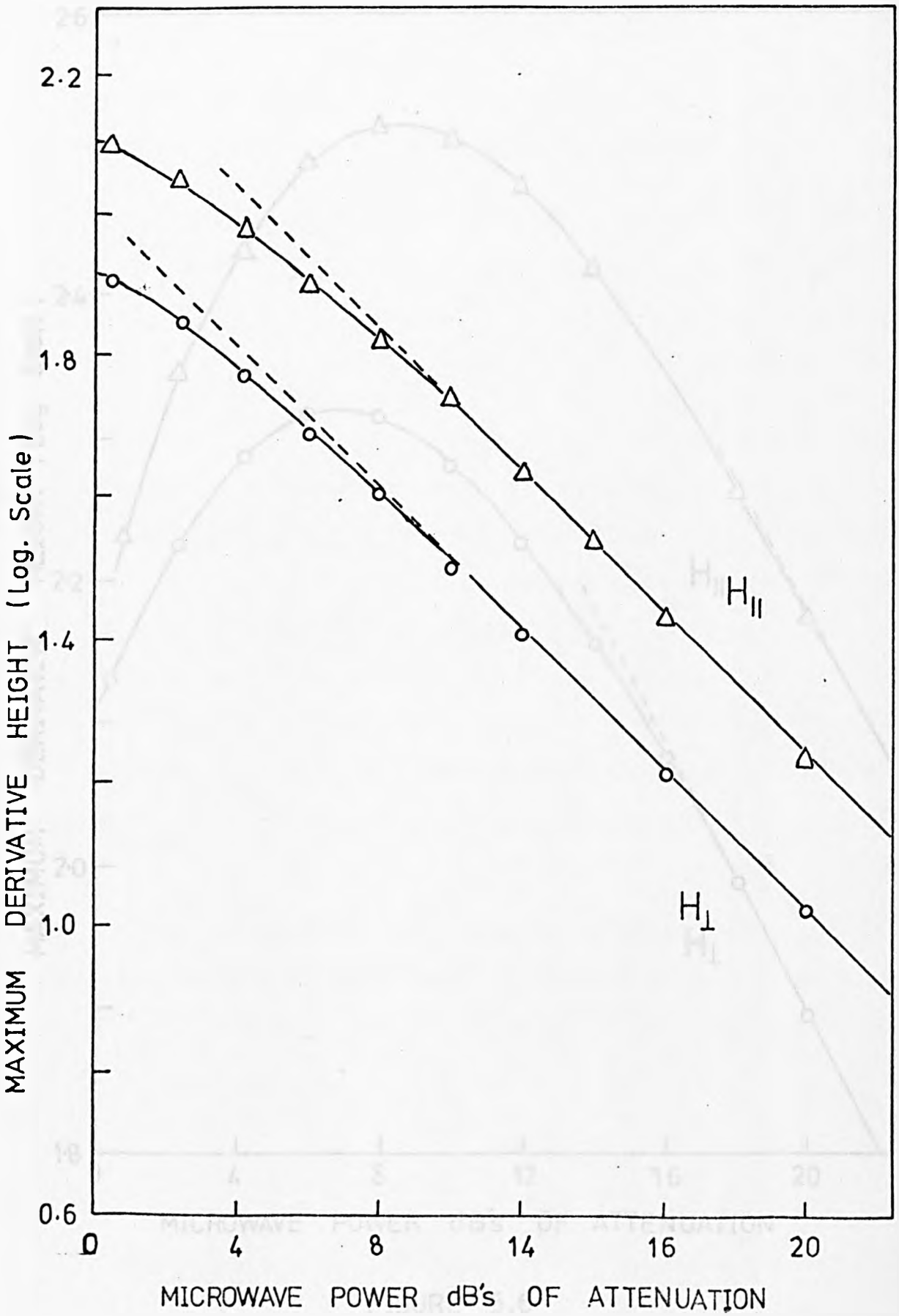

FIGURE 5.7

microwave power.

In practice rather than determining H_1^2 absolutely a comparative method is used, and the following equation holds

$$T_1 = \frac{(H_1^\circ)^2 \Delta H}{(H_1)\,\Delta H^\circ} T_1^\circ \qquad 5.6$$

where H_1°, ΔH° and T_1° refer to the standard.

The tetracene positive ion was used as a primary standard and the manganese reference was mounted with the fibre as a secondary standard. At room temperature the spin-lattice relaxation time for manganese was estimated to be 9.6×10^{-6} secs, assuming the value of the tetracene positive ion to be 7×10^{-6} sec (76).

Plots of the signal height against the microwave power for sample G 6 are shown in Fig's. 5.6 and 5.7, and again anisotropy in the behaviour is observed. In the absence of saturation, a plot of the signal height, (log scale) against the microwave power (dB) is expected to be linear with a slope of 0.05. When saturation occurs deviations from linearity arise, and the signal height goes through a maximum before decreasing.

The manganese resonance reached a maximum height at 15dB $\pm$ 1.0 dB of microwave power attenuation and had an unsaturated line width of 0.95 gauss. With the magnetic field perpendicular to the fibre axis the signal maximum occurred at 7.0 $\pm$ 0.5 dB of attenuation, and with the field parallel to the fibre axis at 8.8 $\pm$ 0.5 dB. Using unsaturated line widths of 0.90 and 0.71 gauss respectively (measured from the slope of the line shape plot) we obtained $T_1(\perp) = 1.4 \times 10^{-6}$ sec and $T_1(\parallel) = 1.63 \times 10^{-6}$ sec. Thus although the saturation behaviour is anisotropic the relaxation time appears to be isotropic and has a value for this fibre in vacuum of $\sim 1.5 \times 10^{-6}$ sec.

When the fibre is examined in air the only evidence of saturation is a small deviation from linearity at the highest microwave powers (See Fig. 5.7). Clearly, however, the presence of air shortens the relaxation time, for if this were not the case then a T_1 of 1.5×10^{-6} sec. together with a line width of ~ 2 gauss would give a maximum in signal height at ~ 4dB of microwave power attenuation. A very rough estimate suggests that T_1 is decreased to ~ 1.5×10^{-7} sec. in the presence of air.

The pulsing method requires a degree of sophistication, the apparatus was set up for use on a Varian Superheterodyne spectrometer employing a reflection cavity, a.f. (400 Hz) magnetic field modulation and detection at 30 MHz.

In order that the frequency of the saturating pulse be at the resonant frequency a low power - several milliwatt - signal from the signal klystron was passed through a GEC TWX8 travelling wave tube giving 30dB gain when on - with a maximum power output of 1 watt - and 60dB attenuation when off.

The travelling wave tube triggered by a pulse generator which could give between 1 and 100 pulses/sec each pulse width being variable between 20 μsec and 1.8 millsec.

Each pulse must be of sufficient power to saturate the transition i.e. to equalise the population difference between the two levels. A low power microwave signal was used to monitor the recovery to the equilibrium population values. The recovery from saturation was exponential and this was compared directly on the oscilloscope screen with an exponential waveform obtained from an exponential generator triggered by the same pulse generator that operated the travelling wave tube. The method was to fit the exponentially generated waveform to that of the experimental curve

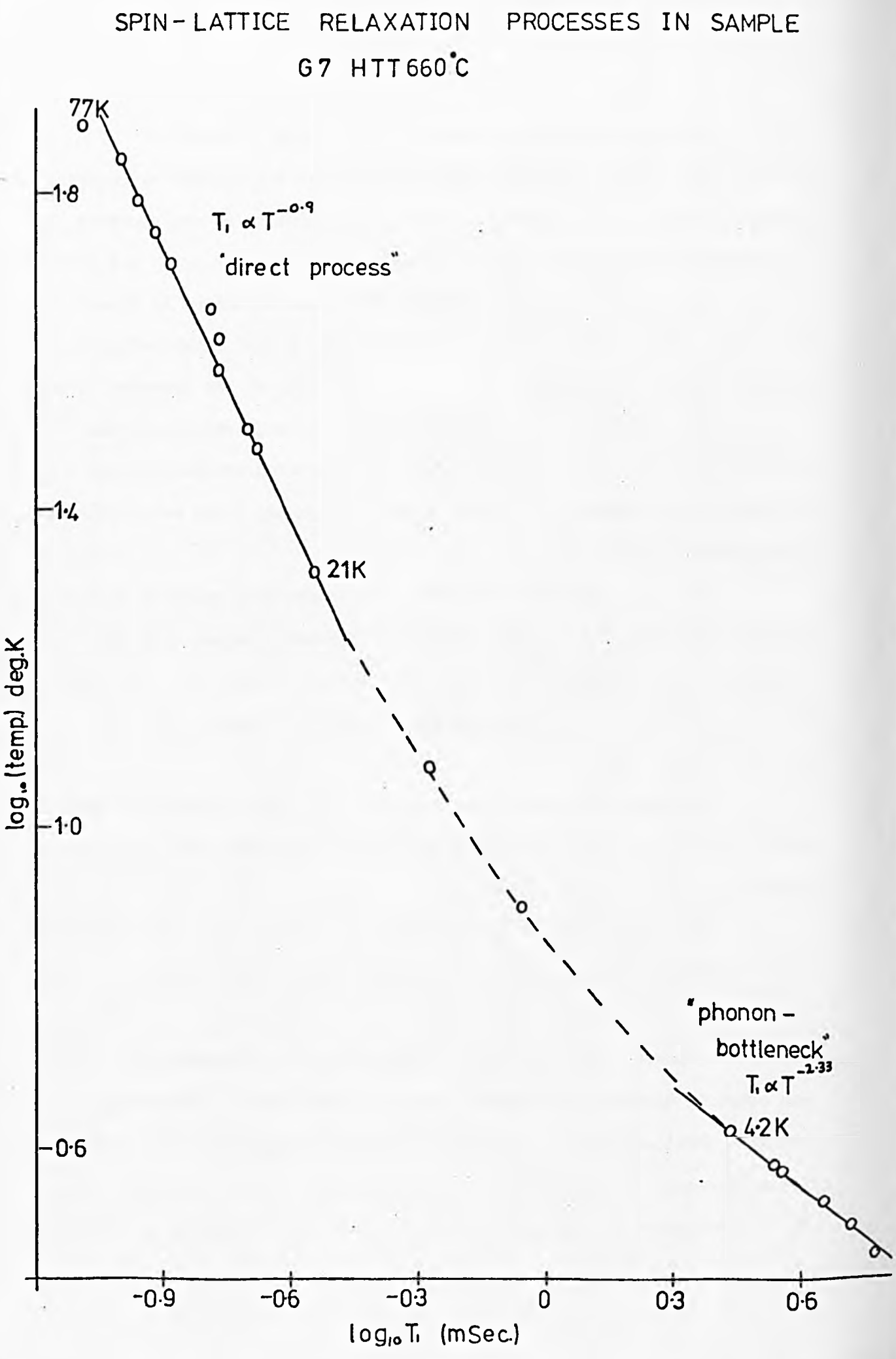
SPIN - LATTICE RELAXATION PROCESSES IN SAMPLE
G 7 HTT 660°C
77K
1·8
1·4
1·0
0·6
$T_1 \propto T^{-0.9}$
"direct process"
21K
"phonon - bottleneck"
$T_1 \propto T^{-2.33}$
4·2K
log₁₀ (temp.) deg.K
-0·9
-0·6
-0·3
0
0·3
0·6
$\log_{10} T_1$ (mSec.)

FIGURE 5.8

SPIN-LATTICE RELAXATION PROCESSES

IN SAMPLE G6 HTT 710°C

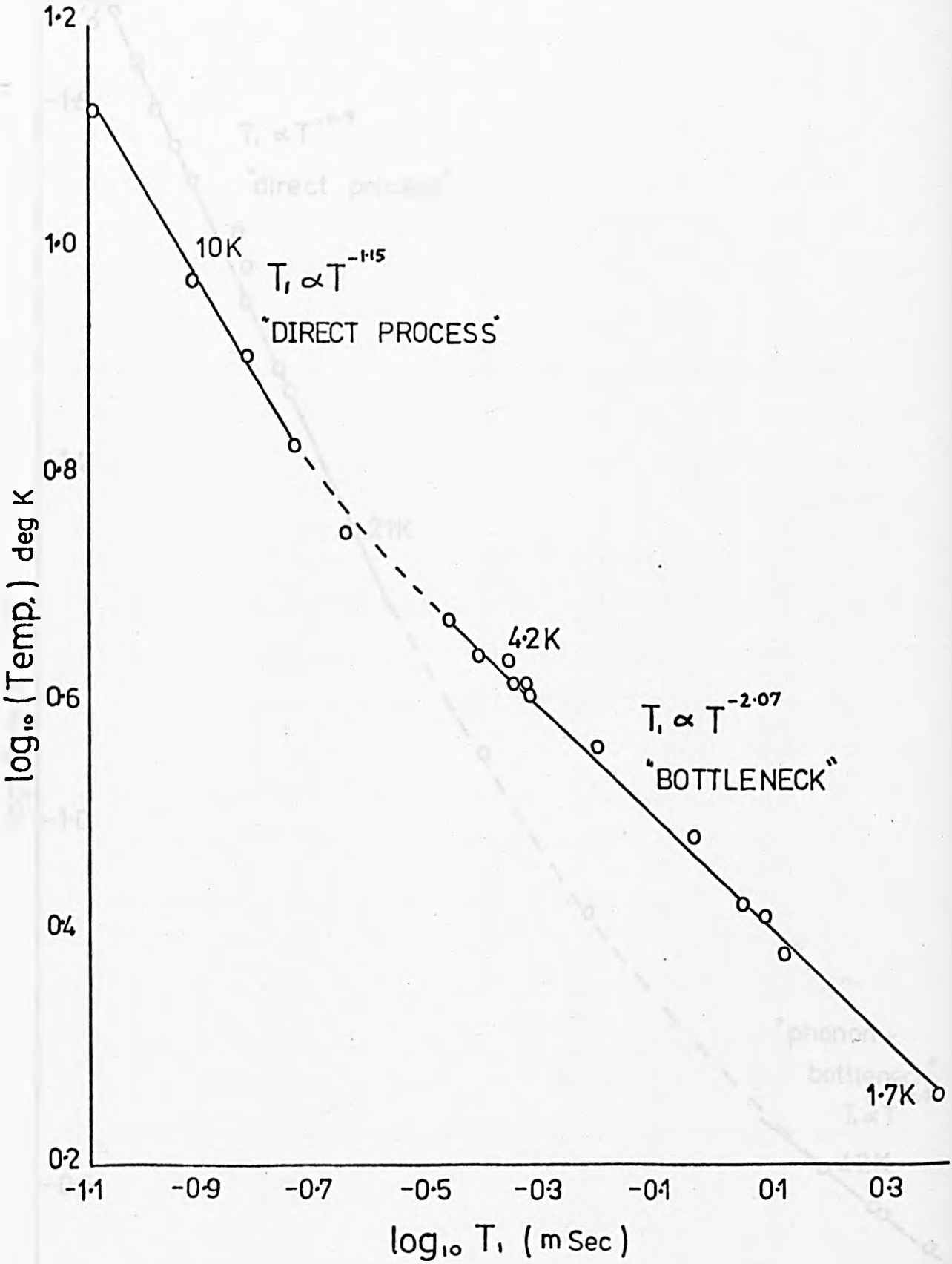

FIGURE 5.9

At 77K the pulse saturated spin-lattice relaxation time for G 7 measured $T_1 \approx 0.08$ m sec. CW saturation results at 77K showed that the signal amplitude peaked at 14.8dB power attenuation with an unsaturated line width of 3.5 gauss, and in comparison the Mn^{2+} signal peaked at 30dB power attenuation with an unchanged line width of 0.95 gauss. This data gives a spin-lattice relaxation time of $T_1 \approx 7.3 \times 10^{-4}$sec for Mn at liquid nitrogen.

Sample G 6, however, with the magnetic field perpendicular to the fibre axis, power saturated at 11dB power attenuation at 77K and had an unsaturated line width of some 2.3 gauss giving $T_1(\perp) = 1.87 \times 10^{-5}$sec. At 300K, however, the spin lattice relaxation time for the evacuated sample was found to be $T_1 \approx 1.5 \times 10^{-6}$sec. If we assume that over this temperature range, 77 - 300K, the relaxation process is of the form $T_1 \propto T^{-n}$ we obtain the value $n = 1.9$.

The pulse saturation results of Fig. 5.9 indicate that at 10K the spin lattice relaxation time is 1.15×10^{-4}sec and if we again assume that over the temperature range 77 - 10K the relaxation process is of the form $T_1 \propto T^{-n}$, then $n = 0.9$. These results indicate that as for sample G 7 the direct process extends to liquid nitrogen temperature above which the rate appears to proceed at T^{-2}.

5.9 Discussion of the ESR and spin-lattice relaxation results.

Fig. 5.3 indicates the fit obtained assuming a synthesized powder spectrum with g-values as shown. This computer synthesis although agreeing with the overall features of the observed spectrum, is obviously lacking in exactness. Furthermore, the fit is obtained using a Gaussian line shape function which is in sharp contrast with the Lorentzian line shape spectra observed in low temperature air treated chars. The computed spectrum

obtained using a Lorentzian line shape function provided a poor fit. The results indicate $g_{\parallel} = 2.0062$ and $g_{\perp} = 2.0033$ which represents a g shift (Δg) of order 0.0029 which is somewhat bigger than the g shift observed in samples such as G 6 (HTT 710°C). (See Fig. 5.5). It would seem probable therefore that the structure observed in these chars is due to either unresolved hyperfine splitting or to two different free spin species.

It is evident that over the narrow HTT range 660°C to 830°C air has a physical reversible effect on certain of the ESR parameters. The line broadening observed is thought to arise as a result of collision broadening - oxygen molecules in the surface of the carbon have sufficient mobility to produce a distortion in the unpaired electrons orbitals. These interactions reduce the lifetime in the excited state by spreading out the energy levels. The overall effect of which would be to produce a shortening of the spin-lattice relaxation time. The results for carbon G 6 HTT 710°C, which has a T_1 when evacuated of order 1.5×10^{-6} sec and a T_1 in air of order 1.5×10^{-7} sec, clearly confirm this proposition in full agreement with Singer's results[54] for charred sucrose.

On lowering the measurement temperature the number of 'collisions' will fall as the mobility of the oxygen molecules is lessened and a narrowing of the ESR line would be expected. In keeping with these ideas we observe that the line width obtained at 77K for sample G 6 HTT 710°C is nominally the same whether or not the sample had been evacuated at room temperature.

The mechanism by which air affects the ESR parameters would appear to be one of spin-lattice interaction, that the integrated intensity is unaffected by air lends further support for this proposition.

Line shape analysis also gives a good indication as to whether the oxygen has been homogeneously absorbed. In our samples the lines were of Lorentzian shape to at least five line widths irrespective of whether the fibres were evacuated.

Previous reported work[55,57] in the carbon field has established that the low temperature chars are inhomogeneously broadened. Consistent with this observation the spectra obtained from our low heat treatment Courtelle chars have a line width ~ 5 gauss, which up to 560°C appears to be independent of the heat treatment temperature and hence is independent of the increasing spin concentration.

The increased line width observed on recording the spectra at Q band, provides a direct confirmation that g anisotropy broadening is at least partly responsible for the observed line width.

Samples heat treated in the range 660°C to 760°C give, on evacuating, Lorentzian lines of width ~1 gauss. Above 760°C line broadening is initiated giving a line width of 36 gauss at 1,000°C.

The narrowing which occurs in carbon has long been established as being a result of exchange interaction between like spins.[60,61]

The nature and origin of the free spin species in carbon has been difficult to establish. Ingram[77] proposed that the free spins may be π electrons, formed during carbonization by bond scission or by removal of edge groups. These electrons are then stabilized in aromatic fragments. The suggestion is consistent with a number of observations: the condensation of aromatic fragments will increase with increasing heat treatment temperature resulting in an increased exchange interaction and line narrowing, further since the number of layer planes will be limited the concentration of unpaired spins will be expected to have a maximum.

The low chemical reactivity of the carbons is also in accord with the π electron proposition.

If the development of the aromatic layers could be hindered the effects would be reflected in those ESR properties which depend upon the extent of the aromaticity.[78]

Pastor and Hoskins[55] prepared two series of charred dextrose, one of which had been entirely inert treated while the other had been given a preoxidation stage. They found that the preoxidized char tended to resist aromatization during further inert heat treatment. In agreement with this observation they found that exchange narrowing occurred at a somewhat higher heat treatment temperature in the preoxidized sample.

It is now well established that conjugated ring type structures are formed during the pyrolysis of polyacrylonitrile (See section 3.2). There is no evidence to suggest that preoxidation hinders the development of such ring structures. However, preoxidation is usually terminated by 300°C and it is worthwhile examining in detail the properties of the chars to ascertain the effect of the excessive preoxidation stage given to our fibres.

Assabghy[50] carried out a series of experiments on Courtelle chars initially preoxidized at 300°C and an interesting comparison can be made between the properties of G 1 and those of his sample which had been carbonized at 1,000°C (A1). The respective spin concentrations for G 1 and A 1 are 1.7×10^{20} and 1.0×10^{20} spin gm^{-1}. However, Fig. 5.4 shows that the spin concentration in the 'G' series is rapidly increasing at 1,000°C while the results of Assabghy show that the spin concentration is rapidly decreasing above 1,000°C.

Assabghy's results predict that the maximum spin concentration

occurs below HTT 1,000°C which is consistent with previous observations in the carbon field[54] - the maximum spin concentration generally occurring in the exchange narrowed region. Our results are clearly at variance with these observations.

We reported in section 5.5 that the spin concentration obeyed a Curie Temperature dependence for the chars heat treated up to 760°C, however, above this temperature departures were noted. Mrozowski and others (See section 3.4) have interpreted this behaviour as arising from a sum of contributions from Curie and Pauli spin species. The former being associated with the localized centres observed in the low temperature chars, while the latter arises from delocalized spin centres associated with conduction electrons. These conductivity observations provide further support for the π electron hypothesis.

Using Mrozowski's analysis (section 3.4) we find that the percentage of conduction carriers in sample G 1 at room temperature measures only 40% while for sample A 1 it measures 80%.

Carbons prepared by heat treatment to temperatures up to 600°C have extremely high resistivities exceeding $10^{7}\Omega$ - cm at 600°C. Beyond this temperature the resistivity falls sharply, levelling off at 1,000°C to take the value $10^{-2}\Omega$ - cm. (See Fig. 3.4) Mrozowski suggested that in the region 500 - 800°C these carbons are intrinsic semiconductors. Dehydrogenation and imperfect layer formation creates 'σ' valencies that act as electron traps creating holes in the valence band. Further heat treatment increases the concentration of traps and this is reflected by a sharp fall in the thermoelectric power and the resistivity. The sharp fall in the spin concentration in this region has provided support for this model. However, although our samples show a fall in both the thermoelectric power and the resistivity in the region 800 - 1,000°C (see next chapter) this is

accompanied by a continuous increase in spin concentration. Singer and Cherry's[79] experiments on charred acenaphthylene show that the flakes exhibit appreciable conductivity in the exchange narrowed region. These results indicate that Mrozowski's interpretation needs to be reconsidered especially as his band model is suspect in view of the non-periodic nature of the lattice. Evidence has now been obtained to show that over this region the carbons behave as disordered materials for which the conduction process is by electron 'hopping' from localized sites (see next chapter).

We can compare the respective room temperature resistivity measurements for samples G 1 and A 1 : 0.0039 Ω - cms and 0.00003 Ω - cm. The resistivity ratio ρ_{77K}/ρ_{300K} falls sharply over the range 800°C - 1,000°C having the value 1.387 for sample G 1 while for A 1 it measured ~ 1.24.

The modulus of carbon fibres provides a good indication of the crystallite order within the fibres, both of the properties increase with increasing heat treatment temperature. The tensile strength, however, passes through a maximum at around HTT 1500°C. For sample G 1 the modulus measured 151 $\pm$ 6 GNm^{-2} with a breaking strength of 1.28 $\pm$ 0.05 GNm^{-2} which compare unfavourably with those obtained by preoxidizing at 220°C before carbonizing at 1,000°C: modulus ~ 245 GNm^{-2} and a breaking stress ~1.7 GNm^{-2}.

The properties measured provide strong evidence that the overall development of the fibre has been inhibited. Marsh and Wynne-Jones[80] prepared a laboratory specimen of polyvinylcyanide from which a series of carbons were obtained by heat treatment in a nitrogen atmosphere. Jackson and Wynne-Jones[78] measured the line width and spin concentration for the carbon series. The maximum spin concentration measured 1.5 x 10^{20} spin gm^{-1}

corresponding to a line width ~0.8 gauss and occurred at a heat treatment temperature of 740°C.

These results are consistent with the observation that excessive preoxidation hinders both crystallite and layer plane development.

The maximum heat treatment temperature to which the carbon fibre is subjected would appear to give an unreliable indication of its properties, this is because the history of the charring process is also of significance in determining the final carbon. These observations are in complete accord with our previous publication[49] where the resistivity ratio was found to give an effective indication of the relative graphitic order within the samples.

The Q band ESR measurements show that g anisotropy broadening contributes to the observed line width. The effect appears to be most significant in the region of minimum line width HTT 660°C to 760°C.

Although the exchange interaction is sufficient to render dipolar interactions incoherent and produce lines of width ~ 1 gauss, the results indicate that the exchange interaction is not strong. Line broadening is observed as the measurement temperature is lowered, thus providing part of the evidence of a weak exchange interaction. Since the spin concentration increases with increasing heat treatment temperature, we should expect a corresponding increase in the exchange integral J. This proposition finds support from a reduction in the amount of line broadening at 4.2 K as the heat treatment temperature increases from 660°C to 760°C.

If the exchange interaction is strong we expect the spin-lattice and the spin-spin relaxation times to become equal $T_1 \approx T_2$, and that both should become independent of the measurement temperature (See section 2.12). It has been shown for DPPH[81] that $T_1 = T_2 = 6.3 \times 10^{-8}$ sec and for a sucrose sample heat treated to 560°C Hoskins and Pastor[61] using CW

saturation techniques showed that $T_1 \approx T_2 \approx 2 \times 10^{-7}$ sec and that both T_1 and T_2 were temperature independent. For sample G 6 and G 7 we see that $T_1 > T_2$, and that T_1 is not independent of the measurement temperature, (See section 5.8) indicating that the exchange interaction is weak. It should be pointed out, however, that T_2 has been estimated from the width of inhomogeneously broadened line.

Above 760°C line broadening is initiated and measures 36 G at HTT 1,000°C.

If we assume that the spin-lattice relaxation time is a major parameter in determining the line width, then uncertainty broadened[82] lines of width 1 gauss to 40 gauss would correspond to a shortening of the spin-lattice relaxation time from 6×10^{-8} sec to 2×10^{-9} sec. Consistent with this proposition the spin-lattice relaxation time is observed to shorten with increasing heat treatment temperature for samples heat treated above 660°C. Sample G 5 (HTT 760°C) has a value for T_1 less than 10^{-7} sec and could not be measured by the available pulse apparatus, neither could it be saturated with the available microwave power.

There are various mechanisms, apart from increased exchange interaction, by which the spin-lattice relaxation times may be shortened. Ingram[83] suggested that the improved interaction of the spins with the lattice was brought about by the increase of charge carriers. However, Singer[54] proposed that the interaction of conduction electrons with impurities could produce a shortened T_1. Increased crystallinity, producing an increased density of lattice oscillators at the spin frequency, would also be effective in reducing the spin-lattice relaxation time. The strong narrowing as the measurement temperature is lowered is indicative of spin-lattice broadening.

It is interesting that the broadening observed with increasing heat treatment temperature is accompanied by an increase in conductivity. We have shown (See next chapter) that the conduction process is by electron hopping between localized sites beyond the nearest neighbour separation. The hopping through the trap like sites is thermally activated, and as the measurement temperature is lowered the conductivity decreases. This is accompanied by a decrease in the line width. The density of traps increases and the activation energy of 'hop' decreases with increasing heat treatment temperature, above 830°C. As a consequence the conductivity decreases by a smaller factor as the measurement temperature is lowered. Similarly Table 5.2 indicates that for the higher HTT samples the line width narrows by a reduced factor as the measurement temperature is lowered. It does appear that the conductivity and the line width show similar variations.

For samples G 6 and G 7, HTT'S 710°C and 660°C, we used a combination of CW and pulse relaxation methods to establish the spin-lattice relaxation processes over the temperature range 300 - 1.7K. Below 4.2K the relaxation process in both samples becomes phonon bottlenecked with the characteristic T^{-2} temperature dependence. Above 4.2K the direct process is observed to dominate with $T_1 \propto T^{-1}$. This is to be expected as a first order direct process would be far more likely to become phonon bottlenecked on lowering the measurement temperature, than a second order Raman process (See section 2.9). An obviously interesting feature of the relaxation results is the extension of the direct process up to liquid nitrogen temperatures without the appearance of the more likely Raman process. Although we have found evidence of anisotropy in the fibres the structure is that of a poorly crystalline material and this may account for the evidently poor thermal access between the spins and the reservoir.

Between 77K and 300K we find $T_1 \propto T^{-2}$ while below 77K the process is direct with $T_1 \propto T^{-1}$, indicating that the samples have a low Debye temperature[84]. It would appear that the resonant spins may utilise a rather limited phonon spectrum in coupling with the lattice. Hence, it is the direct and not the more favourable Raman process that is seen to dominate above 4.2K. If these observations are correctly interpreted the spin-lattice relaxation process should be more efficient as the heat treatment temperature is increased i.e., as the fibre develops a more definite crystalline structure. The spin-lattice relaxation time is observed to shorten with increasing heat treatment temperature, although as we have already discussed there are several possible interpretations to explain this behaviour. These arguments could have been further developed had we been able to establish the spin-lattice relaxation process in the higher heat treatment temperature samples. G 4 HTT 830°C shows evidence of increased exchange interaction having a line width at 4.2K $\sim$ 1 gauss. This sample shows less evidence of inhomogeneous broadening, and might have provided valuable information had we been able to establish its spin-lattice relaxation process.

The existence of ESR g-value anisotropy in fibres processed above 1750°C has now become well established through the work at Keele[46]. This anisotropy is similar in nature to that found in single crystals of graphite and is the result of the preferential orientation of crystallites with their basal planes aligned along the fibre axis. The anisotropy depends sensitively on the interlayer interaction, and as a consequence $g_\perp$ (magnetic field H perpendicular to the fibre axis) is considerably greater than $g_\parallel$ (H parallel to the fibre axis). Typical values are $g_\parallel \sim 2.0026$ and $g_\perp \sim 2.0100$ giving a g-value anisotropy $(g_\perp - g_\parallel)$ of the order $+ 75 \times 10^{-4}$.

While the existence of g-value anisotropy in the resonance of high temperature carbonaceous materials is fairly well known, there are very

few references in the literature to the detection of any g-anisotropy in carbonaceous chars prepared at low heat temperatures. The most recent and detailed of these is due to Singer and Cherry[79]. Small individual flakes of acenaphthylene coke heat treated to 700°C were subjected to a detailed study. The carbon exhibited a sharp symmetrical ESR line, and because the line width was very narrow ($\sim$ 0.12 Gauss) the g-value could be measured very accurately. The g-value with the magnetic field parallel to the c-axis of the flake measured 2.002368 $\pm$ 0.000003 while with the field perpendicular to the c-axis it measured 2.002743 $\pm$ 0.000002. The g-shift was reported to be independent of the measurement temperature between 100 and 300K and it should be noted that the anisotropy is opposite in sign to that observed in single crystal graphite. It is also smaller in magnitude than the anisotropy in high heat treatment temperature fibres by at least an order of magnitude.

As we see from the results contained in Table 5.3 we have unambiguously shown that a similar anisotropy exists in the Courtelle fibres heat treated to less than 1,000°C.

The fibre G 7 HTT 710°C exhibits a sharp symmetrical resonance $\sim$ 0.8 gauss width which is clearly anisotropic with $g_{\parallel}$ = 2.00315 and $g_{\perp}$ = 2.00285 where $\parallel$ and $\perp$ denote the orientations of the magnetic field with respect to the fibre axis. The resonance is symmetrical and as Figure 5.5 illustrates the shift in position on rotation of the magnetic field about the fibre axis is somewhat greater than the line width. In agreement with Singer and Cherry's observations the anisotropy is of opposite sign to that observed in high heat treatment temperature fibres and the results would appear to indicate a preferential orientation of hexagonal layer planes parallel to the fibre axis. This g-anisotropy appears to be unaffected by

the presence of air.

McConnell and Robertson[85] have proposed a qualitative theory of g-values in aromatic radicals which has been shown to fit a wealth of experimental results. For free radicals the g-factors differ only marginally $< 0.05\%$ from that of the free spin value. Although these shifts are small it has been possible to measure, quite accurately, the anisotropy in g-factor for planar radicals. The theory predicts that spin orbit coupling causes mixing of excited states with the ground state, reintroducing some orbital angular momentum. The g-shift is proportional to the spin orbit coupling constant λ, divided by the energy separation between the ground and excited state.

For an axially symmetric planar radical it is suggested that the g-value with the magnetic field parallel to the plane $g_{\|}$ is reduced by $\frac{2\lambda}{\Delta}$, where λ is the $2p$ spin orbit coupling constant for carbon and Δ is the energy separation between the π orbital ground state and the antibonding excited state. However, $g_{\|}$ is increased by $\frac{2\lambda}{\delta}$ for the excitation of the σ bonding electron to the π orbital state, of energy separation δ, and the overall effect is to increase $g_{\|}$ providing $\Delta > \delta$. In contrast contributions to $g_{\perp}$ can only be made by minor transitions such as σ bonding $- \sigma$ antibonding and $g_{\perp}$ remains quite close to the fine spin value.

That we observe similar g-shifts in our fibres would tend to confirm that unpaired electrons are localized on carbon atoms which are themselves associated with planar molecules. This proposition is in accord with the known development of conjugated ring structures (See section 3.2).

The effect of crystallite misorientation upon the values of $g_{\|}$ and $g_{\perp}$ observed experimentally for the high HTT fibres has already been

considered by Assabghy et al.[50] This work has shown that

$$g_{\parallel} = g_1 + A\langle \sin^2\phi \rangle$$

$$g_{\perp} = g_1 + \frac{A}{2}\left(1 - \langle \sin^2\phi \rangle\right)$$

where $A = g_3 - g_1$ and $g_1 = g_2 \neq g_3$ are the principal g-tensors of the crystallite. $\langle \sin^2\phi \rangle$ is an average over all possible values of ϕ, where ϕ is the angle between a layer plane and the fibre axis.

For sample G 7 we have $g_{\parallel} = 2.00315$ and $g_{\perp} = 2.00285$ and if we assume that $g_3 = 2.00230$ then we find that

$$g_1 = 2.00328$$

$$A = -0.00098$$

$$g_3 = 2.00230$$

$$\langle \sin^2 \phi \rangle = 0.133$$

These arguments suggest that the planes show a considerable misorientation with respect to the fibre axis and have a misorientation parameter $Z = \langle \phi \rangle \sim 21^{\circ}$. The anisotropy A observed in this fibre is more than twice that observed by Singer and Cherry for the acenaphthylene coke. This increase in anisotropy could well arise through increased spin orbit interaction; the fibre will have oxygen and nitrogen in its structure and while carbon has a spin orbit coupling parameter λ of 28 cm^{-1} that for oxygen is 152 cm^{-1} and nitrogen 70 cm^{-1}.

The anisotropy in line width is interesting and appears to be most significant in the region of narrowed line widths. The line is broader with the magnetic field perpendicular to the fibre axis and this is to be expected as one would be observing a superposition of lines varying between g_1 and g_3 giving rise to an inhomogeneously broadened line. With the

magnetic field parallel to the axis, however, the fibre would have a g value $\sim g_{\parallel}$. In accord with the above observations the line width measurements at Q band frequencies show an increased broadening in the perpendicular orientation, rather more so than in the parallel orientation.

CHAPTER 6

THE ELECTRONIC PROPERTIES.

6.1 The conduction process in amorphous materials

The group have previously measured various transport properties including the resistivity ρ , the resistivity ratio ρ_{LN}/ρ_{RT} , the thermoelectric power TEP and the magnetoresistance $\Delta\rho/\rho_o$ for samples prepared by heat treating Courtelle fibre between 1,000°C and ~ 2,800°C. An interesting correlation was made between the electronic and ESR properties. While throwing new light on the carbon field the overall development of a number of the transport properties with increasing HTT can be adequately interpreted using Mrozowski's model (See section 3.3). However, it was proposed that below a HTT of 1750°C defects and stresses play an important role in determining the properties of the carbon, 1750°C is the temperature at which the carbon-carbon bond can be thermally broken allowing the structure to anneal removing any stresses. Assabghy(50) suggested that as Mrozowski's band overlap model would appear to fail below HTT 1750°C then any replacement model would necessarily have to take into account the amorphous region of these materials.

In 1967 Mott(86) carried out a most comprehensive review of the properties of electrons in disordered structures and a brief account of certain of the more pertinent ideas will be given. The theories themselves are based on a study of the localized states existing within the material. Localization can be brought about by fluctuations in the atomic separation producing an overlap of atomic orbitals. Disorder in ionic lattices may result in random potentials localizing the electrons in potential wells.

Localized behaviour can produce a low density of states in what might originally be thought a forbidden gap in semiconductors by extending the density of states curve at the top of the valence band and at the bottom of the conduction band. These localized states can effectively reduce the band gap thereby modifying the electronic properties of the material.

If the electron is to move between localized states for which the orbitals overlap, then providing the overlap is not sufficient to produce metallic conduction, the motion will take place by hopping or tunnelling, the necessary quanta being exchanged with the lattice by phonons.

Impurity band conduction in materials which are compensated can give rise to thermally activated hopping from centre to centre. Generally a certain proportion of donors in a compensated semiconductor will lose electrons to acceptors and electrons may tunnel to empty donors.

Hopping always involves an activation energy because each localized state has a discrete energy level associated with it. If the conduction process is derived entirely from localized behaviour the conductivity would be zero at absolute zero of temperature.

The temperature variation of the conductivity (σ) can yield valuable information about the energy band model in a solid. Typically for intrinsic semiconductors a plot of $\log_e \sigma$ against the reciprocal absolute temperature should give a straight line from which the band gap may be estimated. Mott[87] has considered in some detail the conductivity to be expected in the case of thermally activated hopping and a brief account will be given.

It is assumed that the Fermi level lies in the hopping region and that only electrons with energies $\sim$ KT below E_F have a significant hopping probability.

The jump frequency takes the form

$$J_f = \nu_{ph}\,\phi(R)\exp -\frac{W}{KT} \qquad 6.1$$

ν_{ph} is the phonon frequency and W is the hopping or thermal activation energy. The central term ϕ (R) is the tunnelling factor between overlapping nearest neighbour localized states separated by a distance R. If the wave function falls off as exp $(-\alpha r)$ then ϕ (R) will contain the factor $\exp(-2\alpha R)$. The final term is the Boltzman factor and is the probability of mounting the barrier at each attempt. If a is the lattice constant it is readily shown that the diffusivity can be related to the jump frequency by

$$\text{Diffusivity} = a^2 J_f = \nu_{ph}\,\phi(R)\,a^2 \exp -\frac{W}{KT} \qquad 6.2$$

giving a mobility $\mu = \dfrac{e\,\nu_{ph}\,\phi(R)\,a^2}{KT}\exp -\dfrac{W}{KT}$ 6.3

for electrons of $\sim$ KT below E_F the conductivity σ will be

$$\sigma = \frac{N(E_F)\,KT\,\phi(R)\,e^2a^2}{KT}\exp -\frac{W}{KT} \qquad 6.4$$

where $N(E_F)$ is the density of states at the Fermi level.

The conductivity takes the form

$$\sigma = A\exp -\left(2\alpha R + \frac{W}{KT}\right) \qquad 6.5$$

If the electron can hop a distance pR much greater than R i.e., $p \gg 1$ then the choice of accessible hopping sites will be increased by a factor p^3 There will be an increased probability of an electron finding a localized state of energy close to that from which the electron hopped. As a consequence we would expect the activation energy to be reduced to $\frac{W}{p^3}$.

The conductivity may be rewritten

$$\sigma = A\exp -\left(2\alpha pR + \frac{W}{p^3KT}\right) \qquad 6.6$$

This has a maximum, corresponding to a maximum hopping probability when $p^4 = \frac{3W}{2\alpha RKT}$ 6.7

and gives a conductivity of the form

$$\sigma = A \exp\left[-\text{constant}\,(\alpha R)^{3/4}\left(\frac{W}{KT}\right)^{1/4}\right] \qquad 6.8$$

so that for thermally activated hopping a plot of $\log_e \sigma$ versus $T^{-\frac{1}{4}}$ should give a straight line.

This conductivity behaviour for thermally activated hopping has now been substantiated by experiment and it has been possible for previously recorded observations to be reinterpreted according to this model c.f. the observations in amorphous germanium made by Walley and Jonscher[88] and their later interpretation by Mott[89].

It will be of interest to restrict this Mott model to 2 dimensions so that the localizations are contained within planes. By carrying out a similar analysis to that previously given we find the conductivity to be of the form

$$\sigma = C \exp - \frac{B}{T^{1/3}} \qquad 6.9$$

where B and C are constants

The evidence for hopping can therefore be obtained by monitoring the variation of the conductivity as the measurement temperature is varied.

It was suggested by Assabghy[50] that in order to account for the electronic properties observed for samples heat treated to less than 1750°C then the contribution from localized states would have to be considered. While agreeing with this observation it was considered that localized behaviour would more readily be identified, and hence evaluated, in samples heat treated to below 1,000°C. There is evidence that heat treatment produces some disorder in these samples. Bond rupture exposes free valencies

(dangling σ - bonds) which act as electron traps i.e., acceptors so that the electron would be expected to move by thermally activated hopping.

With these ideas in mind the temperature variation of the conductivity was investigated. Carbon fibre is a good thin film material a single strand having a diameter $\sim 10\mu m$. Measurement of the longitudinal resistance in fibres is not subject to interparticle contacts as would samples formed by evaporation of graphite rods and deposited on glass substrates. The techniques used in the measurement of the electronic properties have been well established by Assabghy[50].

6.2 Measurement of the conductivity at room temperature.

A carbon fibre filament was mounted on to a microscope slide parallel to the longest edge of the slide. The filament was secured in position by four contacts painted on to the fibre at its ends and at two points near to its ends. Colloidal silver paint was used and the contacts were extended to the edges of the slide where electrical contacts could be attached.

The resistance between the two central contacts was measured using the four probe technique employing a sensitive potentiometer. Sufficiently low currents were used to ensure the absence of Joule heating.

Microscope slides were selected as suitable mounts for the fibres since a travelling microscope was to be used to measure their length and diameter. The diameter measurements were made using a calibrated eyepiece. It was found necessary to make a number of determinations of the diameter at different points along the length of the fibre; the average value was then used to calculate the resistivity and hence the conductivity. It was necessary to make several determinations of the diameter since although the filaments are of circular cross section the cross sectional area is not

SAMPLE	RESISTIVITY (ρ) (Ω-cms) $\times 10^{-3}$	CONDUCTIVITY (σ) (Ω-cms) $\times 10^{2}$	RESISTIVITY RATIO ρ_{77K}/ρ_{RT}	$\rho_{4.2K}/\rho_{RT}$
G1	3·9	2·58	1·387	3·15
G2	9·94	1·00	2·485	172
G3	6·57×10	1·50×10	11·30	$\frac{\rho_{11.4K}}{\rho_{RT}} \sim 1.35\times10^{4}$
G4	$7·50\times10^{2}$	$1·33\times10^{-2}$	100·0	—
G5	$9·70\times10^{3}$	$1·03\times10^{-3}$	—	—
G6	$1·97\times10^{5}$	$5·08\times10^{-5}$	—	—
G7	$9·50\times10^{6}$	$1·05\times10^{-6}$	—	—

TABLE 6.1

constant over the entire length, thus introducing a 10% error in the conductivity measurement. Similarly conductivity determinations for filaments selected from within the same batch were reproducible only to within ± 10%.

6.3 The resistivity ratio $\frac{\rho_{LN}}{\rho_{RT}}$.

The resistivity ratio $\frac{\rho_{LN}}{\rho_{RT}}$ was calculated using the resistance values obtained at room temperatures and at liquid nitrogen. The resistance at 77K being obtained with the microscope slide immersed in liquid nitrogen. Clearly since this parameter does not involve any diameter measurements a small measurement error might be anticipated. Indeed the results were reproducible to within 1%. This readily measured parameter has been shown to give a good indication of the relative graphitic order within the fibres.

6.4 The resistivity ratio and conductivity results.

Table 6.1 contains the results of the measurement of the resistivity ρ , the conductivity σ and the resistivity ratio $\frac{\rho_{LN}}{\rho_{RT}}$ and $\frac{\rho_{4.2}}{\rho_{RT}}$. The resistivity decreases from a value of the order of $10^{7}\,\Omega$ - cm recorded at a HTT of 660°C to a value of order $0.0039\,\Omega$ - cm at a HTT of 1,000°C. The resistivity ratio $\frac{\rho_{77}}{\rho_{RT}}$ $\sim$ 100 for a HTT of 830°C and only $\sim$ 1.4 for a HTT of 1,000°C while the ratio $\frac{\rho_{11.4}}{\rho_{RT}}$ $\sim$ 13,000 for a HTT of 895°C and $\frac{\rho_{4.2}}{\rho_{RT}}$ $\sim$ 172 for a HTT of 960°C. These results tend to indicate an exponential temperature dependence of the resistivity with a decreasing activation energy as the heat treatment temperature increases. Mrozowski's school attributed the equivalent large fall of the resistivity in soft carbons, over the heat treatment temperature range 600°C - 1,000°C, to an increase in carrier concentration. Free valencies occur, partly as a result of the disorder, acting as electron traps creating holes in the valence band.

6.5 The variation of the conductivity with the measurement temperature.

This was established over the temperature range ~ 4.2K to 300K by monitoring the resistance. From Table 6.1 we observe that the resistivity of some of the samples is extremely large and is accompanied by a rapid increase as the measurement temperature is lowered. For sample G 1 the resistivity corresponds to a monofilament resistance somewhat greater than 20 KΩ. As a consequence small bundles of fibres were mounted and again the resistance was measured by the four probe technique.

The low temperature techniques discussed extensively in section 4.4 were used. The lowest measurement temperatures are achieved by immersing the samples in liquid helium contained within a cryostat, so that a more sophisticated mount was required. The final mount was similar to that used by Assabghy[50] to measure the magnetoresistance of carbon fibres. Eight samples were mounted and the whole experiment was repeated to provide a sufficient number of sample points.

The mount consisted of two strips of perspex each 2 mm thick, 2.5 cm width and 10 cms in length, which were glued in the form of a sandwich. The upper part of the mount was reduced in width ~ 1 cm, and was securely fastened into a stainless steel tube by which it could be lowered into the tail of the cryostat. The stainless steel tube passed through, and was soldered into, a brass plate which during the experiment was bolted to the top plate of the cryostat. The brass plate contained two ~ 1 cms diameter inlets which could be securely plugged. One contained a perspex plug through which the leads from two carbon resistors passed. The carbon resistors were used to monitor the temperature and were secured on the seam of the perspex mount using varnish suitable for low temperature work. The other inlet contained a brass plug which could be removed to allow

FIGURE

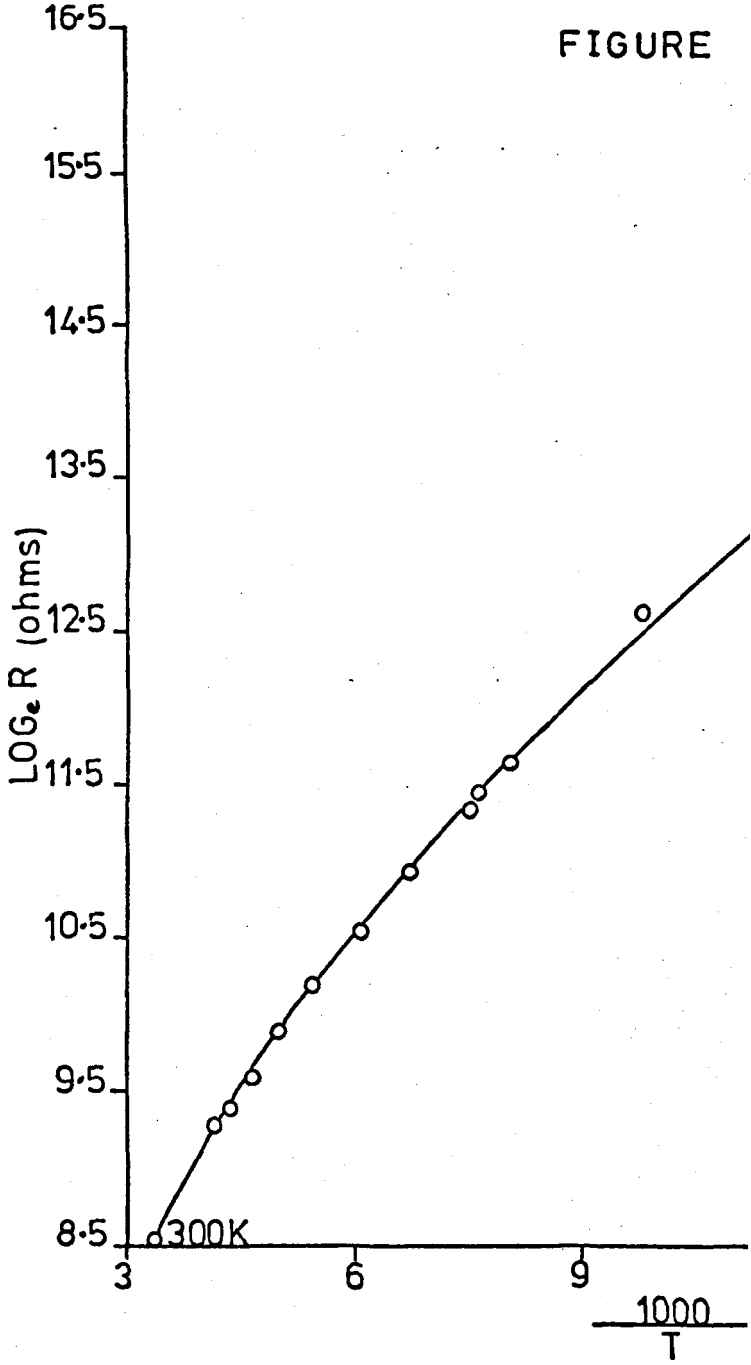

6.1

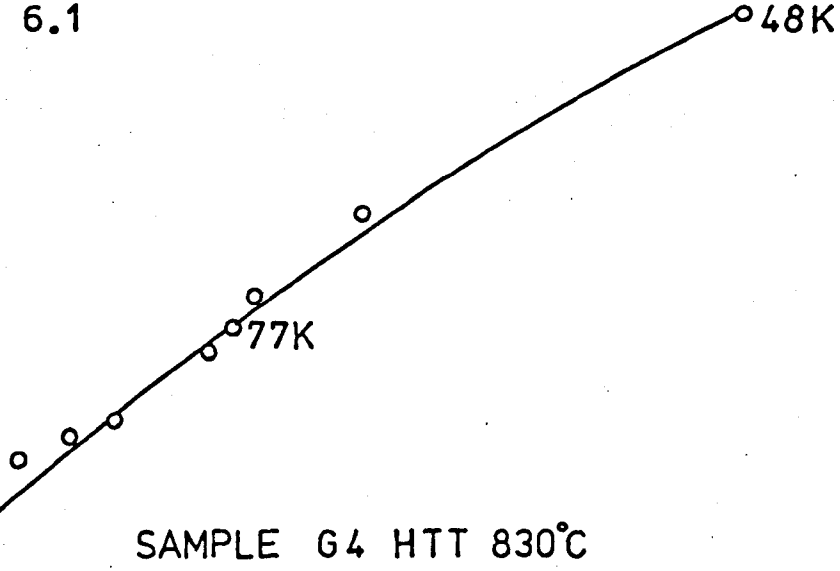

SAMPLE G4 HTT 830°C

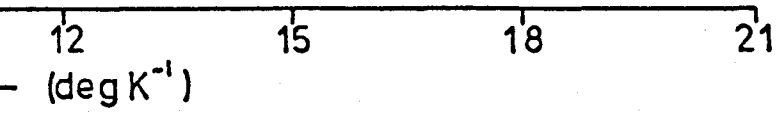

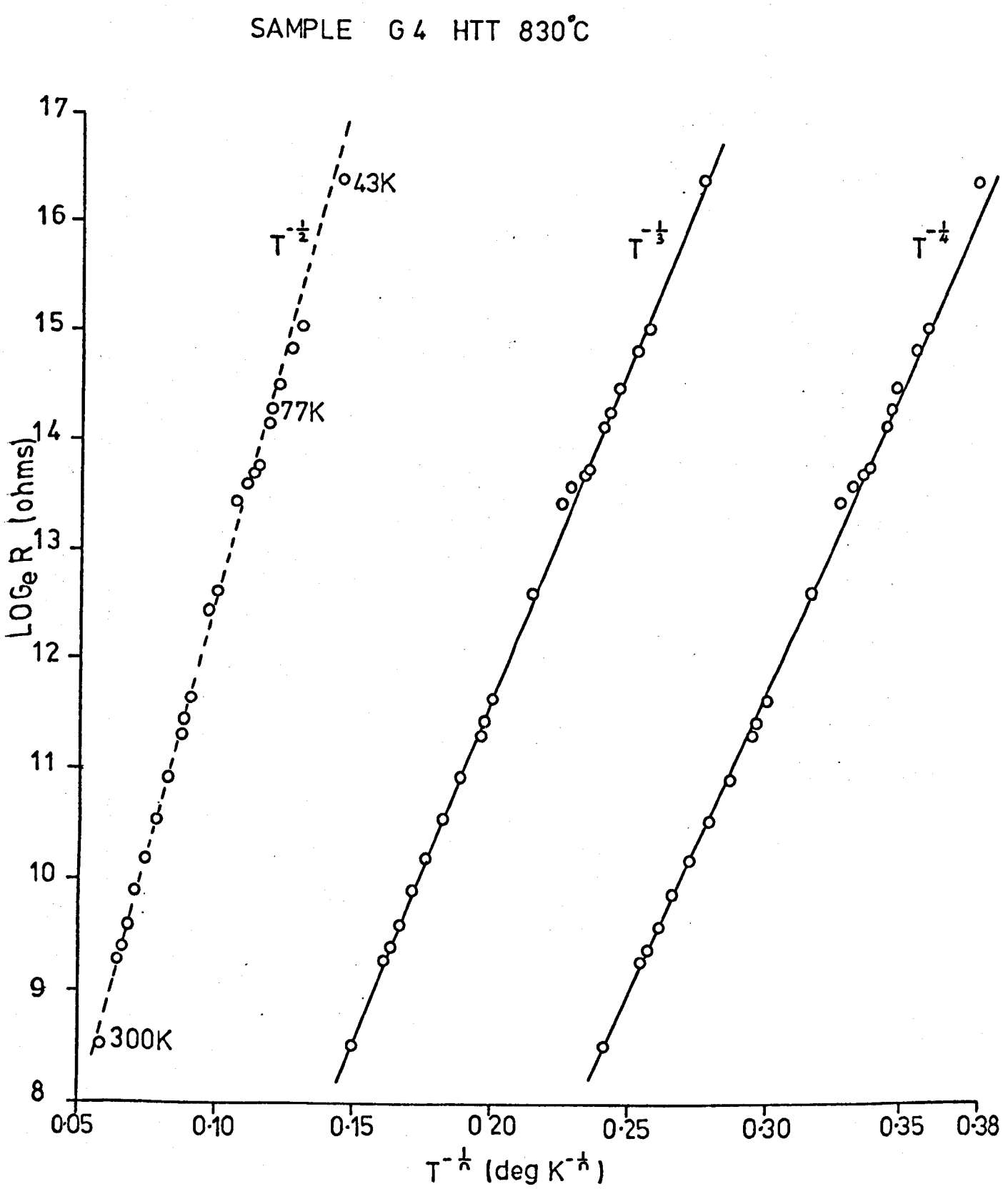
SAMPLE G 4 HTT 830°C
17
16
15
14
13
12
11
10
9
8
LOGe R (ohms)
43K
77K
300K
T^-1/2
T^-1/3
T^-1/4
0·05
0·10
0·15
0·20
0·25
0·30
0·35
0·38
T^-1/n (deg K^-1/n)

FIGURE 6.2

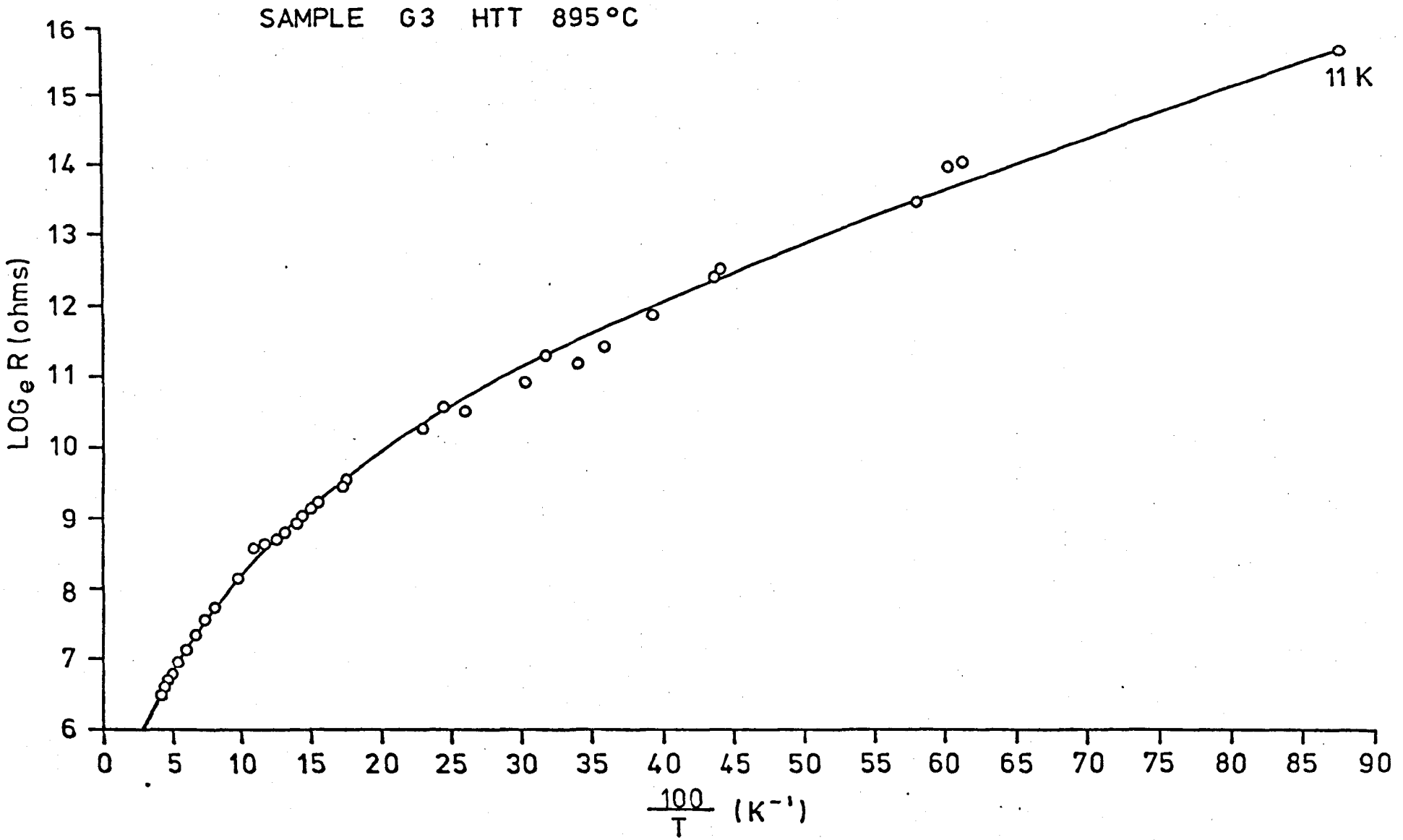
SAMPLE G3 HTT 895°C
11 K
LOG_e R (ohms)
16
15
14
13
12
11
10
9
8
7
6
0
5
10
15
20
25
30
35
40
45
50
55
60
65
70
75
80
85
90
$\frac{100}{T}$ (K^{-1})

FIGURE 6.3

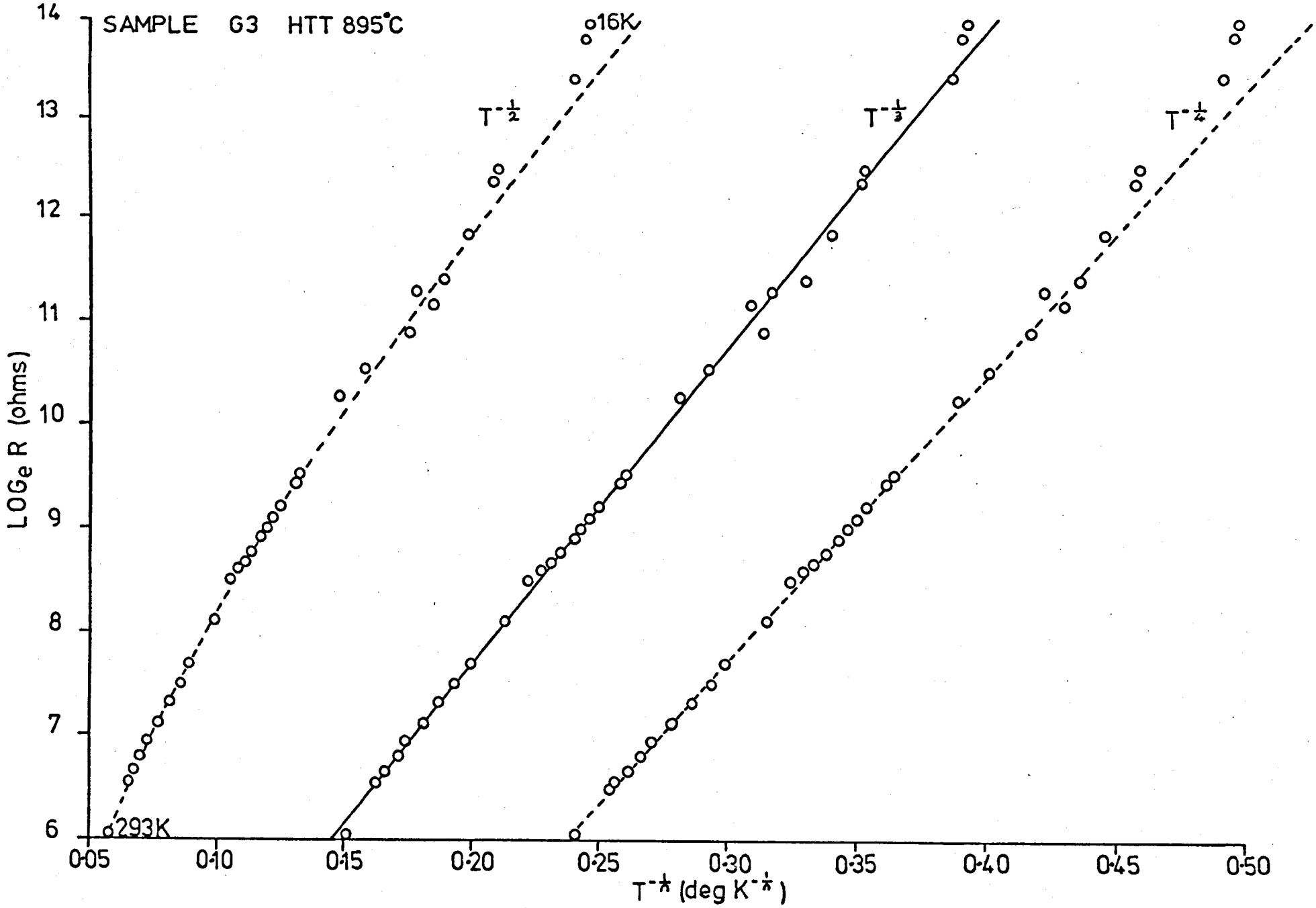
SAMPLE G3 HTT 895°C
16K
293K
$T^{-\frac{1}{2}}$
$T^{-\frac{1}{3}}$
$T^{-\frac{1}{4}}$
LOG_e R (ohms)
$T^{-\frac{1}{n}}$ (deg $K^{-\frac{1}{n}}$)
14
13
12
11
10
9
8
7
6
0·05
0·10
0·15
0·20
0·25
0·30
0·35
0·40
0·45
0·50

FIGURE 6.4

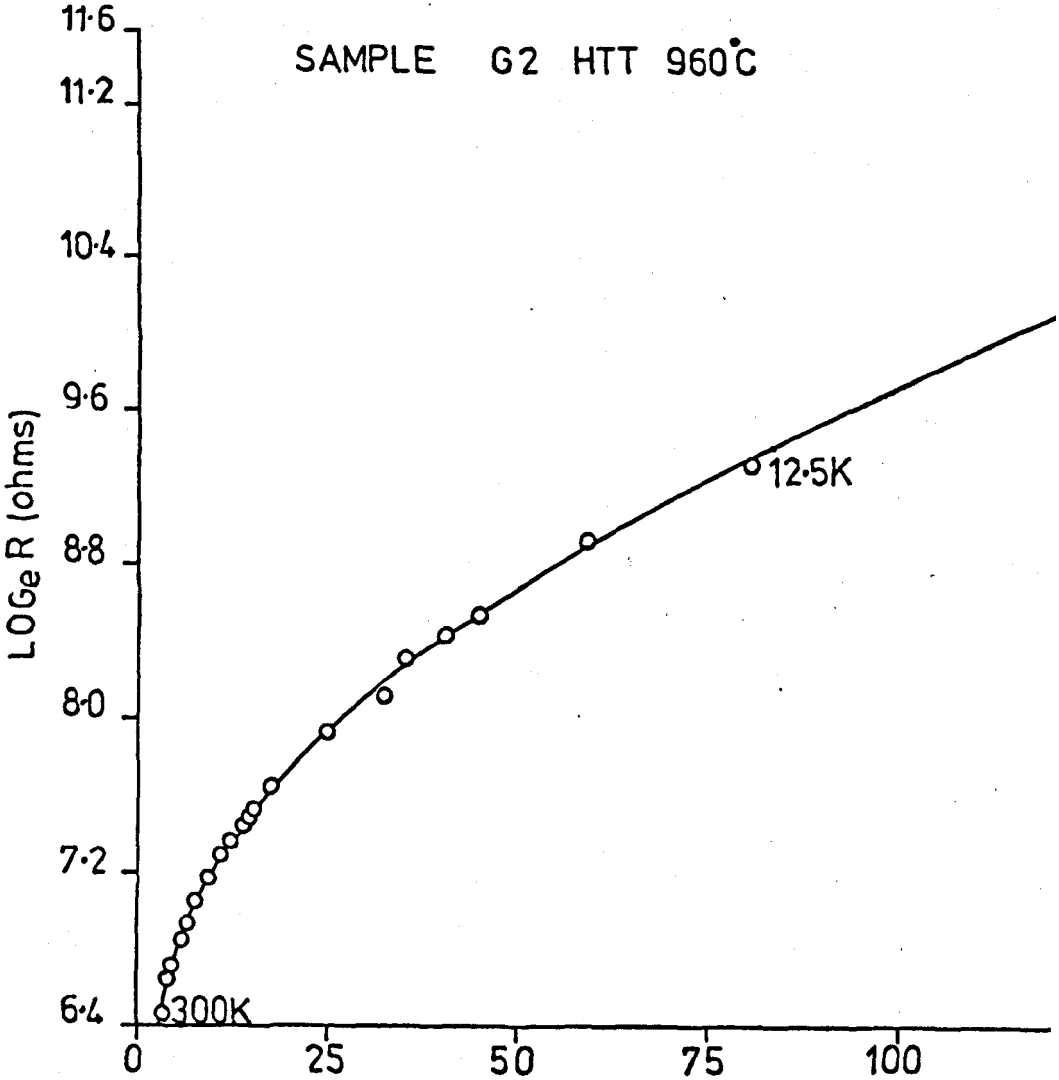
SAMPLE G2 HTT 960°C
11·6
11·2
10·4
9·6
8·8
8·0
7·2
6·4
LOGe R (ohms)
12·5K
300K
0
25
50
75
100
1000/T

FIGURE

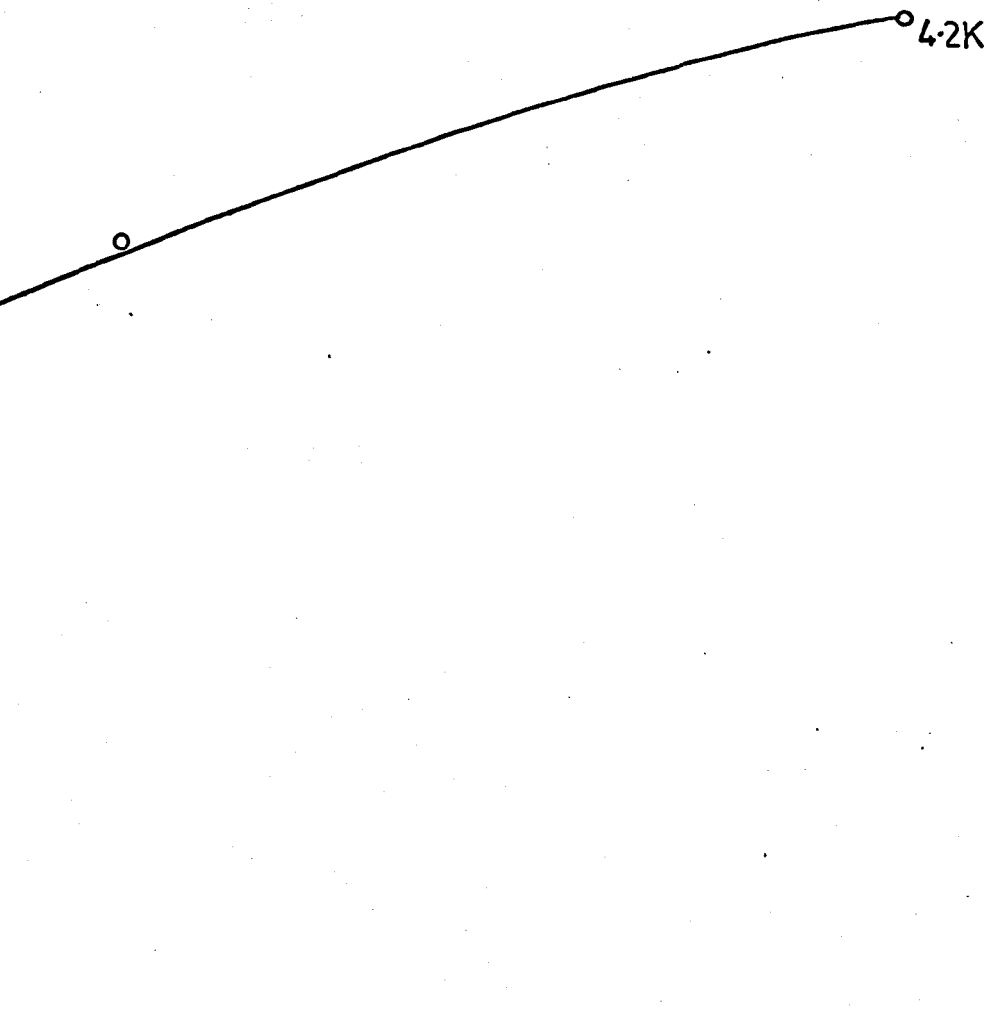

6.5

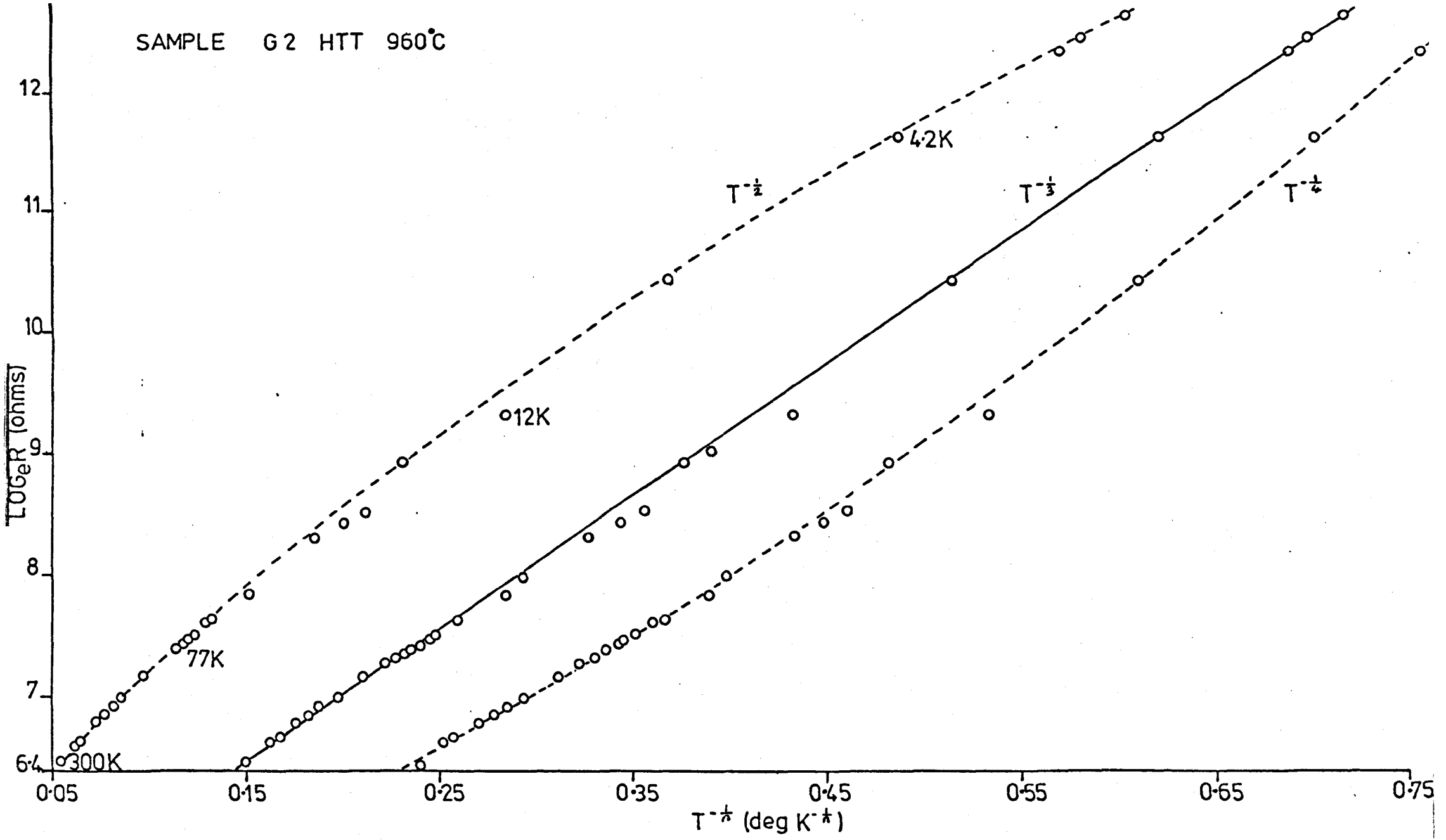
SAMPLE G2 HTT 960°C
12
11
10
9
8
7
6·4
LOGeR (ohms)
4·2K
12K
77K
300K
$T^{-\frac{1}{2}}$
$T^{-\frac{1}{3}}$
$T^{-\frac{1}{4}}$
0·05
0·15
0·25
0·35
0·45
0·55
0·65
0·75
$T^{-\frac{1}{n}}$ (deg $K^{-\frac{1}{n}}$)

FIGURE 6.6

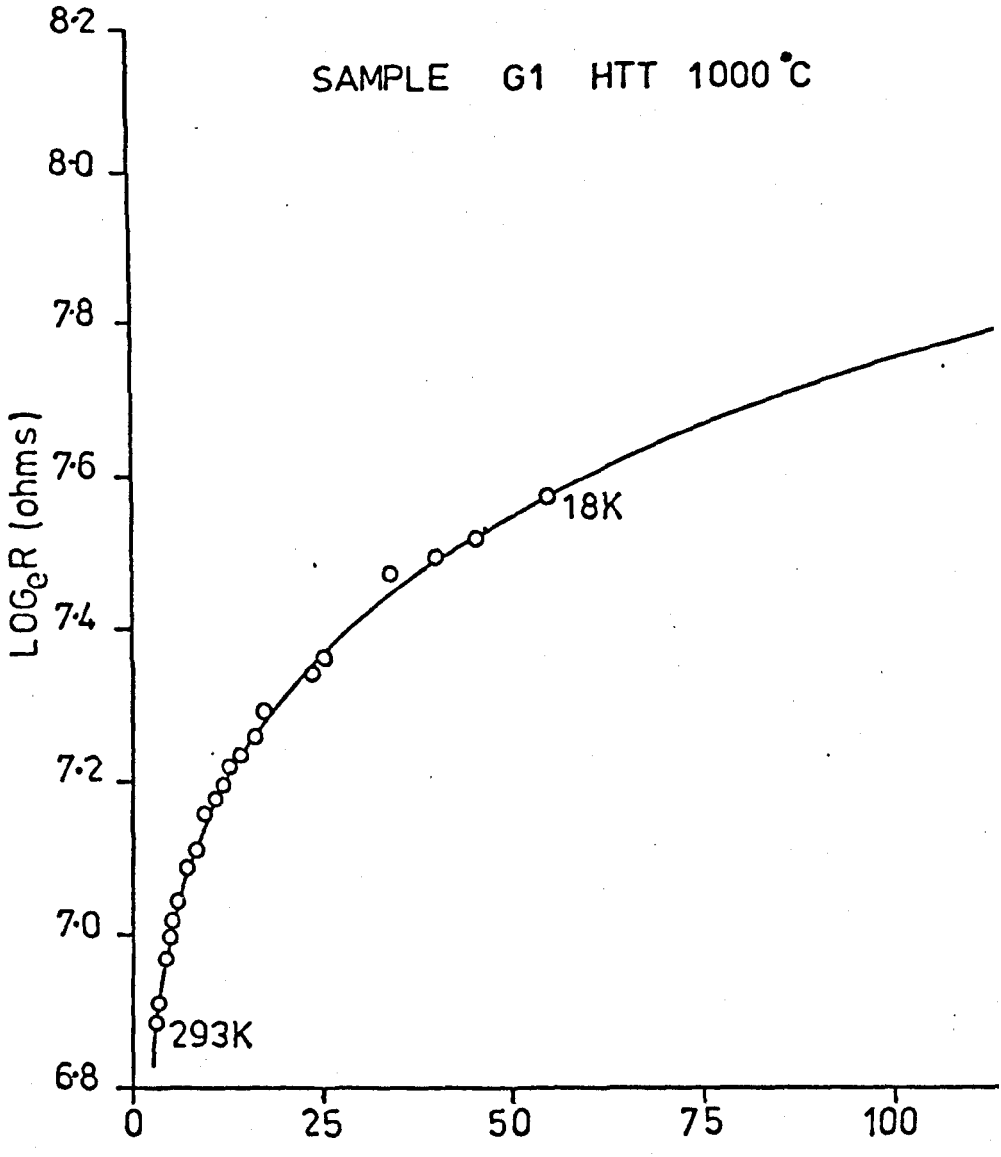
SAMPLE G1 HTT 1000 °C
8·2
8·0
7·8
7·6
7·4
7·2
7·0
6·8
LOGeR (ohms)
18K
293K
0
25
50
75
100

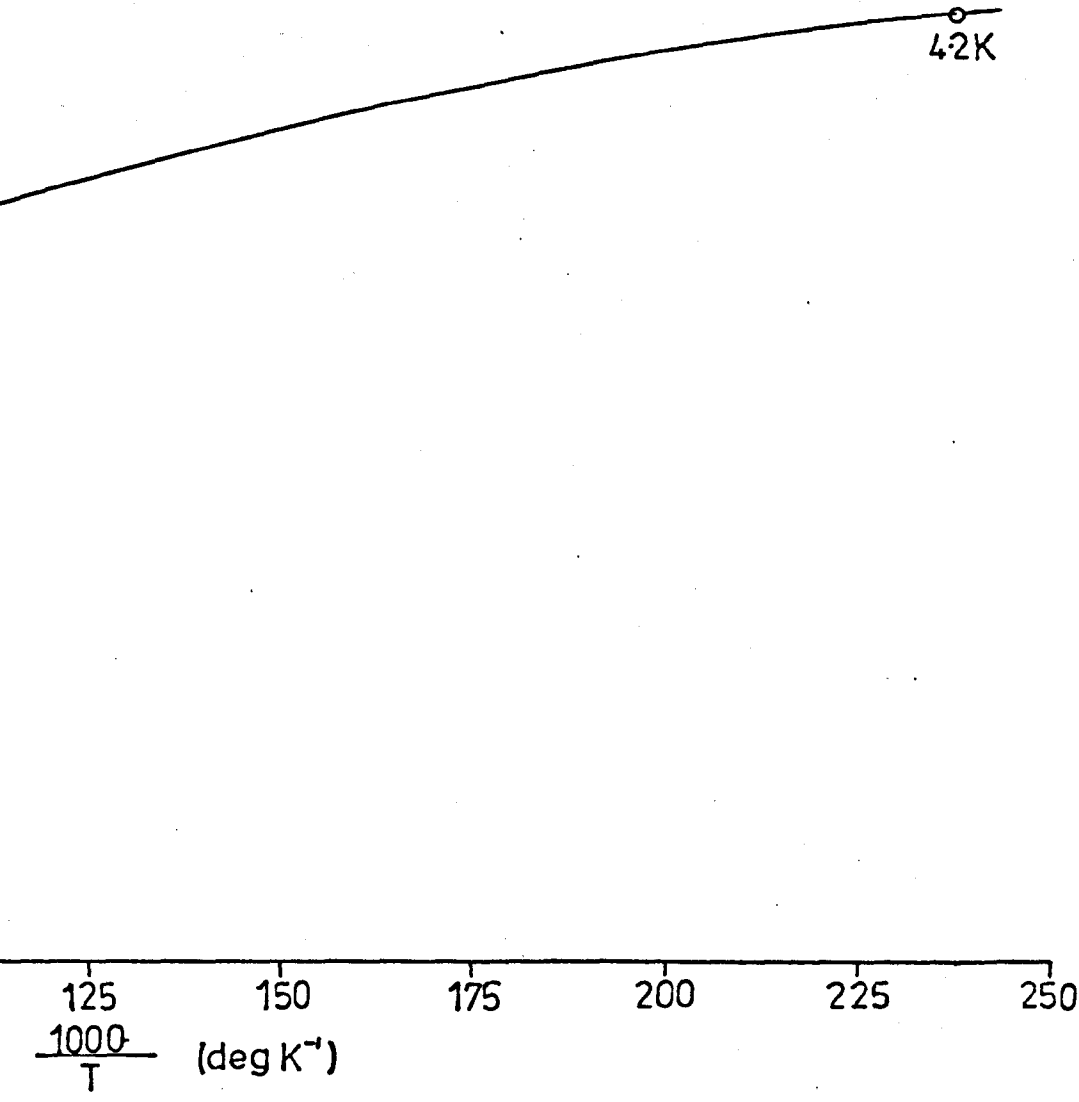

FIGURE 6.7

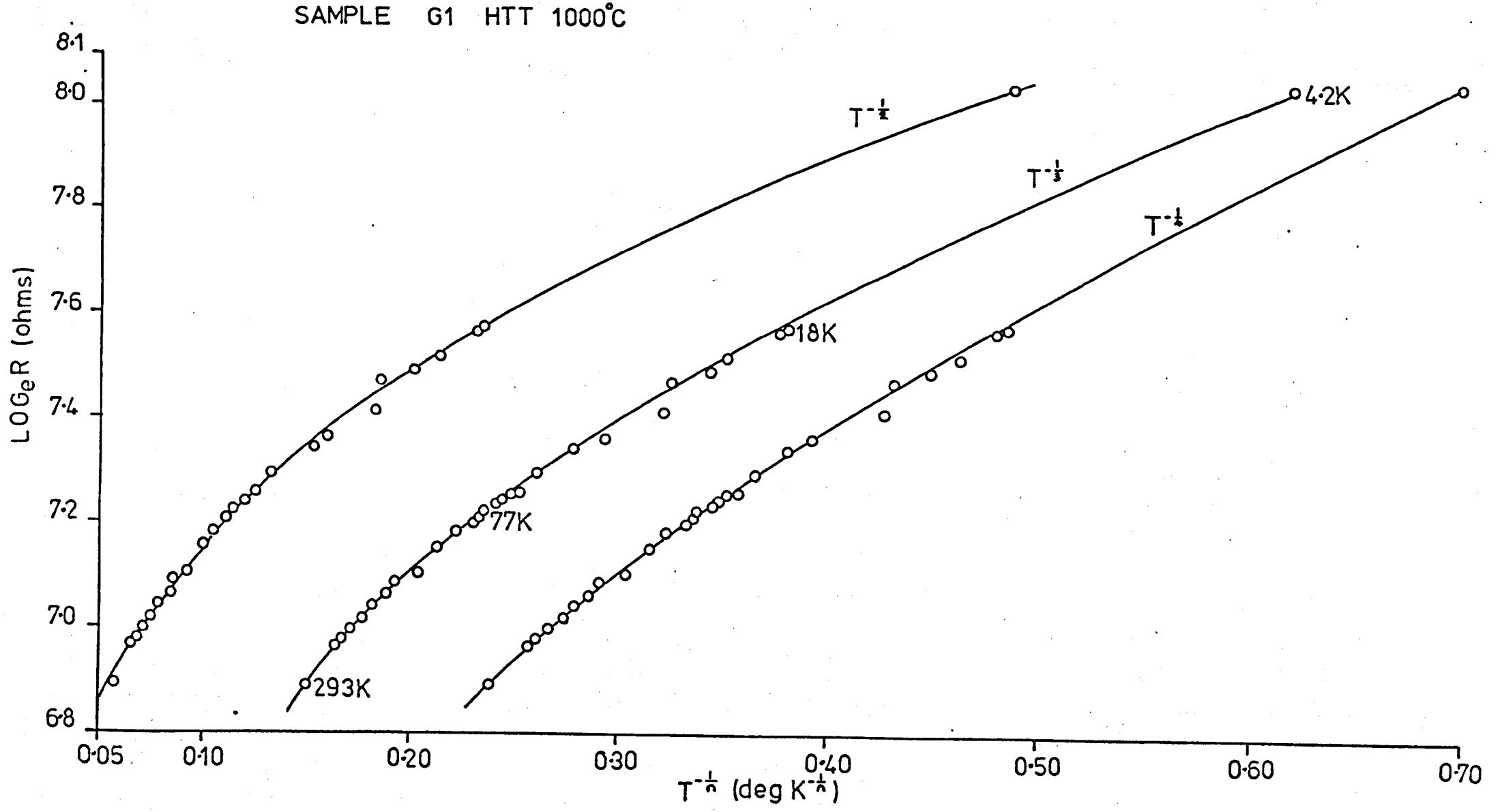
SAMPLE G1 HTT 1000°C
8·1
8·0
7·8
7·6
7·4
7·2
7·0
6·8
LOGeR (ohms)
0·05
0·10
0·20
0·30
0·40
0·50
0·60
0·70
T^-1/n (deg K^-1/n)
T^-1/2
T^-1/3
T^-1/4
4·2K
18K
77K
293K

FIGURE 6.8

the helium transfer tube to be inserted. The wire leads to which the samples were attached passed down the stainless steel tube and were glued between the perspex layers. Four wires were required for each sample and passed through small holes in the perspex layers in such a way that the fibres could be mounted horizontally. The electrical contacts were made as before using colloidal silver paint. Four samples were mounted on each layer with a 1.5 cms spacing between the samples. The top of the tube was sealed with glue and the wires on emerging were attached to veroaboard. A latex cover was put over the samples and was held in position using cellotape. A gauze cage was fastened around the mount and activated charcoal was carefully inserted.

Figs. 6.1, 6.3, 6.5 and 6.7, show plots of $\log_e R\ (\Omega)$ versus $\frac{1000}{T}\ (K^{-1})$ for samples heat treated between 830°C and 1000°C inclusively. It is evident that the resistance increases continuously with no well defined activation energy as the measurement temperature is lowered. As a consequence of these results it would not be justifiable to interpret these low HTT carbons entirely as intrinsic semiconductors as had been attempted by Harker[90].

Figs. 6.2, 6.4, 6.6 and 6.8, show the corresponding plots of $\log_e R\ (\Omega)$ versus $T^{-\frac{1}{n}}\ (K^{-\frac{1}{n}})$ for $n = 2,3$ or 4. Although the results confirm that the principal conducting mechanism is one of hopping it is worth giving consideration to each of the figures as some deviation is observed for the sample heat treated to 1,000°C.

Fig. 6.2 HTT 830°C shows that the results could be well fitted by either a $T^{-\frac{1}{3}}$ or $T^{-\frac{1}{4}}$ temperature dependence with $T^{-\frac{1}{3}}$ providing marginally the better fit.

Similarly the results for samples G 3 HTT 895°C and G 2 HTT 960°C

HYPERFINE INTERACTION IN A $C-CH_3$ FRAGMENT

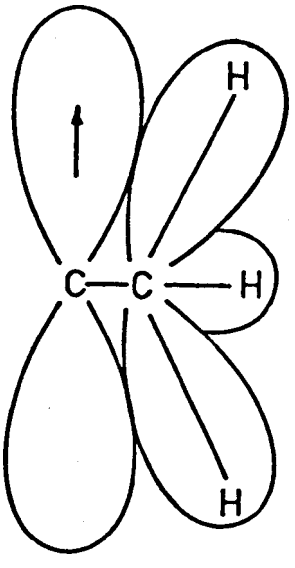

(a)

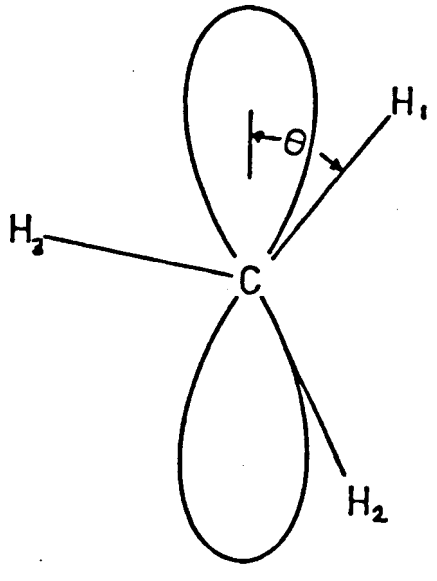

(b)

FIGURE 7.3

shown in Figs. 6.4 and 6.6, are clearly better fitted to a $T^{-\frac{1}{3}}$ temperature dependence than to either a $T^{-\frac{1}{4}}$ or a $T^{-\frac{1}{2}}$ dependence.

The results for sample G 1 HTT 1,000°C are illustrated in Fig. 6.8 where it can be seen that the graphs obtained by plotting $\log_e R$ (Ω) against $T^{-\frac{1}{2}}$, $T^{-\frac{1}{3}}$ and $T^{-\frac{1}{4}}$ all show some degree of curvature. Enhanced electron mobility associated with increased delocalization is the responsible mechanism.

6.6 The thermoelectric power (TEP)

Before discussing more fully the implications of these results it will be of relevance to present the results obtained on measuring the Seebeck thermoelectric power (TEP) for the fibres. The Seebeck effect and the Hall effect are closely related parameters and generally practical considerations determine which property is measured. Measurement of both these properties readily yields the sign of the majority carriers and in addition their concentration may also be determined.

Both the Hall constant[53] and the TEP[52] have been measured for soft and hard carbons and substantial agreement was found for the two properties.

Essentially the Seebeck effect generates a potential difference when a temperature difference is maintained across a conducting material. The carriers at the hot junction diffuse more rapidly and a potential of the same sign as the carriers is developed as they migrate towards the cold junction.

The TEP is measured relative to some standard in a typical thermocouple arrangement.

6.7 Measurement of the TEP.

The measurement of the TEP at room temperature was made using

FIBRES MOUNTED FOR TEP

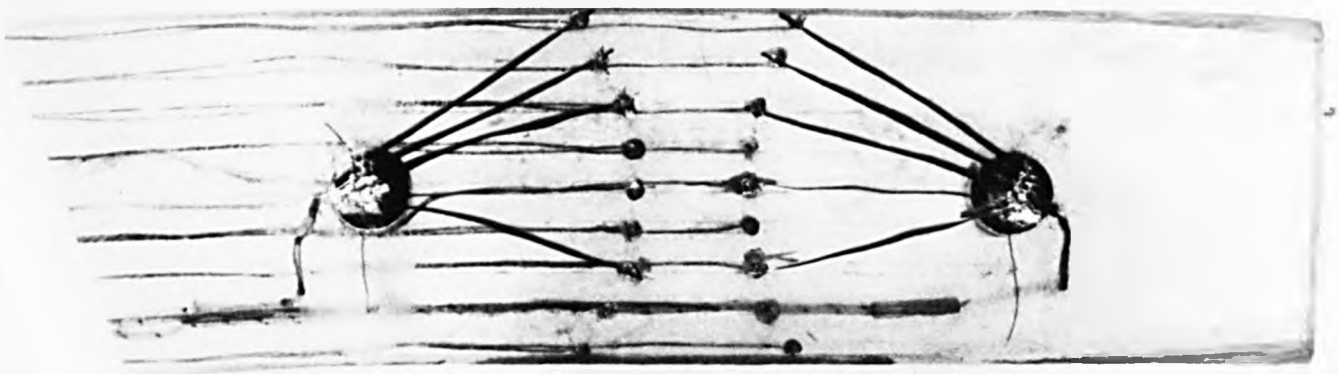

FIGURE 6.9

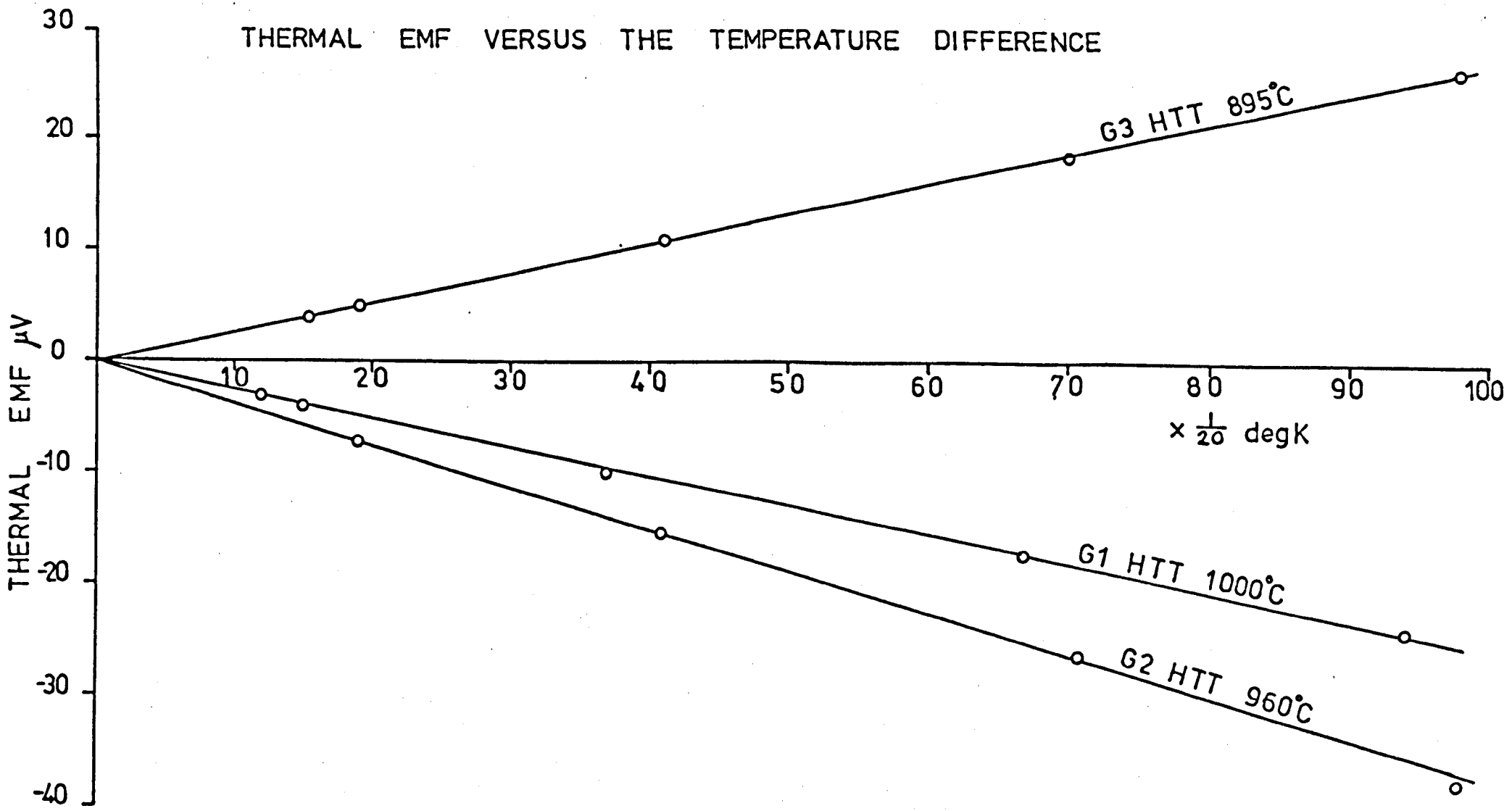
THERMAL EMF VERSUS THE TEMPERATURE DIFFERENCE
THERMAL EMF μV
30
20
10
0
-10
-20
-30
-40
10
20
30
40
50
60
70
80
90
100
× 1/20 degK
G3 HTT 895°C
G1 HTT 1000°C
G2 HTT 960°C

FIGURE 6.10

Assabghy's mount[50] shown in Fig. 6.9 Small bundles of fibre were mounted and as it can be seen the TEP of several samples can be readily measured during a single run. The mount was made of perspex with two brass cylinders fixed into it. One of the cylinders acted as a room temperature heat reservoir and the other as a heater having a few turns of insulated nichrome wire wound around it. Good thermal and electrical contact was ensured by painting the ends of the carbon fibre bundles on to the brass cylinders using colloidal silver paint. Iron/gold against chromel thermocouple wires (See section 4.4) were similarly painted on to the cylinders in order to monitor the temperature. A single strand of 99.999% pure gold wire was connected between the two cylinders in order to complete the thermocouple arrangement with carbon fibres. The thermal e.m.f. developed across the break in the carbon fibre was measured using a sensitive potentiometer.

Graphs of the thermal e.m.f. measured in microvolts against the temperature difference in degrees Kelvin were drawn up. The graphs obtained were linear (See Fig. 6.10) and the slope gives the TEP of carbon fibre relative to that of spectroscopically pure gold. The absolute value is then obtained by adding the value 2.0 μV deg K^{-1} which is the value obtained by Huebener[91] for a sample of gold wire of the same purity.

The following absolute values of the TEP measured in μV deg K^{-1} were obtained:

G 3 + 7.4 G 2 - 5.6 G 1 - 3.2

The following estimates were also made for samples G4 HTT 830°C and G 5 HTT 760°C ~ + 23.0 μV deg K^{-1} and ~ + 41 μV deg K^{-1} respectively. The results are consistent with previous observations in the carbon field, in that the TEP decreases from a large positive value eventually becoming

negative as the HTT increases. The positive TEP observed at low HTT indicates that holes are the majority carriers dehydrogenation, cross linking and imperfect condensation are thought to expose free valencies (dangling σ bonds) which act as electron traps. The fall of the TEP with increasing HTT is attributed to an increasing concentration of such traps. The TEP is sensitive to the position of the Fermi level and this led to Loebner's[52] explanation of the change of sign. It was suggested that the Fermi level crosses the inflection in the E σ K curve, so that $\frac{d^2E}{dK^2}$ and hence the effective mass of the carriers change sign. However, we have shown that hopping is the conducting mechanism and some other explanation needs to be sought for the change in sign of the TEP, observed in samples heat treated above 960°C.

6.8 Discussion

As early as 1967 Harker[90] attempted an alternative to the band model of Mrozowski. He proposed that the carbons should be considered as intrinsic semiconductors over their whole range of preparation temperatures. It was suggested that carbon materials contain ionized layers formed by thermal excitation with charge hopping from layer to layer. This molecular crystal approach is capable of interpreting a number of the observed features. For the low HTT samples we have shown that thermally activated hopping is the process of conduction which is at variance with Harker's interpretation of intrinsic semiconducting behaviour.

Hopping models have been successfully applied by Adkins et al.[92] and Morgan[93] to account for the electrical conduction in thin films of amorphous carbon. Graphite rods were slowly evaporated at low pressure and thin films of carbon were obtained when the carbon particles were deposited on glass substrates. Morgan obtained his conductivity results using a film

of thickness 700 Å while Adkins et al. made their measurements using films 1600 Å thick. Both groups established that the conduction process fitted a hopping model, however, the results indicated that the films were not entirely amorphous. Electron microscope examinations revealed no structure above 30 Å and it was suggested that the crystallite size is typically ~ 10 Å. However, Adkins et al. reported the electrical resistivity to be strongly anisotropic being considerably larger when measured through rather than along, the film. Although they found the structure to be anisotropic, conduction by hopping was confirmed both through and along the film. In contrast, Morgan, found his electrical measurements to be isotropic.

Both groups gave plots of $\log_e \rho$ against $T^{-\frac{1}{4}}$ which showed some degree of curvature. Morgan observed that the resistivity results approximated more nearly to $T^{-\frac{1}{2}}$ than to $T^{-\frac{1}{4}}$ and reported that an even better fit could be obtained by plotting $\log_e \rho$ against $T^{-\frac{1}{3}}$.

They also reported that for fields (E), in excess of 2.5 KV cm^{-1}, the conduction became non-linear with the current (I) and field (E) satisfying a relationship of the form

$$\log_e (I) \propto E^{\frac{1}{2}}$$

which is characteristic of the Poole - Frenkel or Schottky mechanisms.

The g-shift that we obtained confirmed that low HTT Courtelle chars are anisotropic in structure, with the layer planes preferentially aligned parallel to the fibre axis. Singer and Cherry[79] reported similar anisotropic effects in an acenaphthylene char. It would perhaps therefore be anticipated that electrical conduction would take place by hopping between localized sites contained within two dimensional layer planes. We have deduced that under such circumstances the conductivity (σ) should be

of the form $\log_e \sigma \propto A - BT^{-\frac{1}{3}}$. We have seen that for samples G 4, G 3 and G 2 the conductivity fits this relationship with G 1 showing some deviation due to increased mobility.

It has been estimated that for conductivities much in excess of $100 \Omega^{-1} cm^{-1}$ conduction would not be expected to be by thermally activated hopping so that sample G 1 is a borderline sample.

No theory has been developed to account for the magnitude and sign of the TEP observed in disordered structures. It appears that negative Hall coefficients are not uncommon in p - type non-crystalline materials.

Our TEP measurements show some interesting features, at low HTT'S it is large and positive, however, at a HTT of 960°C the TEP becomes negative. Assabghy[50] reported that it became positive again at a HTT of 1750°C.

It is thought that a well defined band of acceptors or traps exist (dangling σ bonds) at the lowest heat treatment temperatures. Discontinuities in the structure due to dehydrogenation, cross linking and imperfect condensation are proposed as the origin of such traps. Electrons from the π band occupy some of these σ orbitals, forming spin pairs, and creating mobile holes in the π band. The positive TEP would tend to confirm this approach, and the observed fall in magnitude is explained as an increase in the concentration of such traps. Compensation by donor impurities could account for the negative TEP. At these heat treatment temperatures a few atomic percent of oxygen, hydrogen and nitrogen are contained within the structure[26]. Nitrogen in particular can readily give rise to a source of donor impurities. A proportion of donors would lose electrons to acceptors and electrons would then tunnel from occupied to empty donors. Interestingly the bulk of impurities are driven off as the HTT is increased to 1750°C [26] and the TEP becomes positive.

HYPERFINE SPLITTING OF THE UNPAIRED ELECTRONS ENERGY LEVELS BY INTERACTION WITH A PROTON

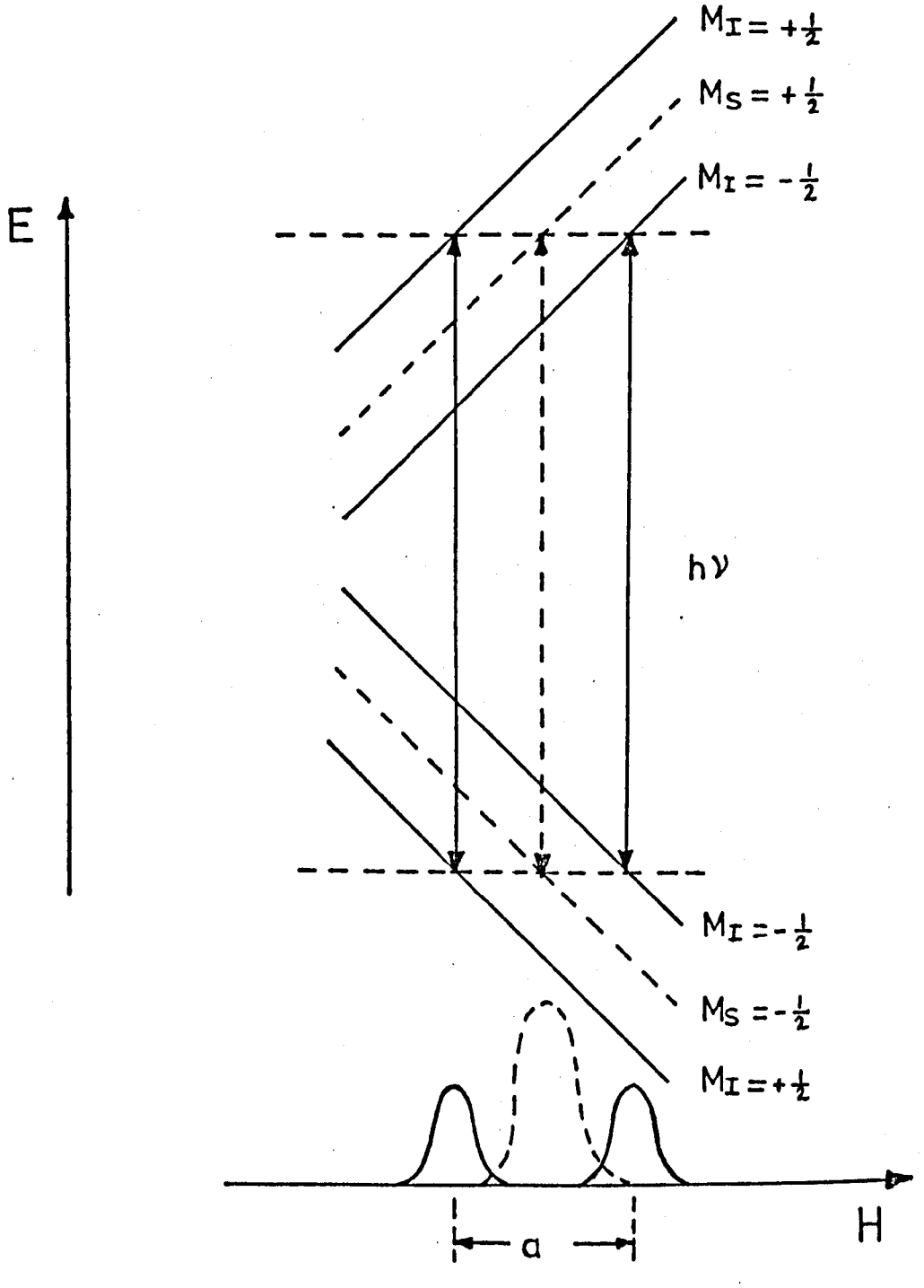

FIGURE 7.1

CHAPTER 7

ESR APPLIED TO FREE RADICALS.

7.1 Hyperfine structure

The production, trapping and subsequent analysis of free radicals in solids at low temperatures has over the years been the subject of considerable research. Free radicals are molecules or molecular fragments formed in such a way that an unpaired electron has been left associated with them.

Electron spin resonance spectroscopy has been applied to the study of such radicals and in a number of cases it has been possible both to identify the radical and also to obtain intimate knowledge of its structure.

Free radicals can be thought of as a crystal field system for which the orbital angular momentum has been quenched. For most radicals the separation of the orbital levels is very large ($> 10^3 cms^{-1}$) and as a consequence very little orbital angular momentum is reintroduced into the ground state by mixing of the ground and excited states, and the g factor differs only marginally ($< 0.5\%$) from that of the free spin value.

The ground state is an orbital singlet having a spin degeneracy of 2 giving rise to the normal Zeeman energy levels. These levels are further split by interaction with magnetic nuclei. For a nuclear spin I each of the electronic levels are split into $(2\ I + 1)$ levels. The selection rules for these transitions being $\Delta\ M_I = o$, $\Delta\ M_s = \pm 1$.

One of the most common and interesting hyperfine interactions is that of the unpaired electron with hydrogen nuclei for which $I = \frac{1}{2}$. Fig. 7.1 illustrates the effect of the interaction of the unpaired electron with a

single proton resulting in a doublet spectrum with a hyperfine splitting a. Similarly the interaction with n equivalent protons gives a spectrum of $(n + 1)$ lines having a binomial distribution of intensities. The interaction with n non-equivalent protons however, results in a spectrum consisting of 2^n lines of equal intensity.

The ESR spectrum that is observed as a result of the hyperfine interaction acts like a fingerprint by which the radicals are identified. The hyperfine interaction consists of both an isotropic and an anisotropic contribution. In studies of radicals formed in polymers and polycrystalline materials the radicals are not well oriented in the static field and the anisotropic interaction causes line broadening, with a consequent loss of resolution, of the hyperfine lines formed from the isotropic interaction. The anisotropic interaction is a dipole-dipole interaction between the unpaired electron and nuclear spin and in liquids can be averaged out by the rapid tumbling of the molecules.

The contact or isotropic hyperfine interaction may be written

$$a\,\underline{I}\cdot\underline{S} \qquad 7.1$$

where $\underline{I}$ is the nuclear spin and if the magnetic field direction is in the Z direction it becomes

$$a\,I_z S_z \qquad 7.2$$

$$= \quad a\,M_I\,M_s \qquad 7.3$$

where M_I takes the 2I+1 values -I, -I+1, ————I

where M_s takes the 2S+1 values -S, -S+1, ————S

The hyperfine coupling constant a is a measure of the S character of the electronic wave functions at the site of the nucleus. Fermi showed using the relativistic Dirac equation that

$$a = -\frac{8\pi}{3}\,g_e g_I \beta \beta_N \left|\psi^2(0)\right| \qquad 7.4$$

SPIN POLARIZATION OF A C-H FRAGMENT

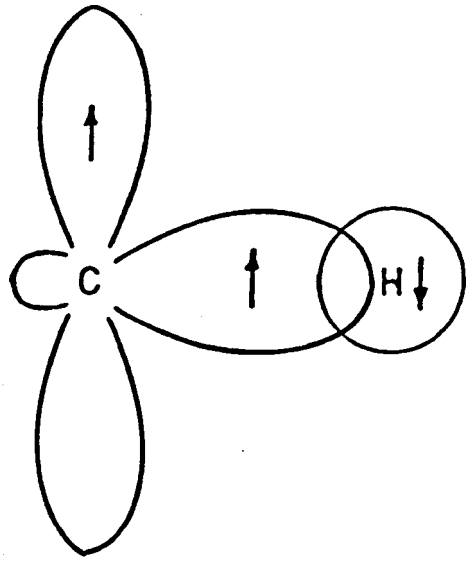

(a)

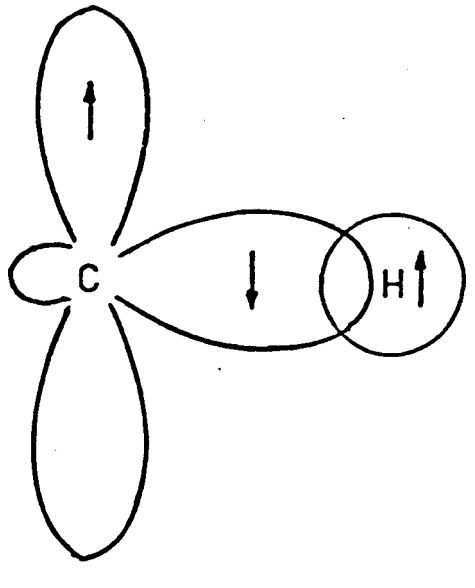

(b)

FIGURE 7.2

where β is the Bohr magneton

where β_N is the nuclear magneton

where g_I is the nuclear g factor

where $\psi(o)$ is the electron wave function at the nucleus

A non-zero wave function for the unpaired electron at the site of the nuclear spin is necessary and this is responsible for the observation of hyperfine structure in the ESR spectra. Clearly then if as is often the case we have an unpaired electron in the $p\pi$ orbital on a carbon atom then an hydrogen nuclei attached to this carbon atom would be expected to produce no hyperfine interaction. However, a very significant isotropic hyperfine coupling to such α protons is found to exist.

7.2 Configuration interaction and spin polarization

It has been shown[94,95,96,97] that configurational interaction plays an important role in the interpretation of this hyperfine interaction. If we consider a $>\dot{C}$ - H fragment as shown in Fig. 7.2 in the ground state configuration it has two electrons in the C - H σ bonding orbital 'σ_B' and one in the carbon π orbital. The σ_B orbital is constructed from a carbon Sp^2 hybrid orbital and the $1s$ orbital of the proton.

The ground state configuration is given by

$$--- \left(\sigma_B^2\right) \pi \qquad 7.5$$

An excited state may exist if one of the paired electrons in the σ_B orbital is promoted to the antibonding orbital σ_A

An excited state configuration may be given by

$$--- \sigma_B \pi \sigma_A \qquad 7.6$$

Configurational interaction can be thought of as the mixing of the ground and excited state as a result of their coulombic interaction.

The ground state spin orbital wave function may be written as

$$\phi_{g.s.} = A\left\| \sigma_B(1)\,\sigma_B(2)\,\Pi(3)\right\| \alpha\beta\alpha \qquad 7.7$$

Because the excited state spin orbital eigenfunctions are to be eigenfunctions of $S_z = +\frac{1}{2}$ (or $-\frac{1}{2}$) and $S^2 = \frac{3}{4}$ the only permissible ones are

$$\phi_1 = A\left\| \sigma_B(1)\,\sigma_A(2)\Pi(3)\right\| \alpha\beta\alpha \qquad 7.8$$

$$\phi_2 = A\left\| \sigma_B(1)\,\sigma_A(2)\Pi(3)\right\| \beta\alpha\alpha \qquad 7.9$$

$$\phi_3 = A\left\| \sigma_B(1)\,\sigma_A(2)\Pi(3)\right\| \alpha\alpha\beta \qquad 7.10$$

Where A is the antisymmetrisation and renormalisation operator and is given by

$$A = \frac{1}{(N!)^{\frac{1}{2}}} \sum (-1)^p P \qquad 7.11$$

where N is the number of electrons, in this case 3 and p is even or odd according as the permutation P is even or odd.

The linear combinations of the orbital eigenfunctions (equations 7.8 - 7.10) which are eigenfunctions of

$S_z = +\frac{1}{2}$(or $-\frac{1}{2}$) and of $S^2 = \frac{3}{4}$ are

$$\psi_1 = \frac{1}{\sqrt{2}}\left(\phi_1 - \phi_2\right) = \frac{1}{\sqrt{2}} A\left\| \sigma_B(1)\sigma_A(2)\,\Pi(3)\right\| \left(\alpha\beta\alpha - \beta\alpha\alpha\right) \qquad 7.12$$

and $\psi_2 = \frac{1}{\sqrt{6}}\left(\phi_1 + \phi_2 - 2\phi_3\right) = \frac{1}{\sqrt{6}} A\left\| \sigma_B(1)\sigma_A(2)\,\Pi(3)\right\| \left(\alpha\beta\alpha + \beta\alpha\alpha - 2\alpha\alpha\beta\right)$ 7.13

where ψ_1 and ψ_2 are normalised by the factors $\frac{1}{\sqrt{2}}$ and $\frac{1}{\sqrt{6}}$ respectively allowing for the spin part of the function.

ψ_1 corresponds to a ground state wave function that is a singlet having paired spins in the σ orbitals and gives no hyperfine coupling with the proton. The hyperfine coupling arises through a mixture of ψ_2 and the ground state resulting in a modified wave function

$$\psi = \phi_{g.s.} + \lambda\psi_2 \qquad 7.14$$

where λ is an admixture coefficient and can be shown[97] to be linearly proportional to the unpaired spin density in the attached carbon nucleus. Because the hyperfine splitting is proportional to the unpaired spin density, it is also proportional to λ.

If the unpaired spin on the carbon atom is as shown in Fig. 7.2 Hund's rules tell us that there exists a slightly greater possibility of (a) than of (b), that is the electron in the Sp^2 orbital will be aligned parallel and by Pauli's principle the electron in the H ($1S$) orbital must be antiparallel to that in the Sp^2 orbital and hence antiparallel to that on the carbon atom. Consequently there will be a net unbalance of spin at the proton and a negative spin-density will result.

7.3 Isotropic coupling to β hydrogens-Hyperconjugation

To explain the observed hyperfine interactions in fragments such as $\rangle\dot{C} - CH_3$ it becomes necessary to introduce the concept of hyperconjugation. As shown in Fig. 7.3 (a) there is overlap between one or more of the σ (C - H) bonds and the p orbitals of the unpaired electrons, occasioning some redistribution of unpaired spin on to the β protons. The interaction will be greatest when the axis of the p orbital and the σ bond are co-planar and to be zero when the σ bond lies in the nodal plane of the p orbital. In Fig. 7.3 (b) θ is the angle between the axis of the p orbital and the projection of the (C - H) σ bond on to the plane that passes through the axis of the p orbital and is perpendicular to the C - C bond, and the interaction is found to follow a $\cos^2\theta$ relation. Hyperconjugation produces a positive spin density at the protons, and for a methyl group in solution, each of the protons are equivalent and a large hyperfine coupling of about 26 gauss results. In the solid state, however, the rotation of the methyl group could be severely hindered and one could possibly envisage a situation

where one proton could be constrained to lie in a position of zero interaction, while at the same time the other two protons could be manifesting large and even possibly unequal hyperfine interactions.

7.4 Anisotropic hyperfine interactions

This stems from a dipole-dipole type of interaction between the electron dipole moment $\underline{\mu}_e$ and the nuclear dipole moment $\underline{\mu}_N$.

The Hamiltonian corresponding to this type of interaction is

$$\mathcal{H} = \left[\frac{\underline{\mu}_e \cdot \underline{\mu}_N}{r^3} - \frac{3(\underline{\mu}_e \cdot \underline{r})(\underline{\mu}_N \cdot \underline{r})}{r^5} \right] \qquad 7.15$$

where $\underline{r}$ is the displacement between the dipoles

if $\underline{I}$ is the nuclear spin and $\underline{S}$ is the electron spin in an external magnetic field $\underline{H}o$ then

$$\underline{\mu}_e = -g_e \beta \underline{S} \qquad 7.16$$

and $$\underline{\mu}_N = g_I \beta_N \underline{I} \qquad 7.17$$

and $$\mathcal{H} = g_e g_I \beta \beta_N \left[\frac{\underline{I} \cdot \underline{S}}{r^3} - \frac{3(\underline{I} \cdot \underline{r})(\underline{S} \cdot \underline{r})}{r^5} \right] \qquad 7.18$$

$$\mathcal{H} = g_e g_I \beta \beta_N \left\langle \left(\frac{1 - 3\cos^2\theta}{r^3} \right) \right\rangle \underline{I} \cdot \underline{S} \qquad 7.19$$

where θ is the angle between the external magnetic field and the line joining the dipoles; the angular part is averaged over the whole orbital of the unpaired electron.

As mentioned earlier, the broadening of individual hyperfine lines and the accompanying loss of resolution for radicals in polymers or polycrystalline materials arises because all orientations occur with equal probability.

7.5 Radicals in polymers

Free radicals exist as intermediates in many organic reactions particularly in polymerization reactions where application of the ESR technique has developed the understanding of both the initial monomer-initiator reactions and the latter stages of polymerization. As the

polymerization process develops the radicals become embedded in the increasing mass of polymer.

Large concentrations of radicals may also be produced as a result of irradiating with such as γ -rays, X-rays, fast electrons, ultra violet or infra red.

These studies and many other chemical applications of ESR are well reviewed by Ayscough.[98]

ESR is being applied to a study of free radicals produced during mechanical degradation of polymeric materials and is providing valuable information of the mechanisms of fracture.

Initial studies were carried out in 1959 by Bresler et al.[99] and Butyagin et al.[100] A number of polymers were studied including polyethylene, polycaprolactum (nylon 6) and polymethylmethacrylate (perspex). The polymers were crushed at liquid nitrogen temperature and the spectra of the resulting fragments were observed at low temperatures, or in an inert medium at room temperature.

As a result of these initial experiments mechanical degradation has been extensively applied to polymers. Campbell[101] and Kausch-Blecken von Schmeling[102] have prepared review articles based on this research.

7.6 Radiolysis

Although each quantum of radiation has more than sufficient energy to produce widespread bond scission it has often been reported, after examination of the resulting radicals, that selective rupture takes place. Still more surprising, is that it is not always the weakest bond that ruptures. The energy transfer to the polymer results in ionization (ejection of an inner electron from a molecular orbital). If the electron is recaptured the resulting excited molecular orbital will undergo bond scission.

After the initial bond rupture various possibilities could occur depending upon the mobility of the radicals.

(i) The radicals could lose their kinetic energy after moving only a few Angstroms apart a process known as 'pair-wise' trapping.

(ii) The radicals become 'caged' if 'pair-wise' trapping has taken place and recombination is not unlikely.

(iii) One of the radicals could be of small size and sufficiently mobile to drift through the lattice where it could combine with a variety of other radicals, or attack sites that have not been broken down by the radiation.

7.7 Photolysis.

For photodissociation to occur the energy of each quanta must be equal to, or even greater than, the dissociation energy of the bond which is ruptured, and the lattice must absorb the light used for irradiation. 'Pair-wise' trapping is likely to result most often since the excess kinetic energy will be less. Irradiation damage is often confined to the surface of the lattice where the light is absorbed.

7.8 Temperature effects.

Because the mobility of the fragments is important, the temperature at which the irradiation is carried out and that at which the ESR analysis is completed could be critical.

For a general example consider an assemblage of free radicals frozen at a low temperature. As the temperature rises two possible types of chemical change may occur:

(i) The radicals may decay by recombination this would occur chiefly in a system where 'pair-wise' trapping predominated.

(ii) one of the free radical species could be converted into another radical prior to decay.

In the former if several free radical species were present in the sample having different rates of decay, then the observed ESR spectrum will show a change in structure as the temperature rises. In the latter we would also expect to see a structural change in the ESR spectrum as the temperature rises because the population of the radicals would change. One would expect such changes to be irreversible with temperature, however, physical reversible changes may also occur. For example, the radical $CH_3\dot{C}H(COOH)$ observed at room temperature[103,104] gives an ESR spectrum that suggests the methyl protons are freely rotating. The rotation becomes hindered as the temperature is lowered, and at liquid nitrogen the results indicate that rotation has ceased and the protons are no longer equivalent.[105]

During mechanical degradation at liquid nitrogen temperature the primary radicals observed are chain end radicals formed as a result of homolysis of the main chain. However, at higher temperatures the radicals migrate and stable secondary radicals may be formed by a process of proton abstraction. The secondary radicals produced by mechanical degradation of a number of samples resemble the spectra observed as a result of high energy irradiation.

7.9 Mechanical degradation in stressed fibres

Free radical formation during polymer loading processes were first investigated by Zurkov et al.[106, 107] The samples studied included nylon 6 and silk fibres. Zurkov,[108] at the IPPS conference on yield and fracture, presented these results together with those obtained by stretching low pressure polyethylene (PE) and polyethylene terephthalate (PET) at -30°C; the ESR measurements being made at liquid nitrogen temperatures. He also reported that polystyrene (PS) and polymethylmethacrylate (PMMA) produced

an insufficient concentration of free radicals to be detected by ESR. However, Zurkov et al.[109] had previously observed free radicals in both these polymers as a result of grinding at 77K.

To date ESR applications to stressed polymers is limited to high strength, well oriented, semicrystalline fibres.

By straining the fibres and thin polymer films directly within the ESR cavity free radical formation has been studied as a function of time and of applied stress.[107,108,110]

Zurkov et al.[107,108] carried out experiments in which the load was increased stepwise at two minute intervals and on the assumption that the rate of production of the free radicals depended only upon the stress the results were seen to fit an equation of the form

$$\frac{dR}{dt} = A \exp(\gamma\sigma) \qquad 7.20$$

where R is the free radical concentration

where σ is the applied stress

and A and γ are constants

In 1943 Tobalsky and Eyring [111] proposed an exponential stress dependency for a materials lifetime (the time during which a particular stress will produce fracture).

$$\tau = B \exp\left[\left(U_o - \frac{\alpha\sigma}{KT}\right)\right] \qquad 7.21$$

where τ is the lifetime under a stress σ at absolute temperature T

where Uo is a potential barrier and is a measure of the energy required to produce bond scission.

where, B, α and K are constants.

At constant temperature the equation reduces to

$$\tau = A \exp -\beta\sigma \qquad 7.22$$

This led Zurkov et al.[107] to relate the lifetime of the polymer to the rate of radical formation. They argued that β and γ should be equal if the rate of radical formation is the factor determining the lifetime of the polymer. This was verified by plotting $\log \frac{dR}{dt}$ against $\log \tau$ for the results obtained at the three measurement temperatures -50°C, o, +50°C. A linear plot was obtained for each of these temperature.

Roylance et al.[110] while confirming the above results also carried out experiments at constant load and showed that the free radical concentration reached a saturation value. This was interpreted as being due to an exhaustion of breakable bonds. Becht et al.[112] verified this by loading a sample and when the saturation concentration of radicals had been reached the sample was unloaded and the radicals allowed to anneal. On reloading no new radicals were formed until the previous loading had been passed.

The bulk of man-made fibres can be thought of as being semicrystalline, that is, they are composed of both amorphous and crystalline regions. It is generally assumed that the long chain molecules pass through several consecutive crystalline and amorphous regions.[102,113] The individual molecular chains that comprise the crystallite, may, on emerging from a crystallite, fold and re-enter the crystallite, or enter another crystallite, so that in the amorphous region the chains will be tangled. The chains in the amorphous region are called tie molecules and it is these molecules that hold the crystalline regions together. On stretching degradation can take place either by (a) chain scission of the tie molecules in the amorphous region, the radicals being detected by ESR when a sufficient number have been accumulated or (b) by scission of bonds that hold the chains together within the crystallite-dipolar, hydrogen or Van der Waals bonding. This type of degradation will result in loss of

crystalline structure, however, no molecular chain scission need take place until eventual fracture. Zurkov et al.[107] found for nylon 6 and silk fibres that free radicals were observed by ESR at 70% of the fracture stress. Also if process (a) dominates one would expect a decrease of molecular weight - a 25% decrease of molecular weight has been observed in nylon 6.[114] Becht and Fischer[114] have also shown that free radicals are formed within the amorphous regions. They found that if a sample of nylon 6 was stretched after swelling in methacrylic acid, the signals observed were not those of the nylon 6 radicals but the polymerization radical of methacrylic acid.

Becht et al.[113] studied the effect of slicing a nylon 6.6 sample above and below the glass transition temperature Tg. They argued that at temperatures far below Tg cutting the sample with a knife will produce a brittle fracture, whereas at or above Tg plastic deformation by slip will result, and the number of broken bonds will be lessened. In their experiment samples were sliced at temperatures between -40°C and 100°C and the free radical concentration was measured at each temperature. At temperatures of the order of Tg (55°C) the free radical concentration was observed to fall markedly.

Spencer-Smith [115] has studied the property known as 'frozen-in' strain produced in a variety of man-made fibres. Among his studies he included several acrylic fibres - Courtelle, Acrilan and Orlon.

Frozen-in strain is the residual strain in a fibre as a result of straining to a point between the yield and fracture points and then releasing the stress.

The frozen-in strain can be best introduced into a fibre by heating and cooling under stress. Frozen-in strain in acrylic fibre can be

recovered either by heating under zero tension in steam or in dry air at 140°C. A Courtelle fibre will when heated under zero tension in steam lose 50% of its frozen-in strain in 32 sec, whereas a Nylon 66 sample would require 3,800 sec and Orlon 5,800 sec.

It was proposed that the frozen-in strain was produced in the amorphous regions of the textile fibres as a result of straining of the tie chains. Evidence for this was obtained by soaking the polymer in dilute solvents that penetrate the amorphous region and weaken or break the extended tie bonds resulting in shrinkage and hence recovery of the frozen-in strain.

To improve the mechanical properties of textile fibres they are generally produced with a high draw ratio and in this state would be expected to contain their maximum degree of frozen-in strain.

MECHANICAL DEGRADATION - THE PEROXIDE RADICAL

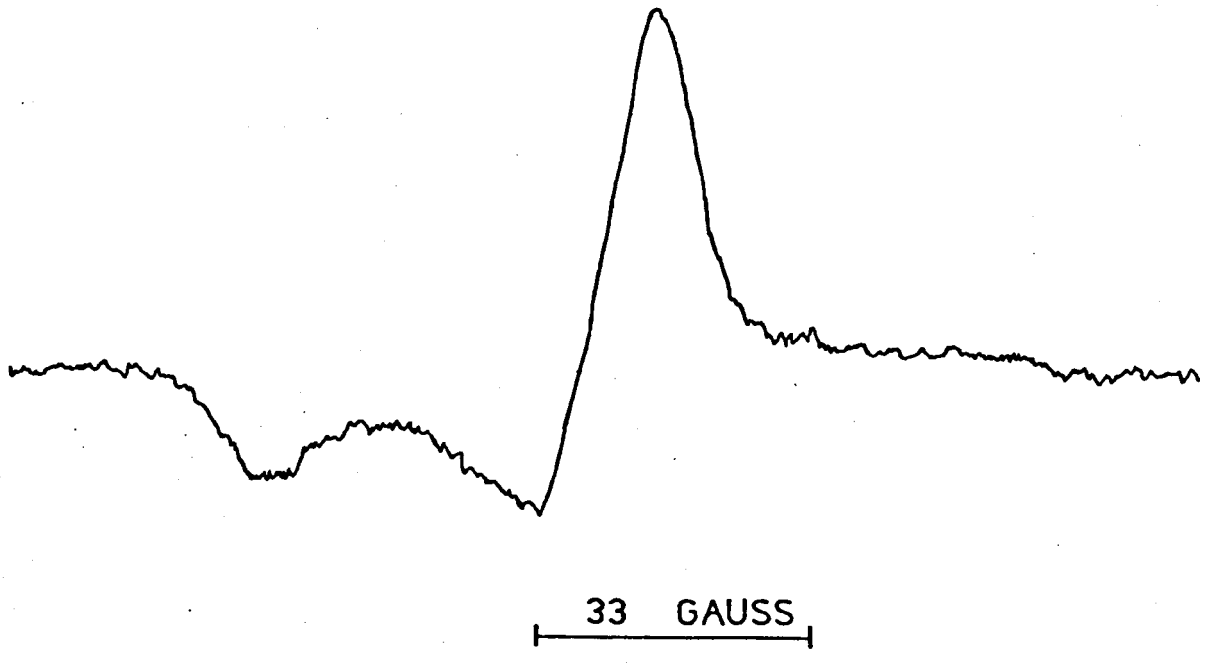

(a)

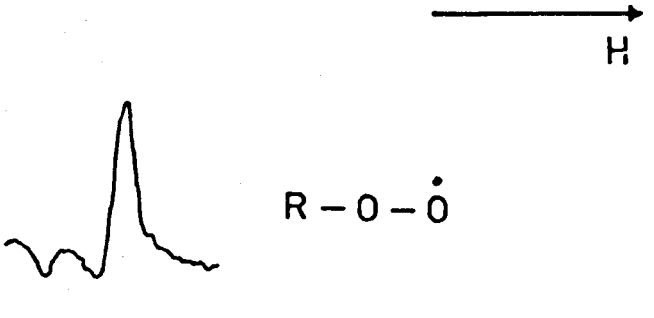

(b)

FIGURE 8.1

CHAPTER 8

AN ESR STUDY OF MECHANICAL DEGRADATION AND IRRADIATION DAMAGE INDUCED IN THE PRECURSOR MATERIALS.

8.1 Mechanical degradation

Degradation was effected by cutting the fibre, under liquid nitrogen in a small plastic beaker, using a pair of sharp scissors. The spectrum obtained is shown in Fig. 8.1 (a) The radical does not appreciably power saturate at 77K. At room temperature it decays rapidly in air and no signal remains after about 30 mins. The spin concentration was estimated to be 5×10^{15} spins cms^{-3} by comparison of the spectra with that obtained from a phosphorous doped silicon chip containing 2.5×10^{14} spins. No ESR spectrum was observed at 77K when the fibre was cut in air followed by immediate quenching in liquid nitrogen.

Similar spectrum shown in Fig 8.1 (b) were observed during ESR analysis at 77K, when polyethylene terephthalate fibres and low pressure polyethylene films were stretched at -30°C in cooled hexane.[108] The radicals are probably secondary radicals as the primary radicals produced in low pressure polyethylene, polycaprolactum and polymethylmethacrylate, by mechanical crushing at 77K, all gave spectra similar to that of Fig. 8.1 (b) during ESR analysis at 300K in air. Indeed the effects of oxygen on a number of free radicals produced during polymer irradiation give similar spectra which have been identified as the corresponding peroxide radical.[116, 117]

Although the spin concentration of the radicals formed during our degradation experiments was not large, it might well be possible to study the primary radicals. It would seem necessary to remove any oxygen absorbed within the fibre, since for low concentrations of radicals there

may be sufficient oxygen for most of the primary radicals to be immediately oxidised even at 77K. The degradation experiments would then need to be repeated in an oxygen free environment at liquid nitrogen.

8.2 ESR investigations of fibres under stress.

The ESR cavity was arranged with its axis horizontal and containing a flow dewar. The fibres included a variety of acrylics: Courtelle, Dralon T, Orlon, Acrilan and Rhodiceta. The fibres passed through the flow dewar and one end of this bundle was attached to a hook whose position was adjustable along the line of the axis of the cavity, while the other end was attached to the piston of an Enots double acting pneumatic cylinder. The cylinder being bolted to a metal casting that sat firmly on the yoke of the magnet. The piston had a two inch stroke and the operating force was obtained using a cylinder of nitrogen gas. By using a flow dewar it was possible to carry out the stretching experiment at any temperature between 77K and room temperature. Before stretching the fibre an ESR spectrum of its length was recorded to ensure that no impurities that might give rise to an ESR signal were present. Spectra were observed only occasionally on stretching bundles of fibre and never at any temperature other than room temperature. The signals observed appeared to be anisotropic. These results are difficult to explain, however, it would seen possible that the radicals would be highly mobile and may be trapped and accumulated at impurity sites within the fibre. Such sites would provide a weak crystalline field resulting in a variety of observed spectra and could possibly account for the anisotropy.

When a polymer is crushed or milled to a fine powder it will have a much larger surface area than the bulk film or fibre form. Hence free radicals would more likely be observed in the crushed polymer. Indeed while free radicals have been detected in crushed Polystyrene[118,109] and

Polymethylmethacrylate[109] no free radicals have been recorded by uniaxially straining these polymers[119,108] in bulk form. As a result one might expect a weak signal from stretching acrylic fibres. Radicals have only been observed when highly - oriented semicrystalline polymers have been subjected to stress. Acrylic fibres seem to be reasonably crystalline polymers. Both Beevers et al.[120] and Houtz[121] have shown that X-ray scattering in polyacrylonitrile and acrylonitrile + methylmethacrylate copolymers give a sharp peak arising from the 110 planes.

These commercial man-made acrylics have a high draw ratio (in some cases ~ 11:1) and would be expected to contain the maximum degree of frozen-in strain. If these fibres are subjected to stress, disruption could be caused by rupture of secondary bonds along a slip plane and total shearing of one fibril from the adjacent one, thus resulting in a partial disruption of the crystalline region. Fracture may then eventually take place without a great deal of molecular scission and hence without a considerable build up of free radicals. It would seem necessary to either repeat the experiments on an acrylic that has been drawn to a small extent, or to chemically remove the frozen-in strain using a 1% solution of ethyl carbonate[115] and then to repeat the experiment.

We also studied, using ESR, the effects of UV and electron irradiation on acrylics. It was hoped that such studies might give some insight into the mechanical degradation results, because it has been found that in some polymers a close correlation exists between the free radicals produced by mechanical degradation and those by high energy irradiation. The free radical spectra obtained by mechanical degradation of polymethylmethacrylate[122] and nylon 6[110] are the same as those obtained by γ irradiation of polymethylmethacrylate[123] and nylon 6[124].

SPECTRA RECORDED ON UV IRRADIATING A COURTELLE SAMPLE AT 77K

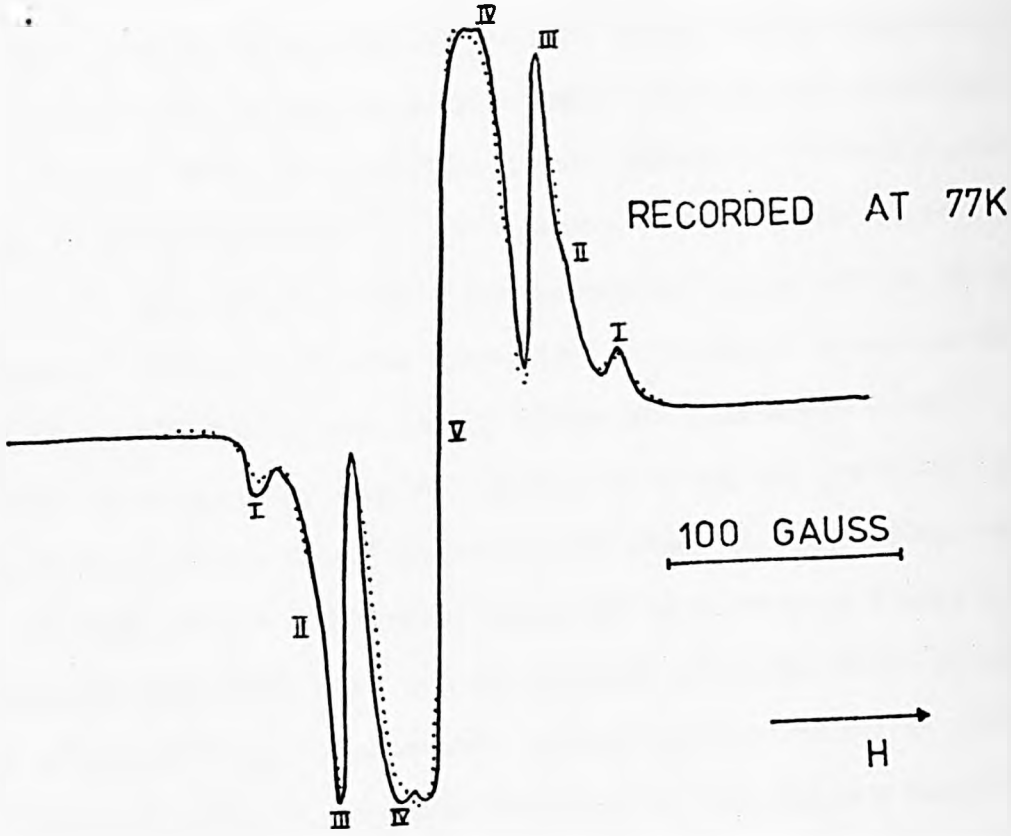

(a)

(b)

FIGURE 8.2

The fibres were UV irradiated using a low pressure mercury lamp (mineralight UV lamp) radiating predominantly at 2537Å together with some short wavelength (1800 Å) emission that was responsible for the unpleasant concentration of ozone produced when the lamp was in use. A 2 M rad doseage of electron irradiation was supplied by a Van de Graaff Accelerator.

8.3 THE UV experiment

A number of experiments were attempted. The fibres were placed in spectrosil tubes and either evacuated or left open to the atmosphere, and were irradiated at liquid nitrogen with the lamp a few mms from the dewar. In some of the initial experiments the fibres were irradiated in situ within a varian Hoii cavity having irradiation slots. However, it was found that identical results were obtained by irradiating external to the cavity in a large finger dewar, containing approximately 0.5 litres of liquid nitrogen. The samples were then quickly transferred to the smaller finger dewar, for ESR observation at liquid nitrogen.

It was found that the radicals, produced during irradiation, power saturated quite readily and to avoid such effects it was necessary to operate at less than 2 m watts power. A typical spectrum of Courtelle irradiated at liquid nitrogen is shown in Fig. 8.2 (a) together with the computed spectrum.

We also include in Fig. 8.2 (b) the spectrum obtained by irradiating with an Osram* lamp for a period of 10 hours at liquid nitrogen temperatures.

* An osram lamp emits the bulk of its radiation with wavelengths greater than 3000Å.

Generally the samples were irradiated for a period of several hours producing a marked yellow to tan colour on the exposed portion of the fibre. Similar colorations have been introduced into acrylic fibres as a result of heat treatment to less than 230°C, and have been interpreted as a conjugation of the nitrile groupings giving structures containing carbon nitrogen double bonds[23]. In our UV experiments the colouring was confined to the surface of fibres as indeed was the concentration of free radicals, which is often found to be the case with UV irradiation. It was also found that identical spectra were recorded when individual samples were irradiated either under vacuum or left open to the atmosphere.

A flow system was set up and the temperature of the sample was allowed to rise slowly from 77K. By 100K the hyperfine structure began to decay. An irreversible chemical process takes place probably by recombination of some of the free radical pairs giving non-paramagnetic species. At room temperature the whole hyperfine structure is lost within a very few minutes leaving a single resonance line having a peak to peak line width of between 16 and 18 gauss. UV irradiation of our samples at room temperature either under vacuum or open to the atmosphere resulted in a single resonance line again having a peak to peak line width of between 16 - 18 gauss and also resulted in the same coloration of the samples as before.

These results tend to imply at least two free radical species, however, it was found impossible to synthesize the spectrum using a model consisting of two radicals. A very striking feature of Fig. 8.2 is the non binomial distribution of lines I and III (approximate ratio III : I of 11 : 1) whereas one might expect a binomial distribution of intensities. From this we concluded that lines III comprise a doublet of some 87 - 88 gauss separation. Also in Fig. 8.2 there is evidence of a shoulder marked II

SPECTRA RECORDED ON UV IRRADIATING A DRALON T SAMPLE AT 77K

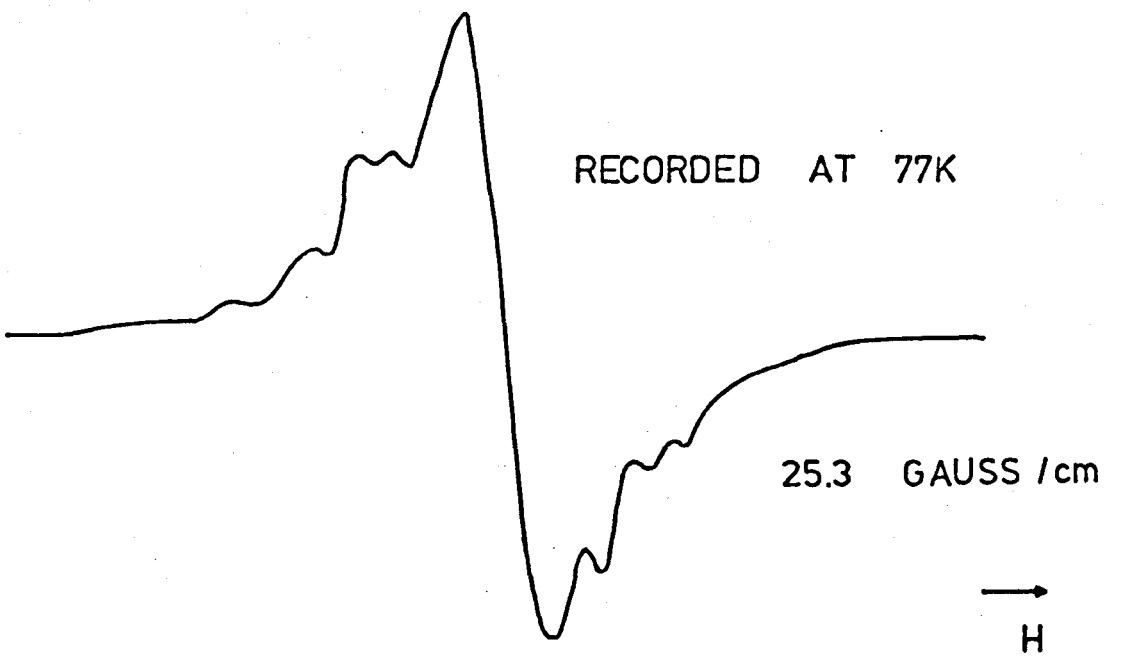

(a)

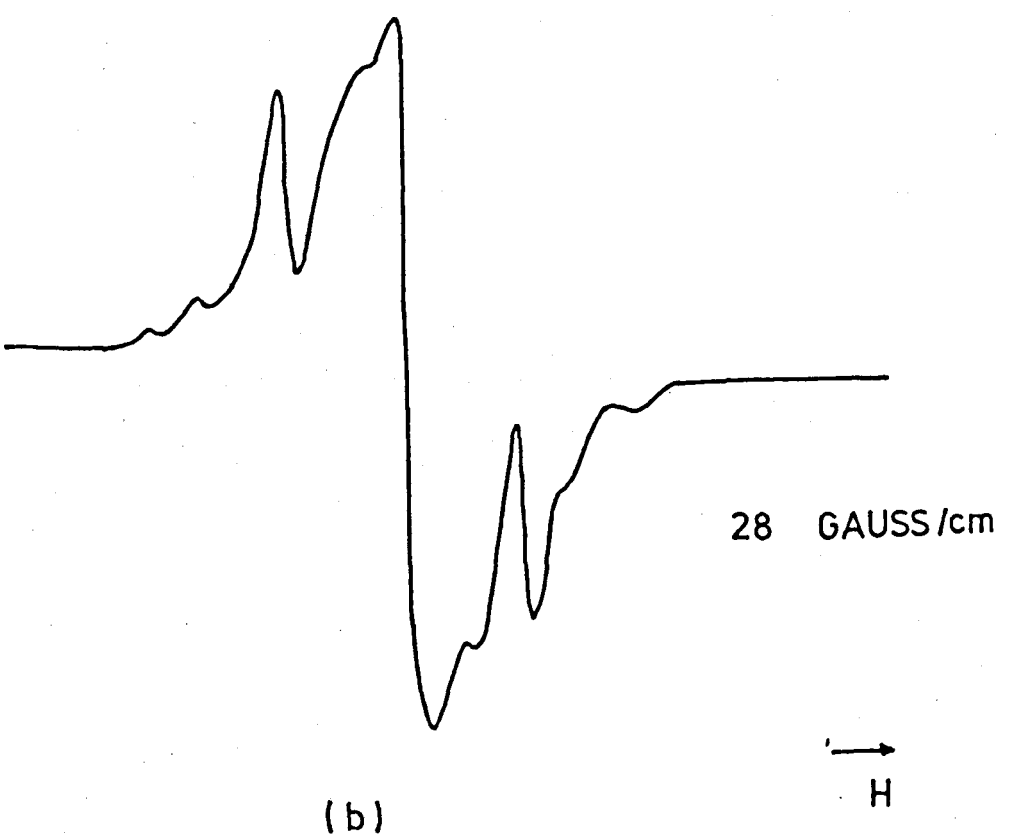

(b)

FIGURE 8.3

on each of the lines of the doublet and also we see indications of two lines marked IV. An estimate was made of the line spacing and height and it was concluded that the lines I, II, IV, IV, II, I approximated a hyperfine set having an approximate distribution 1 : 5 : 10 : 10 : 5 : 1 and possibly representing an interaction with five equivalent protons. We also notice from Fig. 8.2 that the doublet marked III appears quite narrow in relation to the bulk of the spectrum (the actual line width measures approximately 9 gauss) and yet our lines do not cross the base line of the spectrum. Similarly the lines marked I, although well removed from the main body of the spectrum, are not symmetrical about the base line indicating that there could well be a very broad fourth line. A further feature of the spectrum is the slight asymmetry of the spectrum indicative of several free radical species having slightly different g centres.

Fig. 8.3 (a) shows the ESR spectrum of Dralon T (pure polyacrylonitrile) under conditions of power saturation and one of its obvious features is that it is noticeably asymmetric. Fig. 8.3 (b) illustrates the low power spectrum and the essential difference between this and the corresponding Courtelle spectrum is the slightly increased concentration of the central line. Similar spectra were observed as a result of UV irradiation of Orlon, Acrilan and Rhodiceta. These acrylics are prepared by different manufacturers and do not contain the same degree of copolymerization, indeed Rhodiceta is a different copolymer. Rhodiceta has a pale violet silky finish and florescence was observed during irradiation. In spite of this we appear to observe very similar spectra. Crimpled fibre and fibre placed in spectrosil tube in a random fashion produced identical spectra and tend to indicate an absence of anisotropy in the ESR property of the free radical species.

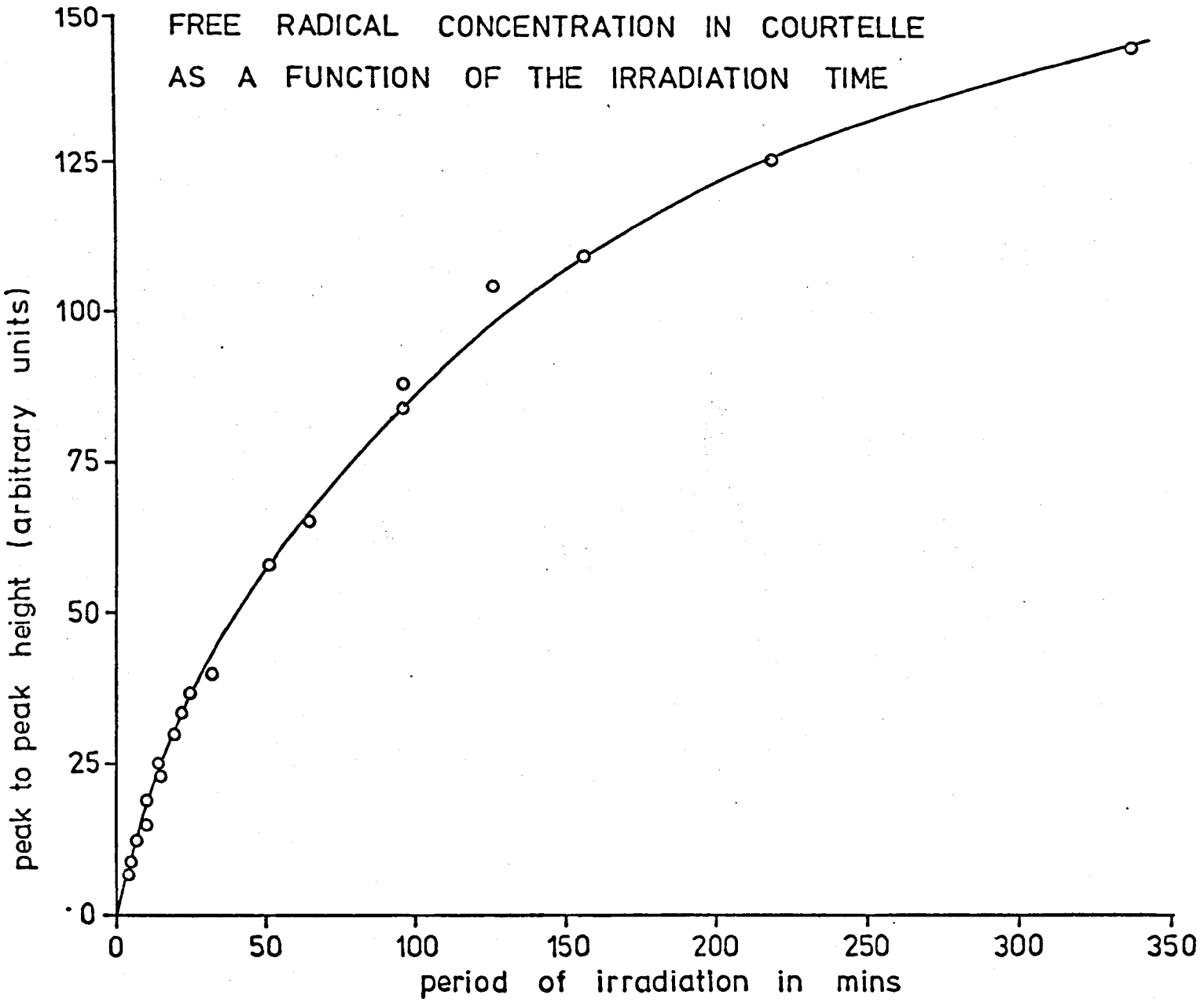
FREE RADICAL CONCENTRATION IN COURTELLE
AS A FUNCTION OF THE IRRADIATION TIME
peak to peak height (arbitrary units)
150
125
100
75
50
25
0
0
50
100
150
200
250
300
350
period of irradiation in mins

FIGURE 8.4

FREE RADICAL CONCENTRATION IN DRALON T
AS A FUNCTION OF THE IRRADIATION TIME

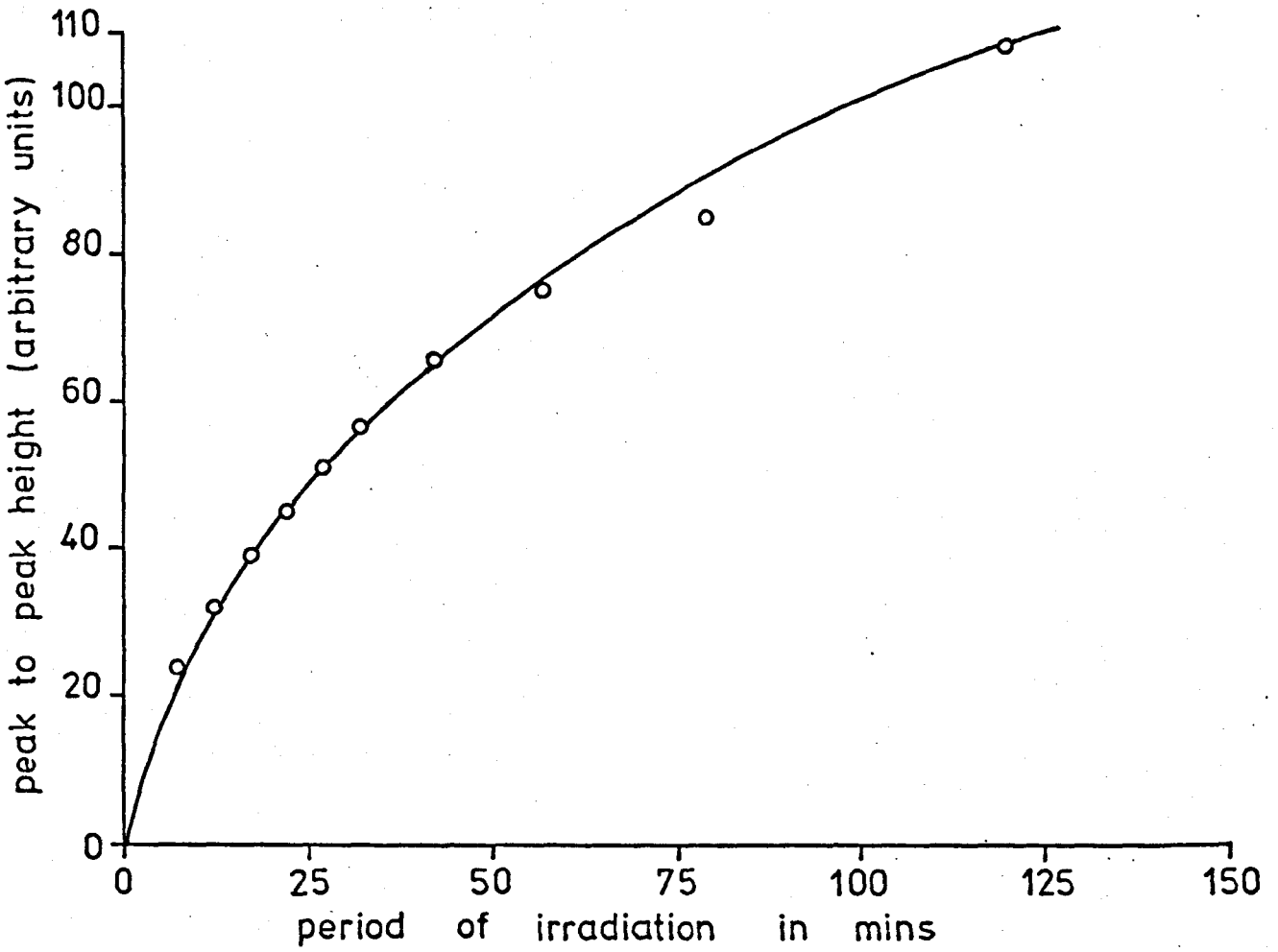

FIGURE 8.5

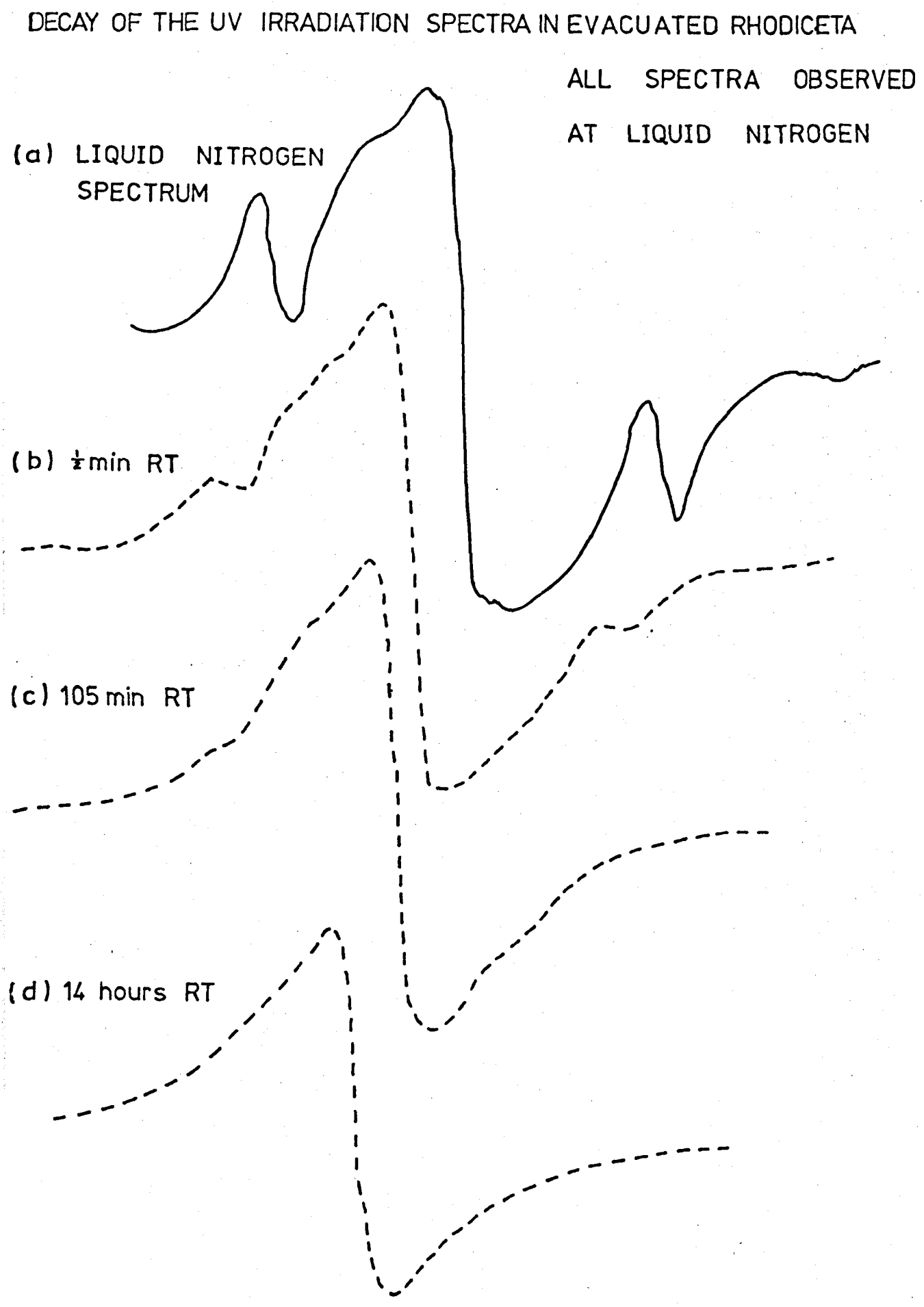
DECAY OF THE UV IRRADIATION SPECTRA IN EVACUATED RHODICETA
ALL SPECTRA OBSERVED AT LIQUID NITROGEN
(a) LIQUID NITROGEN SPECTRUM
(b) ½ min RT
(c) 105 min RT
(d) 14 hours RT

FIGURE 8.6

ELECTRON IRRADIATION SPECTRA (a) DRALON T (b) COURTELLE

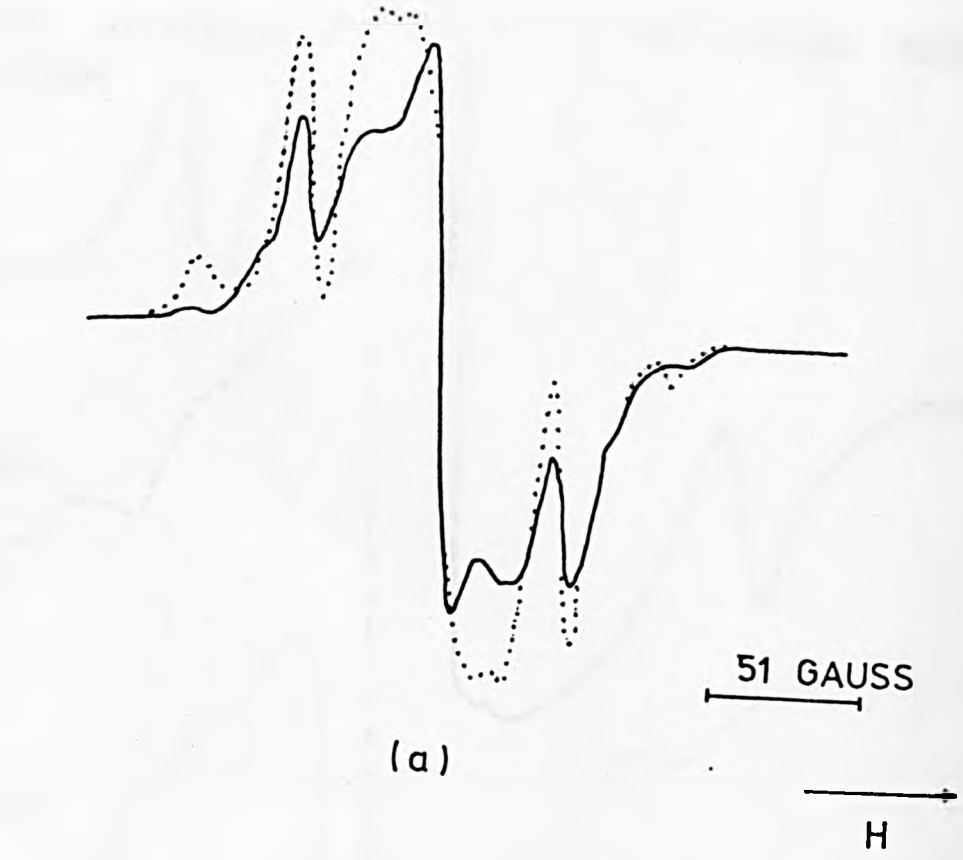

(a)

(b)

FIGURE 8.7

Figs. 8.4 and 8.5 show the respective concentration of free radicals accumulated in Courtelle and Dralon T as a function of irradiation time.

Fig. 8.6 (a), (b), (c), and (d) show the spectra obtained by UV irradiation at liquid nitrogen of an evacuated sample of Rhodiceta together with the spectra obtained after ½ min, 105 min and 14 hours at room temperature respectively. An immediately obvious feature is the rapid loss of hyperfine structure at room temperature while the central line decays more slowly. Very similar effects were observed with the other acrylics. On opening each of the spectrosil tubes containing the irradiated samples, a noticeable odour was released.

8.4 Electron irradiation results.

A 2 M rad dose was given to each of the samples using a Van de Graaff Accelerator. This was provided in 17,000 pulses at a distance of two metres, each pulse containing 55.5 rads. An eight cms square window was cut in a compressed polystyrene bucket. The portion removed was replaced by a similar sized piece made of low density polystyrene and held in position by an Araldite resin. The window was lightly greased so as to prevent excessive seepage when the bucket was filled with liquid nitrogen. During the irradiation experiment the electrons passed relatively unattenuated through the window. Evacuated and unevacuated samples to be irradiated under liquid nitrogen were contained in spectrosil quartz tubes and arranged on a perspex platform behind the polystyrene window. A similar arrangement of samples to be irradiated at room temperature were held by insulating tape on the outside of the bucket.

Fig. 8, 7 (a) and 8.7 (b) show the respective spectra recorded after irradiating Dralon T and Courtelle at room temperature. For comparison the spectrum obtained on irradiating Courtelle with UV at 77K is shown

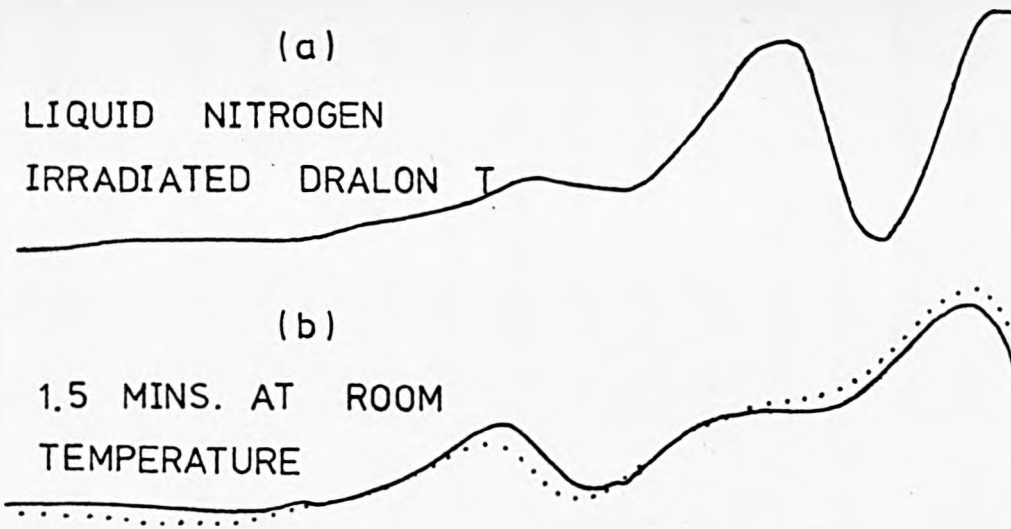
DRALON T ELECTRON
(a)
LIQUID NITROGEN
IRRADIATED DRALON T
(b)
1.5 MINS. AT ROOM
TEMPERATURE

FIGURE

IRRADIATION SPECTRA

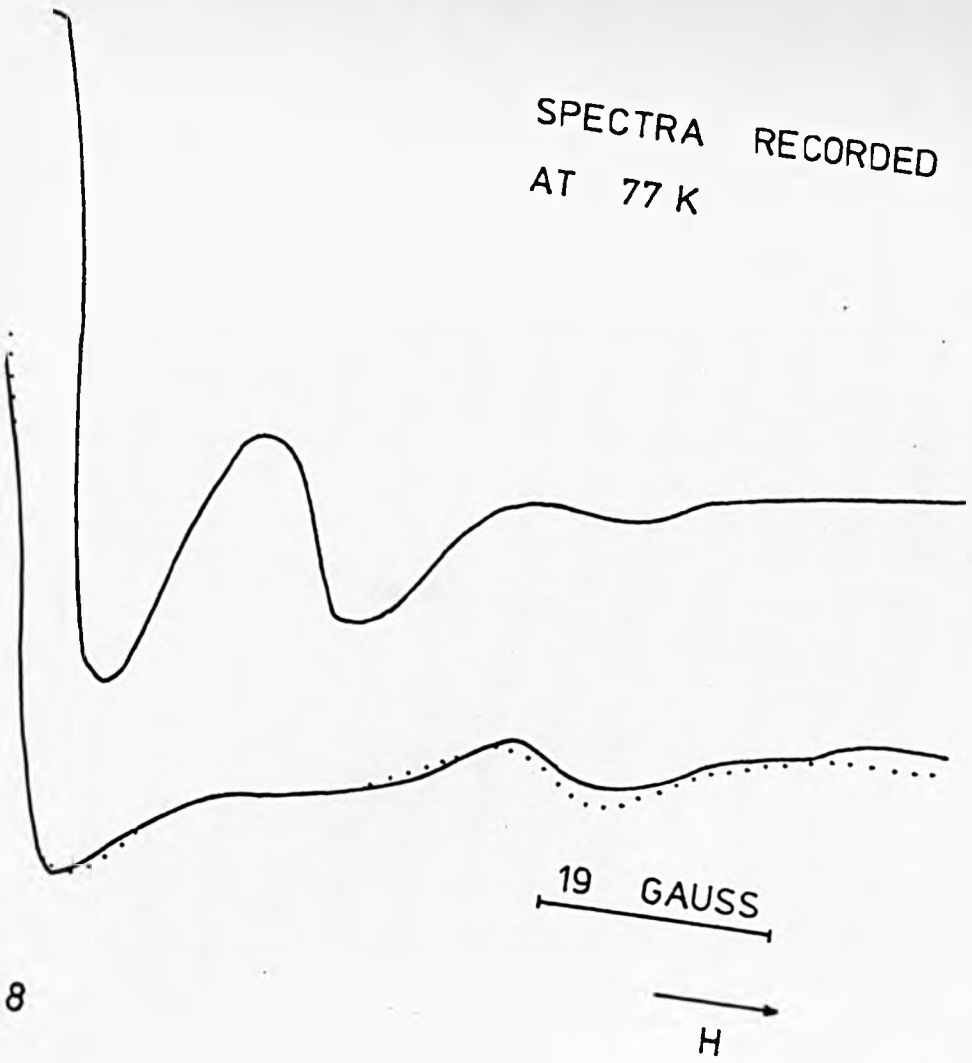

8.8

RHODICETA (EVACUATED) ELECTRON

AT LIOUID NITROGEN

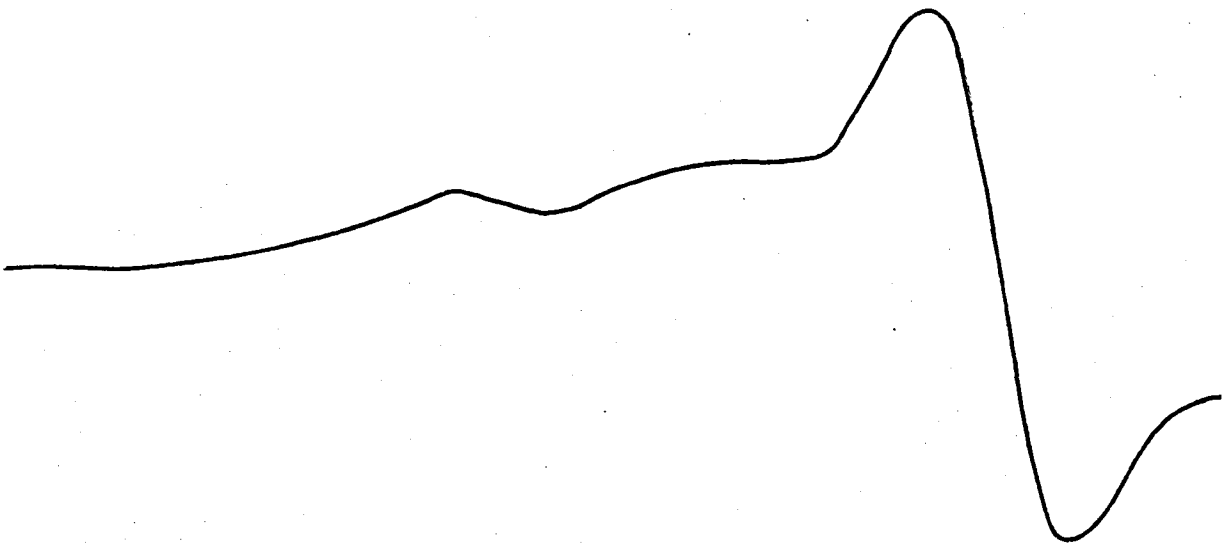

FIGURE 8.9

IRRADIATED

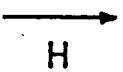

superimposed. Clearly these spectra show remarkably similar features and any model proposed should be capable of explaining all of them. The power saturation behaviour is very similar, and within the limits of experimental error, the g-value of the electron and UV irradiated spectra seem to be the same having the value 2.0021 ± 0.0003 which is very close to the free spin value.

Fig. 8.8 (a) shows the spectrum obtained by electron irradiating Dralon T at liquid nitrogen and Fig. 8.8 (b) illustrates the corresponding signal agter 1½ mins at room temperature. There appears to be an unstable doublet which decays irreversibly on raising the temperature of the sample. Evidence of this doublet was obtained in all acrylics - with the exception of Rhodiceta (See Fig. 8.9) - on electron irradiating under liquid nitrogen whether or not the samples were evacuated. Using a flow system the doublet first begins to decay at 100K, and appears to reveal the presence of a broad line. It was found impossible to computer fit the liquid nitrogen irradiation spectrum without in fact assuming the broad line to be present, and hence it would seem unlikely that the doublet decayed to a broad singlet.

The rather unstable doublet observed on electron irradiating at 77K could possibly arise from bond scission:-

$$-CH_2-\underset{\underset{CN}{|}}{CH}\;+\;CH_2-\underset{\underset{CN}{|}}{CH}-$$

$$-CH_2-\underset{\underset{CN}{|}}{\overset{\bullet}{C}H}\qquad \overset{\bullet}{C}H_2-\underset{\underset{CN}{|}}{CH}-$$

I II

Radical (I) could then possibly rearrange to give

$$-CH_2-C\equiv C-\overset{\bullet}{N}H$$

resulting in a doublet. Radical II could represent the broad line some 59 gauss wide. The doublet is unstable as evidenced by the decay on raising the temperature to 100K, and to be observed at all, it requires high

FREE RADICAL DECAY IN A SAMPLE OF ACRILAN

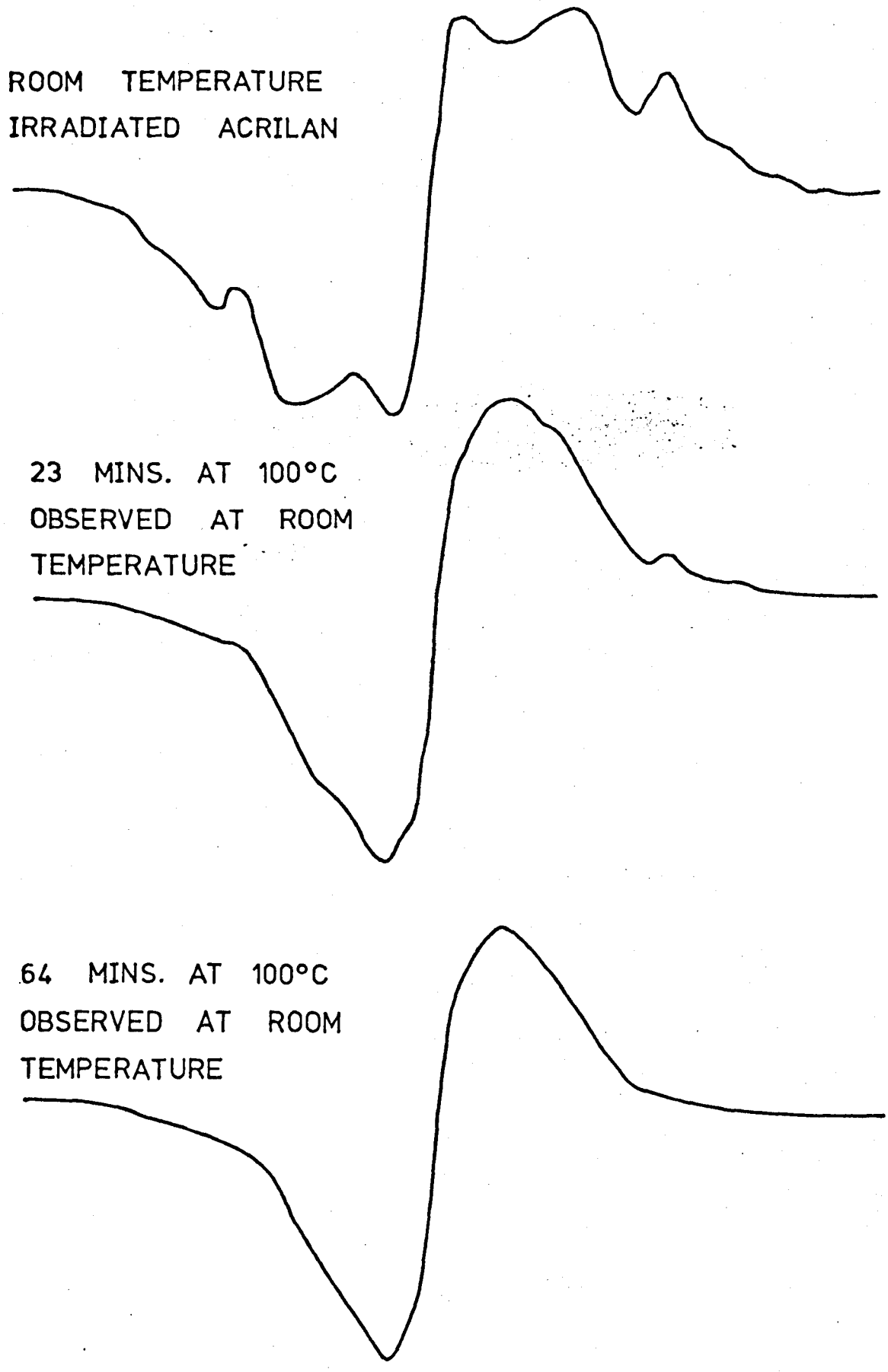

FIGURE 8.10

energy irradiation giving the fragments sufficient excess kinetic energy on separation to isolate a proportion of radicals of type I preventing their decay. However, on raising the temperature of the sample the radical could remove a proton from the polymer chain.

$$-CH_2-C\equiv C-\dot{N}H + -CH_2-\underset{\underset{CN}{|}}{CH}-CH_2-\underset{\underset{CN}{|}}{CH}-$$

$$-CH_2-C\equiv C-NH_2 + -CH_2-\underset{\underset{CN}{|}}{CH}-\dot{C}H-\underset{\underset{CN}{|}}{CH}-$$

The spectrum obtained as a result of electron irradiating Courtelle at room temperature decays only slowly on storing the sample at room temperature. After thirty minutes at room temperature the spin concentration decreases by about 12% and after a total of five days at room temperature the total decay of spin concentration measured under 20%.

When such samples were recorded as a function of storage time at 100°C, the glass transition temperature[120], the rate of decay was more noticeable as can be seen in Fig. 8.10. The hyperfine structure disappears most quickly and after 23 mins it has all but disappeared. This is followed by a general narrowing of the spectrum leaving a single resonance line which slowly decays by 75% after a further six hours at 100°C. A comparative study of Rhodiceta showed that the hyperfine structure is lost after 45 mins at 100°C and the single line takes 23 hours to decay to 25%. It was found that the overall pattern of decay extended throughout the series of acrylics.

As we have already noted the spectrum obtained by electron irradiating Dralon T at liquid nitrogen temperature includes a doublet which rapidly decays on observing the ESR spectrum at room temperature

FREE RADICAL DECAY IN A SAMPLE OF DRALON T

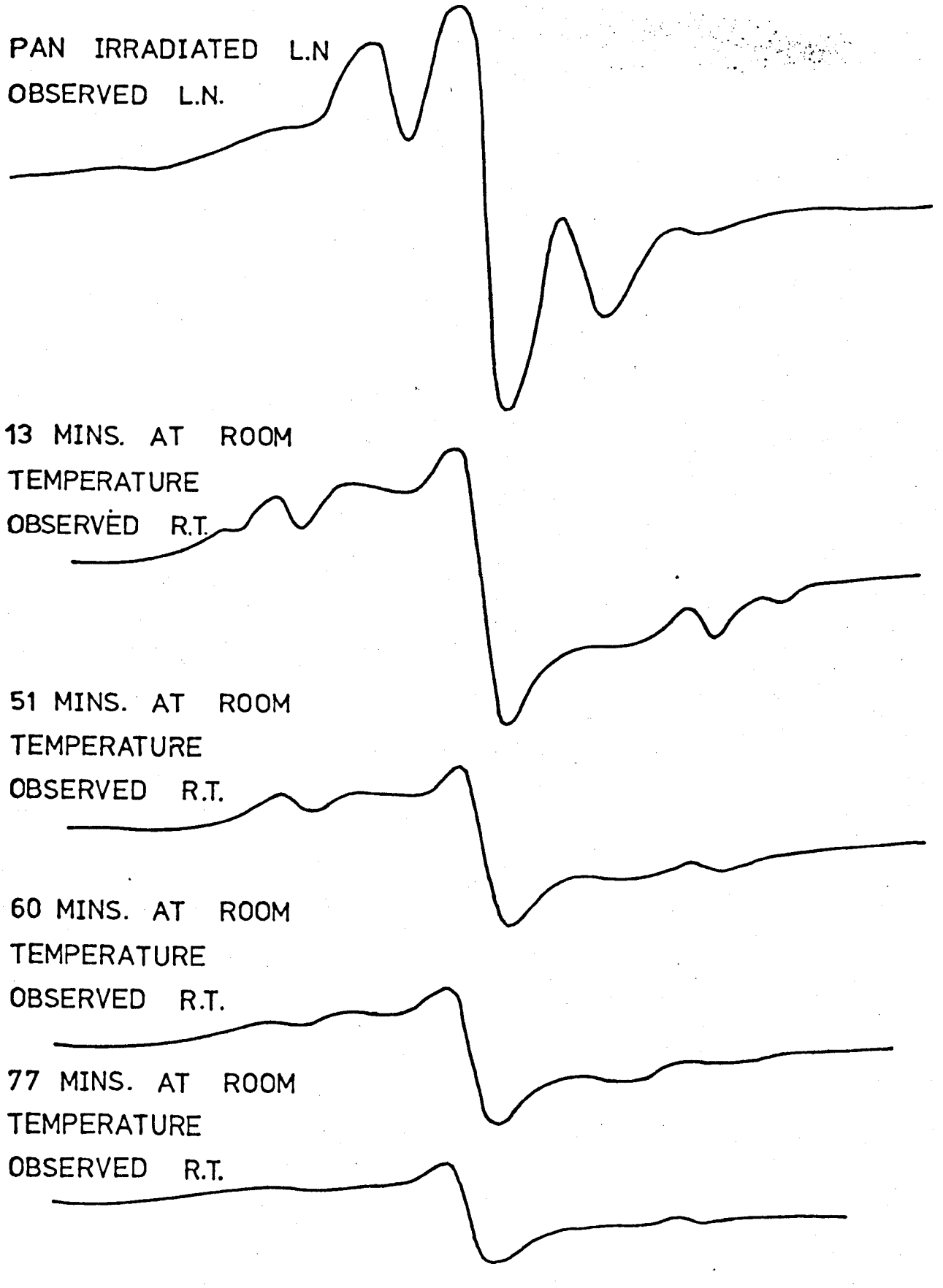

FIGURE 8.11

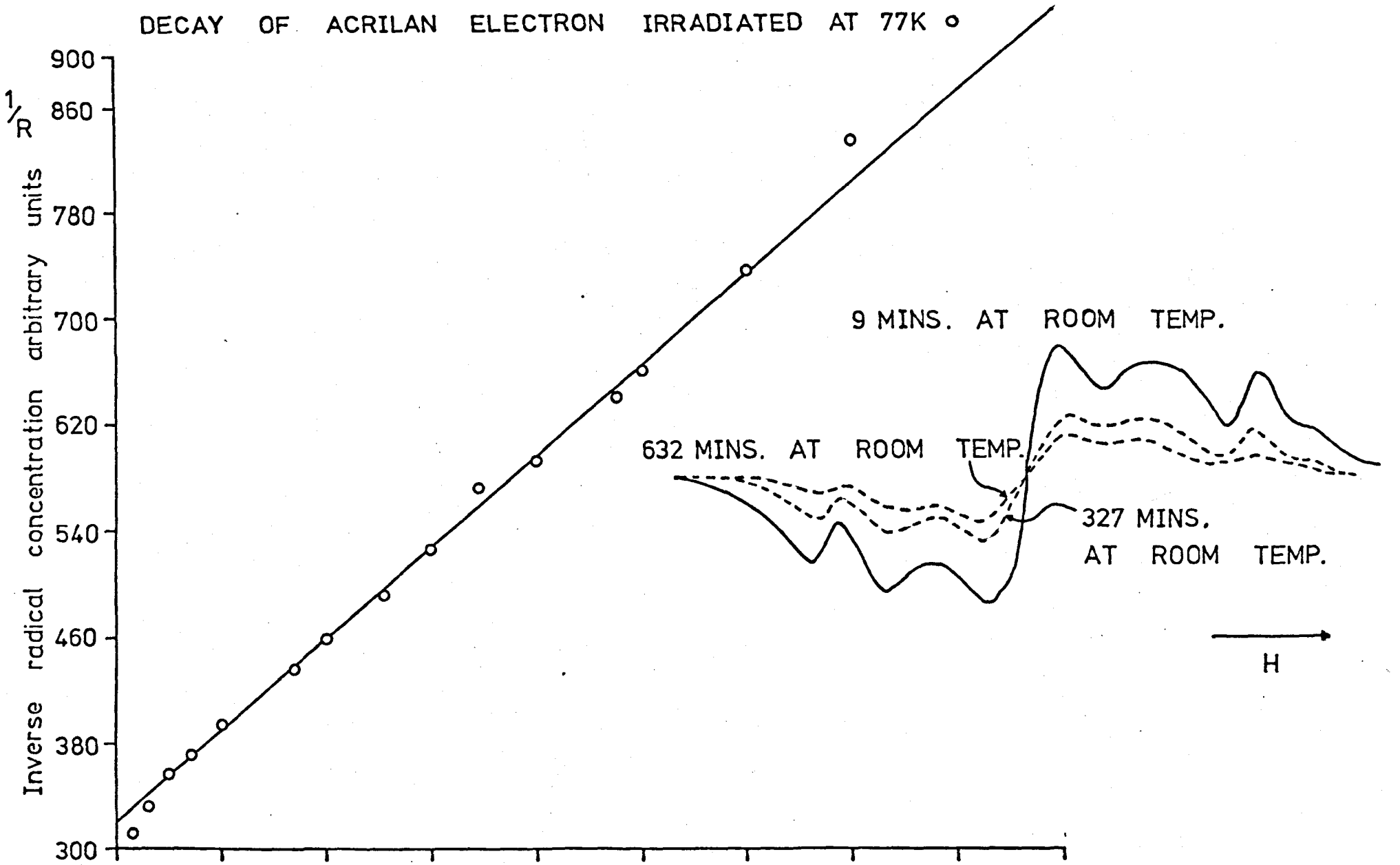
DECAY OF ACRILAN ELECTRON IRRADIATED AT 77K
1/R
Inverse radical concentration arbitrary units
900
860
780
700
620
540
460
380
300
0
80
160
240
320
400
480
560
640
720
mins at R.T.
9 MINS. AT ROOM TEMP.
632 MINS. AT ROOM TEMP.
327 MINS.
AT ROOM TEMP.
H

FIGURE 8.12

	SPIN CONCENTRATION spin/gm × 10^{17}
COURTELLE	10
DRALON T	20
ORLON	7
ACRILAN	5

TABLE 8.1

THE EFFECT OF UV IRRADIATION ON A PREVIOUSLY ELECTRON IRRADIATED COURTELLE SAMPLE

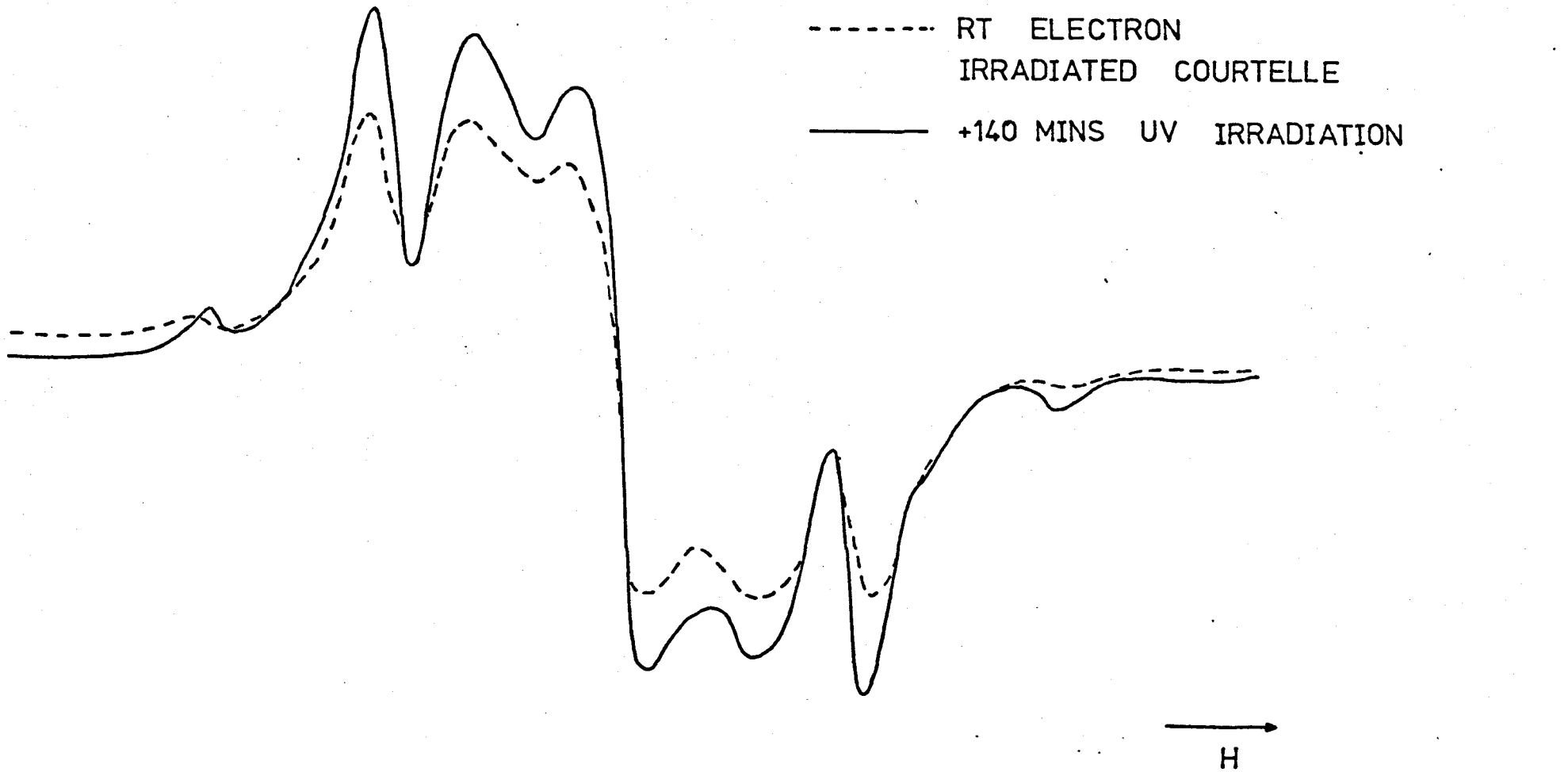

FIGURE 8.13

see Fig. 8.11. After this initial decay the spin concentration decays by a further 85% after twenty hours. Orlon decays similarly to 14% after twenty four hours, and in both samples the envelope of the spectrum is retained during the period of decay.

Fig. 8.12 shows the inverse radical concentration of Acrilan (electron irradiated at liquid nitrogen) plotted against the time in minutes for which the sample was maintained at room temperature. The rate of decay would appear to be second order, a second-order rate being represented by the equation

$$\frac{1}{R} - \frac{1}{R_o} = Kt$$

where R is the free radical concentration and t is the time,
K is the second order constant.
Also shown are three of the spectra obtained after different periods of time at room temperature and once again the overall envelope appears to be retained as the radicals decay.

Electron irradiation of the acrylics produced radicals that did not appear to be confined to the surface of the fibres, and an estimate was made of the spin concentration produced on irradiating under vacuum at 77K (See Table 8.1).

In the usual way the spin concentration was estimated (see section 5.4) against an equivalent volume of carbon standard (powdered pitch in chalk sample containing 5×10^{17} spin/gram). Powdered Mn^{2+} in MgO being used as a secondary standard to monitor 'Q' changes. A numerical Runge Kutta Quartic double integration program was used.

A further interesting experiment that was carried out was the UV irradiation at 77K of some of the electron irradiated samples. Fig 8.13 shows the effect of 140 mins UV irradiation on a Courtelle sample that had been electron irradiated at room temperature. Fig. 8.14 illustrates the

THE EFFECT OF UV IRRADIATION ON A PREVIOUSLY ELECTRON IRRADIATED ORLON SAMPLE

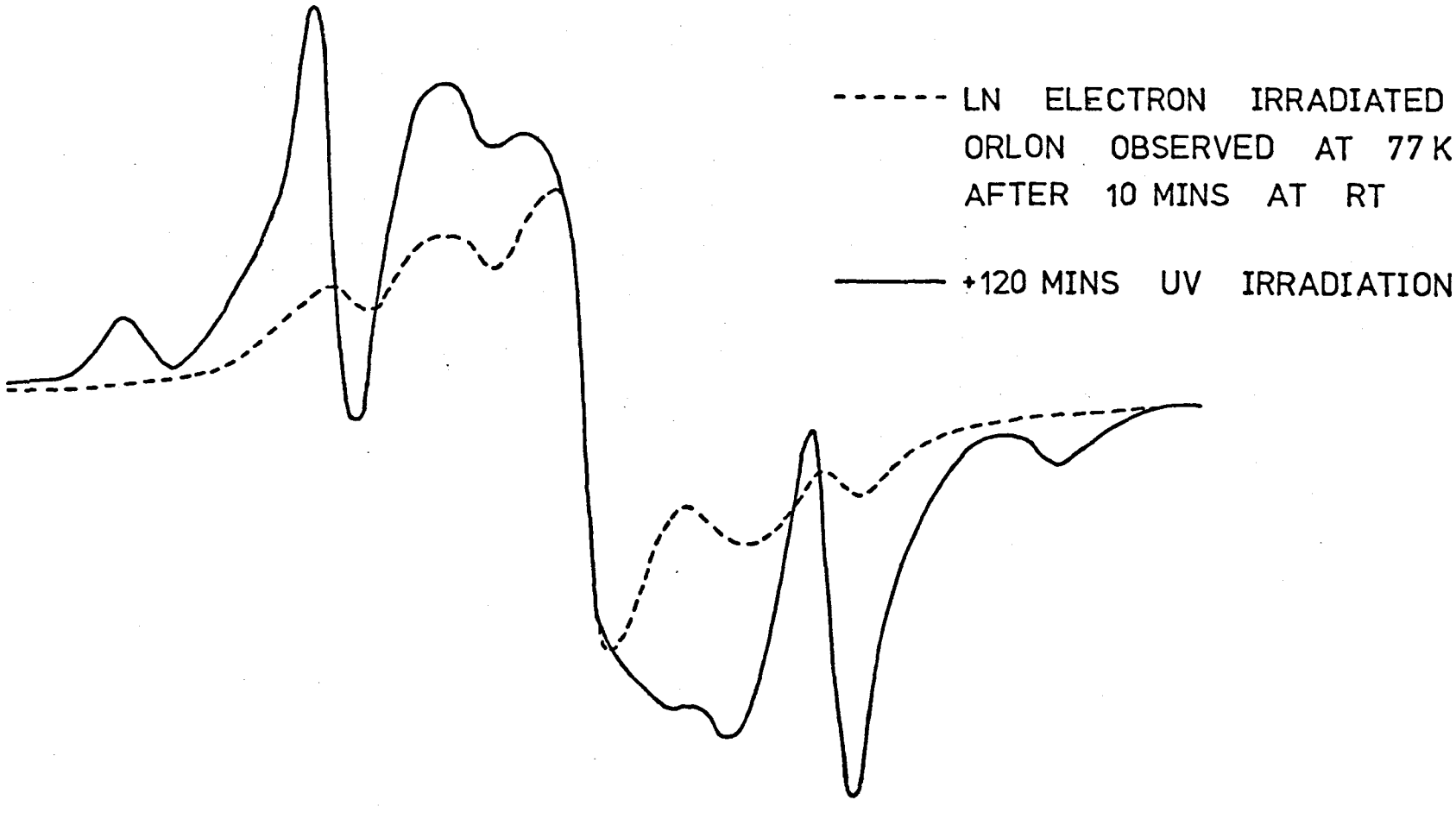

FIGURE 8.14

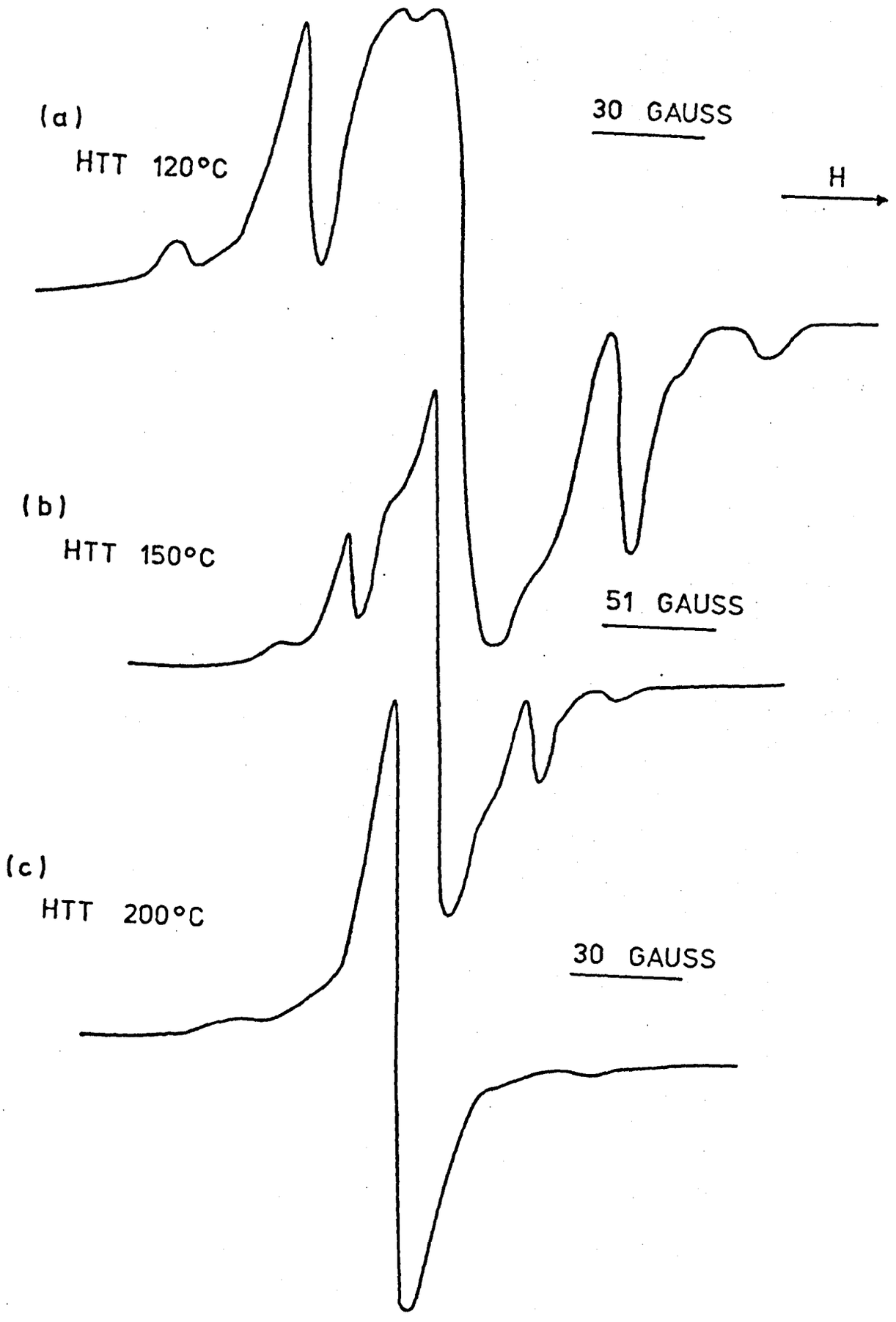
UV IRRADIATION SPECTRA -CHARRED COURTELLE
(a)
HTT 120°C
30 GAUSS
H
(b)
HTT 150°C
51 GAUSS
(c)
HTT 200°C
30 GAUSS

FIGURE 8.15

effect of 2 hours UV irradiation at 77K on an Orlon sample that had been electron irradiated at 77K and then taken to room temperature for 10 minutes.

As we have already stated the effect of low temperature heat treatment has been shown to result in the formation of carbon-nitrogen double bonds and ultimately to lead to nitrile 'zipping' (See section 3.2) giving stable ring structures. A further experiment that we considered was the effect of UV and electron irradiation on partially carbonized samples. Irradiation treatment has less effect as the heat treatment is increased. No irradiation signal was observed on irradiating fibres that had been heat treated in excess of 200°C.

Fig. 8.15 (a) and (b) and (c) illustrate the effect of UV irradiation at 77K on a Courtelle sample previously heat treated to 120°C, 150°C and 200°C respectively.

8.5 The computer synthesis

We have shown so far that identification of the radicals is complicated by broad overlapping lines. In our model all lines in the spectrum of a given radical are assumed to have the same width. Although one might expect Gaussian line shapes from a random distribution of radicals, in our model both Lorentzian and Gaussian functions were given consideration.

If we consider the first derivative Gaussian presentation the n^{th} line of the spectrum of a given radical takes the form:

$$y_G = \frac{-BA_n(H-H_o)}{\sigma \exp(-0.5)} \exp\left\{-\frac{1}{2}\left(\frac{H-H_o}{\sigma}\right)^2\right\}$$

and the corresponding Lorentzian

$$y_L = \frac{-BA_n(H-H_o)\sigma^3}{\left[0.75\sigma^2 + (H-H_o)^2\right]^2}$$

See Fig. 2.6 for an interpretation of certain of the parameters in terms of the peak to peak height and width.

where An is the binomial coefficient of the n^{th} component line

where B is the normalising parameter which adjusts the absolute amplitude of the computed spectrum to the orbitrary amplitude of the experimental data.

where H is the magnetic field strength

where Ho is the centre of symmetry of the spectrum of a given radical

where σ is the line width.

If one or more radicals exist the spectrum observed will merely be given by the superposition of the individual lines.

If the unpaired electron interacts with non-equivalent nuclei and produces a primary and a secondary splitting then this must be accommodated into the theory:

$$y_G = \sum_{n=0}^{N-1} \sum_{m=0}^{M-1} \frac{-BA_{mn}(H - E_{mn})}{\sigma \exp(-0.5)} \exp\left\{-\frac{1}{2}\left(\frac{H - E_{mn}}{\sigma}\right)^2\right\}$$

$$y_L = \sum_{n=0}^{N-1} \sum_{m=0}^{M-1} \frac{-BA_{mn}(H - E_{mn})\sigma^3}{\left[0.75\sigma^2 + (H - E_{mn})^2\right]^2}$$

where $$E_{mn} = \left[n - \frac{N-1}{2}\right]b_1 + \left[m - \frac{M-1}{2}\right]b_2$$

where b_1 is the primary hyperfine splitting parameter

where b_2 is the secondary hyperfine splitting parameter

where N is the number of lines of primary splitting

where M is the number of lines of secondary splitting

where Amn = Am x An = relative amplitude of $(mn)^{th}$ line

If more than one radical is present then we will have a set of terms like those above for each radical. Thus for a spectrum arising from r radicals the spectrum will be given by:

$$y_G = \sum_{q=1}^{r} \sum_{n=0}^{N_q-1} \sum_{m=0}^{M_q-1} -\frac{B_q A_{mnq}(H - E_{mnq})}{\sigma_q \exp(-0.5)} \exp\left\{-\frac{1}{2}\left(\frac{H - E_{mnq}}{\sigma_q}\right)^2\right\}$$

$$y_L = \sum_{q=1}^{r} \sum_{n=0}^{N_q-1} \sum_{m=0}^{M_q-1} \frac{-B_q A_{mnq} (H - E_{mnq}) \sigma_q^3}{\left[0.75\sigma_q^2 + (H - E_{mnq})^2\right]^2}$$

where $E_{mnq} = \left[n - \frac{N_q - 1}{2}\right] b_{1q} + \left[m - \frac{M_q - 1}{2}\right] b_{2q} + H_{oq}$

where Hoq is the centre for the spectrum of the q^{th} radical.

For any particular Nq, Mq and r we can obtain approximate values for the parameters b_{1q}, b_{2q}, Hoq, Bq and σq from the experimental spectrum and a computer program was written to synthesize Y_G and Y_L using these values. A plotter output being selected to enable a direct comparison with the experimental presentation.

Marquardt et al.[125] and others[126] have used a non-linear least squares algorithm* written by Marquardt[127] to obtain the best fit to the experimental spectra obtained as a result of irradiation damage. (Although the routine has a far wider application).

For a given choice of parameter the subroutine E04GAF (See note below) finds the minimum of the sum of squares of m non-linear functions, or residuals, each of n variables.

i.e. $S(\underline{x}) = \underline{f}^T \underline{f} = \sum_{i=1}^{m} \left[f_i(x_1, x_2 \text{-----} x_n)\right]^2 \quad m \geq n$

where $x_{i\text{---}n}$ are the n experimental parameters and m is the number of data points taken from the spectrum and the function f_i represents the residual between the calculated function value y_G^c and the experimental value at the i^{th} data point y_G^i

$$f_i = y_G^c - y_G^i$$

* This algorithm is found in the Nottingham Algorithm Group Library Manual routine E04GAF DOCUMENT NO 427 THIS IS AVAILABLE AS A SUBROUTINE E04GAF ON LINK WITH THE MANCHESTER COMPUTER.

The Jacobian matrix of the first partial derivatives of the functions $J_{ij} = \frac{\partial f_i}{\partial x_j}$ is required and the user simply supplies subroutines to calculate this and the value of their functions f_i for any set of values of the n variables. The method is iterative and at any point $\underline{x}$ given a parameter $\lambda > 0$ it is necessary to find the correction $\underline{\delta}$ to yield a new sum of squares $S(\underline{x}+\underline{\delta})$ less than the previous sum $S(\underline{x})$; this is found by solving for $\underline{\delta}$

$$(J^T J + \lambda D)\underline{\delta} = -J^T f$$

where D is a diagonal matrix $D_{jj} > 0 \quad j = 1,n,1$

The experimental chart was digitised using the 'D' Mac device the information being outputed on paper tape.

8.6 The interpretation and discussion of the irradiation results.

We have obtained sufficient experimental evidence to suggest that several radical species are produced on irradiating at low temperatures with either UV or fast electrons. In particular we are of the opinion that the ESR spectrum obtained by UV irradiation arises from four radicals. Even so before attempting a computer fit based on a four radical model, various two and three radical models were tried, none of which proved acceptable. The two radical models failed primarily because of the failure to fit the non-binomial ratio of lines III : I (See Fig. 8.2) which from the experimental chart measures approximately 11 : 1. The lines marked III were taken to comprise a doublet in all of the three radical models. The computed spectrum had the overall appearance of the experimental spectrum however it could not be said to be a good fit.

Fig. 8.2. shows the computer fit using a four radical model to the spectrum obtained by UV irradiating a Courtelle sample at liquid

ELECTRON IRRADIATED COURTELLE
(OPEN TUBE)

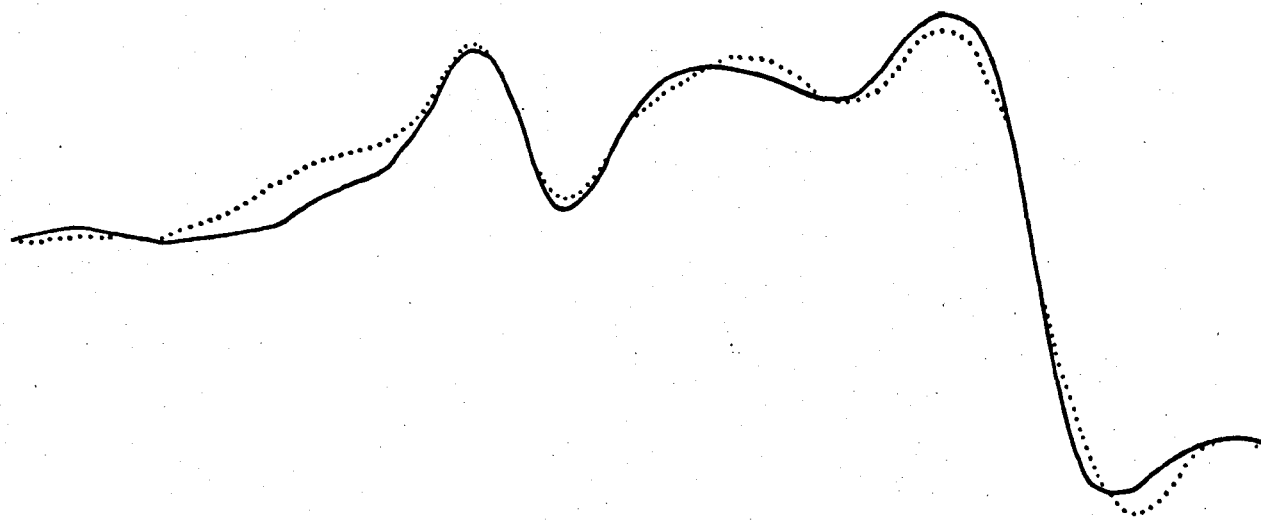

FIGURE 8.16

— ROOM TEMPERATURE

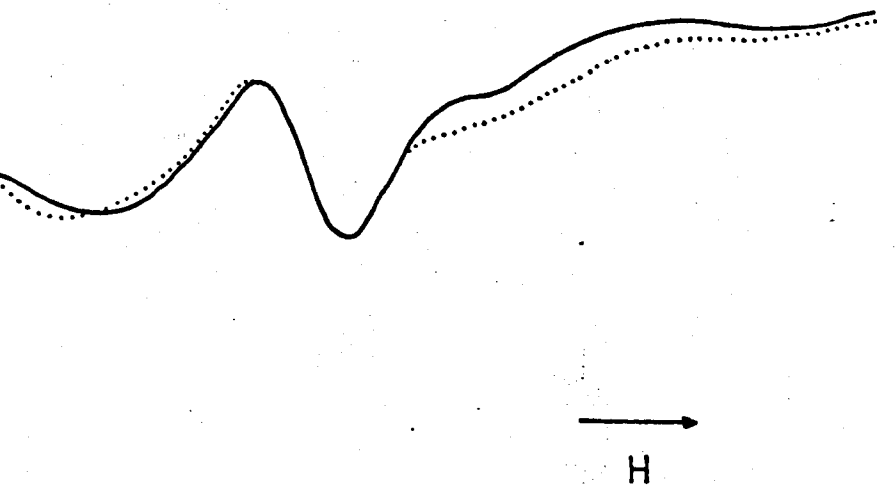

nitrogen. Similarly the spectrum obtained by electron irradiating Courtelle at room temperature was fitted (See Fig. 8.16) using an identical model to the extent that only the concentration of radical species was altered.

The construction of the four radicals that comprise figure 8.2 proceeded as follows:

1st RADICAL.

Chosen to represent the hyperfine lines I, II, IV, IV, II, I of the set n=2 m=5. The best fit being obtained using a primary doublet splitting of 22 gauss, and a secondary quartet splitting of 32 gauss. The peak to peak line width of each line was 13.3 gauss.

2nd RADICAL.

Represents the doublet lines III n=2 m=1 having a hyperfine separation of 87-88 gauss and a peak to peak line width of 10 gauss.

3rd RADICAL.

Represents the central line marked V . The peak to peak line width is 16 gauss, and this was obtained directly from the chart.

The single line observed by allowing the sample to warm up to room temperature, and also the single line obtained by irradiating at room temperature, gave a line width of 16 gauss.

4th RADICAL.

This represents the main underlying broad line having a peak to peak line width of 59 gauss. The approximate line width was obtained from the spectrum observed on electron irradiating a sample of Dralon T at liquid nitrogen and then allowing the sample to warm up to room temperature for a few minutes before final ESR observations at liquid nitrogen. The line is also readily observed in Rhodiceta electron irradiated at liquid nitrogen.

The results of the 1st radical suggest an interaction consisting of four equivalent protons and one non-equivalent proton. By comparison with the irradiation results of related polymers the radical is almost certainly $-CH_2 - \dot{C}H - CH_2 -$. However, due to the α proton we would expect anisotropic hyperfine coupling and yet there is no evidence for this. Indeed although we tended to observe spectra with the magnetic field perpendicular to the axis of the fibre, an identical spectrum was obtained when the irradiated samples were placed in the finger dewar with their axes arranged in a random fashion. Since the radical is isotropic then we must assume that the α proton adopts randomly all directions with respect to the fibre axis, clearly, this would be the situation in the amorphous regions of the fibre. However, Peacock and Khan[128] in a private communication to Spencer - Smith[115] noted from their birefringence results that increasing the draw ratio in acrylics increases the preferred orientation but this is offset somewhat by an increased randomisation of the CN grouping along the chain.

Since the proton is attached to the same carbon atom as the CN group then by mutual interaction of two highly polar groups, the proton could be randomised along the chain.

Both Libby et al.[129] and Kiselev et al.[13] studied the spectra of stretched PE. Kiselev et al. studied the radical $- CH_2 - \dot{C}H - CH_2 -$ as a function of the orientation of the applied magnetic field. They found as expected that with the magnetic field (Ho) parallel to the axis of orientation the spectrum was a sextet 1:5:10:10:5:1, and perpendicular to the axis gave a ten line spectrum having binomial distribution 1:1:4:4:6:6:4:4:1:1. They estimated the isotropic part of the α and the β protons to be 22.4 ± 2.8 and 33.1 ± 0.4 gauss respectively. These compare

with our isotropic α and β proton couplings of 22.0 and 32.0 gauss respectively.

Libby et al.[129] presented the following values for the coupling constants in the principal directions.

Ho $\perp^{r}$ to the axis

$$a_{H_\beta} = 30 \text{ gauss} \quad a_{H_\alpha} = 14 \text{ gauss} \quad \Delta H_{msl} = 11.5 \text{ gauss.}$$

and with Ho $\parallel$ to the axis

$$a_{H_\beta} = 30 \text{ gauss} \quad a_{H_\alpha} = 32.5 \text{ gauss} \quad \Delta H_{msl} = 8.5 \text{ gauss}$$

which give $$a_{H_\alpha \text{ isotropic}} = \frac{2\,a_{H_{\alpha\perp}} + a_{H_{\alpha\parallel}}}{3}$$

$$= 20 \text{ gauss}$$

$$a_{H_\beta \text{ isotropic}} = 30 \text{ gauss}$$

which compare with our results

$$a_{H_\alpha} = 22.0 \quad a_{H_\beta} = 32 \text{ gauss} \quad \Delta H_{p\text{-}p} = 13.3 \text{ gauss.}$$

The colouring produced when irradiating at room temperature and at liquid nitrogen would seem to be an indication of conjugation possibly resulting in polyene structures. Again this result is typical of similar polymers. The greater the extent of the conjugation the greater will be the number of hyperfine interactions and the smaller the interactions until the lines coalesce into a singlet. The central 16 gauss wide singlet that we observe is thought to arise from such a radical having the structure.

$$- CH = CH - CH = CH - \dot{C}H(CN) - CH_2 -$$

The fourth line is difficult to observe and to explain. However, we have already suggested that the radical could arise from chain scission amd having the structure

$$\cdot CH_2 - \underset{\underset{CN}{|}}{\overset{\overset{H}{|}}{C}} -$$

A single line resulting from overlap of broad hyperfine lines. We have fitted the room temperature electron irradiated Courtelle spectrum and its liquid nitrogen UV irradiated spectrum with the same mathematical model. It would seem logical therefore to assume the presence of the broad line in the UV spectrum since it is clearly established in the electron irradiated spectrum.

The doublet with 87-88 gauss hyperfine splitting proposes some difficulty and we have to compare our results with those of Cochran et al.(131) for the radical H_2CN. The radical being prepared by photolysis of hydrogen cyanide and acetylene using a low pressure mercury lamp emitting 2537 Å UV radiation. They proposed the structure $H_2\dot{C}N$ and observed a triplet of triplets the main triplet splitting of 87.4 gauss arising from the β proton coupling. The mechanism of interaction being hyperconjugation and it was proposed that theunusually large β proton coupling arose because the short carbon nitrogen double bond forces the $p(\pi)$ orbital close to the CH σ-orbital resulting in considerable overlap. The β protons being almost perpendicular to the nodal plane.

The suggested mechanism by which the $- CH_2 - \dot{C}H - CH_2 -$ allkyl radical could be formed is by removal of the (CN) grouping

$$- CH_2 - \underset{\underset{CN}{|}}{\overset{\overset{H}{|}}{C}} - CH_2 \quad - \underset{\underset{CN}{|}}{\overset{\overset{H}{|}}{C}} - CH_2 -$$

$$- CH_2 - \dot{C}H - CH_2 - \underset{\underset{CN}{|}}{\overset{\overset{H}{|}}{C}} - CH_2 - + \dot{C}N^-$$

The $(\dot{C}N)$ radical could abstract a proton from a neighbouring chain resulting in the evolution of hydrogen cyanide gas and initiating the conjugated double bond system leading to the formation of the polyene radical.

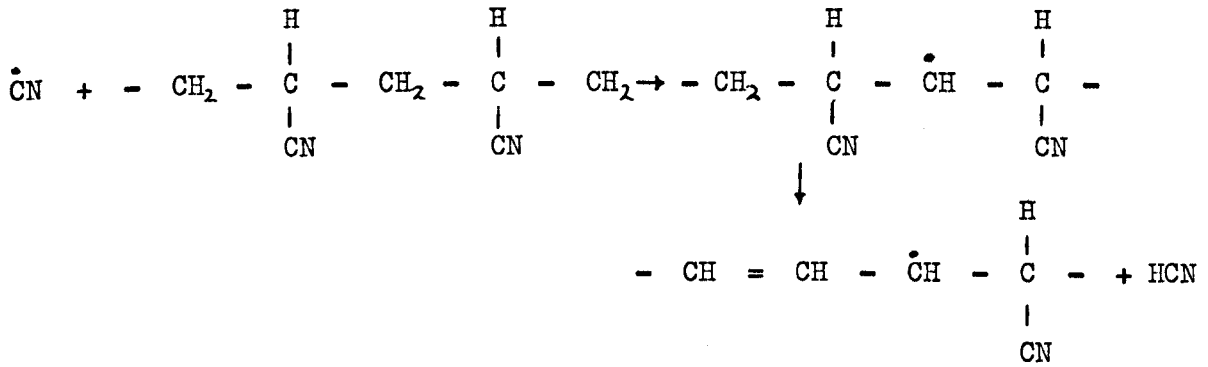

As we have already pointed out the doublet of some 87-88 gauss splitting is difficult to explain, however, if our interpretation is correct we feel it must arise from β proton coupling to a nitrogen nucleus. The radical involved could be formed by a removal of protons at the CH site followed by chain rupture and rearrangement.

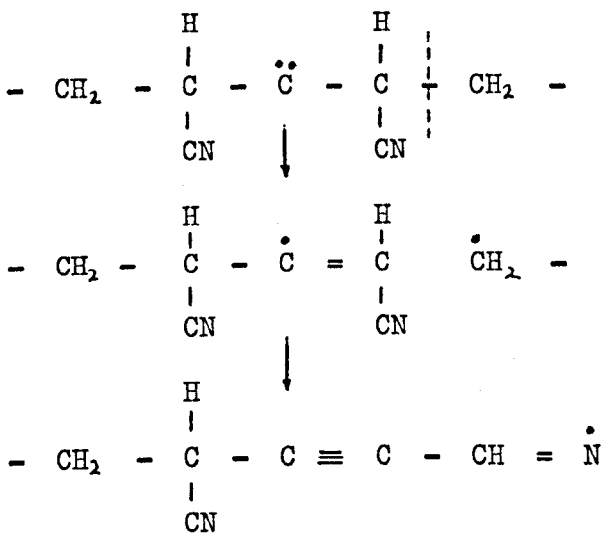

Considering how successfully ESR has been applied to the study of polymers both during polymerization and degradation, ESR has been applied in a limited way towards an understanding of polyacrylonitrile. The initial study was by Ingram et al.[132] who applied ESR to a study of radicals occluded in aggregates during polymerization. A technique that they successfully applied to certain polymers, it was thought that the radicals produced would be embedded in the precipitated polymeric material thereby preventing recombination. The samples were photopolymerized, at room temperature, by

PREVIOUSLY REPORTED IRRADIATION STUDIES OF PAN

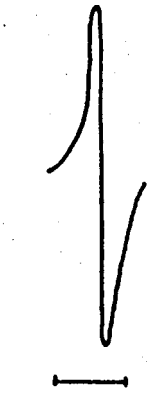

100 GAUSS

(a)

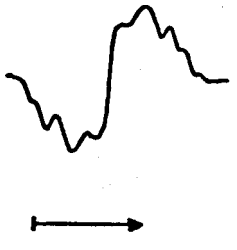

80 GAUSS

$1{\cdot}0 \times 10^{7}$ rads

(b)

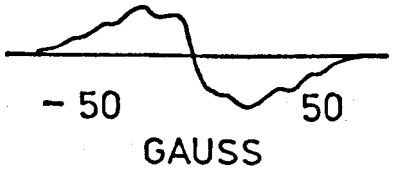

$0{\cdot}1 - 1{\cdot}0 \times 10^{6}$ rads

(c)

FIGURE 8.17

exposure to diffuse sunlight or to 3650Å light. They observed a slight yellow coloration after several hours irradiation and reported observing a single resonance line of half width of some 28 gauss and total spread of 100 gauss. (See Fig. 8.17 (a)). They attempted to explain the absence of any resolvable hyperfine structure as a result of a coincidence of significant but different hyperfine interactions giving a single unresolved line. However, as we have already shown, the temperature at which radicals are produced is critical and it is likely that the initial assumption that the radicals do not combine does not hold for polyacrylonitrile. Indeed the yellow coloration is again an indication of conjugation and the single line is probably the polyene radical that was identified in our studies. Bamford et al.[133] extended this work to consider the effect of copolymerization. They found that when methyl acrylate or methyl methacrylate or vinylidene chloride were photocopolymerized with acrylonitrile at room temperature only the acrylonitrile type signal was observed with a reduced spin concentration. They found this behaviour difficult to explain, however, it could be readily understood if it was assumed that only the polyene radical was being observed. Ohnishi et al.[134] and Abraham and Whiffen[135] observed the spectra shown in Fig. 8.17 (b) and (c) respectively, on γ-irradiating polyacrylonitrile at room temperature. Ohnishi et al.[134] gave their sample a 10 M rad dose and Abraham and Whiffen[135] stated that all spectra reported in their paper received between 0.1 and 1 M rad. In both cases no attempt was made to interpret the spectra. Both spectra show a resemblance to certain of our own spectra and it is clear that the concentration of the hyperfine radicals represents only a small percentage of the overall concentration suggesting that the hyperfine structure appears to be superimposed on a very broad line which again tends to strengthen our own interpretation.

It is instructive to compare our results with the irradiation results obtained for similar polymers.

Polyethylene:

At least three types of radical are produced on γ irradiating at low temperatures.[136] The radical species dominating at low temperatures and low doses of radiation (less than 1 M rad) is the sextet $-CH_2-\dot{C}H-CH_2-$ [137,138] On annealing the sample at 142°C before ESR observation a septet, having average separation 21.3 gauss, is observed and having the suggested structure:

$$-CH_2-\dot{C}H-CH=CH-CH_2-$$

This radical is seen to dominate at medium doses (between 10 and 100 M rad).

The third radical is a singlet of peak to peak width of about 20 gauss and dominates after a dose of at least several hundred M rad. This radical is also observed in a variety of polymers including polypropylene,[134,135] polyvinylchloride,[134,135] polyvinylacetate[134] and nylon 6 [134] on irradiating with similar large doses.

We have already mentioned the results of Libby et al.[129] and Kiselev et al.[130] (See section 8.6) who independently γ irradiated stretched polyethylene films and studied in detail the anisotropy of the $-CH_2-\dot{C}H-CH_2-$ radical.

Polyvinylchloride:

As to be expected three types of radical are again produced[140] and the analysis is similar to that for polyethylene. Irradiation at liquid nitrogen temperature again produces the allkyl radical $-CH_2-\dot{C}H-CH_2-$ [141]. The polyenyl radical has a peak to peak width

of about 26 gauss and accounts for about 7% of the spin concentration at 77K.

The proposed mechanism for the formation of the free radicals and the consequent elimination of hydrogen chloride from irradiated polyvinylchloride is closely related to that for the formation of radicals and the elimination of hydrogen in irradiated polyethylene.

Polyvinylchloride:

$$-CH_2-CHCl\ -CH_2-CHCl- \longrightarrow -CH_2-\dot{C}H-CH_2-CHCl- + \dot{Cl}$$

$$\dot{Cl} + -CH_2-CHCl-CH_2-CHCl- \longrightarrow -CH_2-CHCl-\dot{C}H-CHCl$$

$$\downarrow$$

$$-CH=CH-\dot{C}H-CHCl + HCl$$

Polyethylene:

$$-CH_2-CH_2-CH_2-CH_2- \longrightarrow -CH_2-\dot{C}H-CH_2-CH_2- + \dot{H}$$

$$\dot{H} + -CH_2-CH_2-CH_2- \longrightarrow -CH_2-CH_2-\dot{C}H-CH_2-$$

$$\downarrow$$

$$-CH=CH-\dot{C}H-CH_2 + H_2$$

Polytetrafluoroethylene:

Another similar polymer is polytetrafluoroethylene and in this polymer a doublet quintet structure with some overlapping lines has been observed at room temperature. This primary radical has a doublet splitting of 87 GAUSS and a quintet splitting of 32 GAUSS and the proposed structure is $^{(142)}$ $-CF_2-\dot{C}F-CF_2-$

It might be expected that the mechanism for the formation of free radicals in polyacrylonitrile to be closely related to that for the above polymers. Our work would seem in part to confirm this expectation, however, the argument would be strengthened by confirmation of the formation of hydrogen cyanide. It could also prove worthwhile to carry out a program of high energy irradiation both at room temperature and at 77K. By using a range of doses extending from less than 1 M rad to several hundred M rad and studying in detail the ESR properties of any radicals formed, it might be possible to obtain a positive identification of the radicals produced. We also attempted to study the ESR of irradiated stretched film, however, the ESR signals were masked by damage signals arising from absorbed solvent molecules. If the technique of preparation of such film could be improved to reduce the presence of solvent molecules then it is possible that interesting information could be obtained from such experiments.

CHAPTER 9

CONCLUSIONS

We have made ESR, electrical conductivity and thermoelectric power (TEP) measurements on a series of carbon fibres prepared by slowly heating Courtelle fibre to 400°C in a continuous stream of air, prior to carbonizing in an Argon atmosphere to various temperatures up to 1000°C. The techniques developed by Assabghy and other workers in the carbon field were widely used in our study of these fibres.

In common with Assabghy's observations made on fibre heat treated in excess of 1750°C we have established the g-value of the ESR spectrum to be anisotropic indicating that even in the early stages of heat treatment the spin centres are associated with layer planes which are preferentially aligned along the fibre axis. The g-shift observed on rotating the magnetic field from a position parallel to the fibre axis to a position perpendicular to the fibre axis is of opposite sign and an order of magnitude smaller than that observed by Assabghy.

It is interesting that in all of the parameters measured there is every indication that the unusually protracted preoxidation period given to our samples delayed the structural development within the fibres. This has provided further confirmation that the maximum heat treatment temperature to which the carbon is subjected would appear to give an unreliable indication of the electronic properties. In our previous publication we reported that the resistivity ratio gave an effective indication of the relative graphite order within the samples, the heat treatment temperature being an unreliable guide as the charring history of the fibres is important.

Over the region HTT 660-760°C exchange interaction is the mechanism responsible for the narrow resonance lines. Because the ESR lines were narrow it was possible, with the aid of pulse and CW saturation techniques, to investigate the spin-lattice relaxation processes in the fibres. The temperature variation of the spin-lattice relaxation time was monitored and it was evident that the spin system was not well coupled to the lattice. It would appear that the samples have a low Debye temperature and as a consequence the resonant spins have a limited phonon spectrum accessible to them in coupling with the lattice. The direct process dominates above liquid helium temperature while below 4.2K the relaxation process becomes phonon bottlenecked with a characteristic T^{-2} temperature dependence.

Over the range of HTT 660-830°C air absorbed into the surface of the fibre has a physical reversible effect on certain of the ESR parameters. In particular the spin-lattice relaxation time is shortened and the ESR signals broadened, the mechanism would appear to be one of spin-lattice interaction.

The spin-lattice relaxation time shortens on increasing the heat treatment temperature and as we discussed in section 5.9 there are several possible interpretations to explain this behaviour. The shortening of the spin-lattice relaxation time coincided with a marked increase in the conductivity and it was most unfortunate that the spin-lattice relaxation time was too fast to be measured using the available pulse apparatus. Further monitoring of the spin-lattice relaxation time in this region could prove highly significant in obtaining a more complete picture of the electronic processes in these samples.

Assabghy suggested that as Mrozowski's band overlap model would appear to fail below HTT 1750°C then any replacement model

would necessarily have to take into account the amorphous regions of these materials. It is to be expected that as the structure is not periodic then specific band models would not be applicable to carbon fibres.

In 1967 Mott carried out a most searching review of the properties of electrons in amorphous materials the process of electrical conduction being by thermally activated hopping between localized sites. We monitored the temperature variation of the conductivity and showed that conduction takes place by electron hopping between localized sites beyond the nearest neighbour separation. Consistent with the anisotropic features of the fibres the process of electrical conduction appears to take place along the layer planes, however the structure is that of a poorly crystalline material and this is in part responsible for the poor thermal access between the spin system and the lattice.

Discontinuities in the structure due to dehydrogenation, cross linking and imperfect condensation are thought to provide a well defined band of acceptors resulting in a positive TEP. Compensation by donor impurities could account for the negative TEP in the higher heat treatment samples a proportion of the donors would lose electrons to acceptors and electrons would then tunnel from occupied to empty donors.

In addition to the study of carbon fibres we also applied the ESR technique to a study of the free radicals produced in the precursor materials by mechanical degradation and also by irradiation damage.

By cutting the fibre under liquid nitrogen using a sharp pair of scissors a rather weak ESR signal was observed, and most probably corresponds to the peroxide radical. It might be possible to observe the spectrum due to the primary radical, however it would be necessary to remove any absorbed oxygen molecules before carrying out a similar

experiment in an oxygen free environment.

It was not possible to make a study of the mechanism of fracture in acrylic fibre by uniaxially straining the fibre within the ESR cavity. We have thought it likely that insufficient radicals were produced probably because fracture resulted after fibrillar shearing rather than by molecular scission. It would be most interesting to repeat the experiment on acrylics that have been drawn to a small extent or on acrylics in which the frozen-in strain has been chemically removed.

In contrast free radical spectra were readily observed on irradiating with UV or high energy electrons. The spectra observed are complicated and thought to arise from several free radical species.

Satisfactory computer fits to the UV and electron irradiation spectra were made assuming a four radical model and if our interpretation is correct then the mechanism of degradation by irradiation is similar to that in related polymers.

REFERENCES

1. Weisskopf, V.F.Rev. Mod. Phys., 21 305 (1949).
2. Van Vleck, J.H. "Theory of Electric and Magnetic Susceptibilities". Clarendon Press, Oxford. (1932).
3. Pake, G.E., "Paramagnetic Resonance", Benjamin, New York (1962).
4. Van Vleck, J.H. Phys Rev., 74 1168 (1948).
5. Anderson, P.W. and Weiss, P.R., Rev. Mod. Phys., 25 269 (1953).
6. Bloembergen, N., Purcell, E.M., and Pound, R.V., Phys Rev., 73 679 (1948).
7. Bloch, F., Phys. Rev., 70 460 (1946).
8. Portis, A.M., Phys Rev., 91 1071 (1953).
9. Orbach, R., Proc. Roy.Soc. A264 458 (1961).
10. Waller, I., Z. Physik 79 370 (1932).
11. Kronig, R. de L., Physica 6 33 (1939).
12. Van Vleck, J.H., J. Chem. Phys., 7 72 (1939).
13. Manenkov, A.A. and Orbach, R., "Spin Lattice Relaxation in Ionic Solids", Harpur, New York (1966).
14. Bloembergen, N. and Wang, S., Phys. Rev., 93 72 (1954).
15. Ubbelohde, A.R.,and Lewis, F.A., "Graphite and its Crystal Compounds", Clarendon Press, Oxford (1960).
16. Wallace, P.R., Phys Rev., 71 622 (1947).
17. Slonczewski, J.C., and Lewis, P.R., Phys Rev., 109 272 (1958).
18. Soule, D.E., Phys, Rev., 112 698 (1958).
19. Ganguli, N., and Krishnan, K.S., Nature 144 667 (1939)
20. Reynolds, W.N., "Physical Properties of Graphite".

21. Houtz, R.C., Text. Res. J., 20 786 (1950).

22. Shindo, A., Report No. 317 (Government Industrial Research Institute - Osaka) (1961.)

23. Grassie, N., and Hay, J.N., J. Polymer Sci., 56 189 (1962).

24. Takata, T., Hiroi, I., and Taniyama, M., J. Polymer Sci., A2 1567 (1964).

25. Kennedy, J.P., and Fontannna, C.M., J. Polymer Sci., 39 506 (1959).

26. Turner, W.N., and Johnson, F.C., J. Appl. Polymer Sci., 13 2073 (1969).

27. Watt, W., 3rd Carbon Conf. Soc. Chem. Ind. Paper 7.3. London April (1970).

28. Bandrup, J., and Peebles, L.H., Macromolecules 1 64 (1968).

29. Standage, A.E., and Prescot, R., Nature 211 169 (1966).

30. Watt, W., Phillips, L.N., and Johnson, W., The Engineer 221 (1966).

31. Standage, A.E., and Prescott, R., Brit. Pat. No. 1,128,043 April (1965)

32. Rose, P.G., Scott, G., and Johnson, J.W., 3rd Carbon Conf. Soc., Chem. Ind. Paper 7.5. London April (1970).

33. Watt, W., Proc. Roy. Soc., Lond. A. 319 5 (1970).

34. Moreton, R., 3rd Carbon Conf. Soc., Chem. Ind. Paper 7.11, London April (1970).

35. Franklin, R.E., Proc. Roy. Soc., A 209 196 (1951).

36. Kipling, J.J., and Shooter, P.V., 2nd Carbon Conf. Soc. Chem. Ind. London (1965).

37. Johnson, W., and Watt, W., Nature 215 384 (1967).

38. Badami, D.V., Joiner, J.C., and Jones, G.A., Nature 215 386 (1967).

39. Bacon, R., and Tang, M.M., Carbon 2 221 (1964).

40. Johnson, J.W., and Thorne, D.J., Carbon 7 659 (1969).

41. Johnson, D.J., and Tyson, C.N., J. Phys. D. Appl. Phys., 2 787 (1969).

42. Thorne, D.J., 3rd Carbon Conf. Soc. Chem. Ind. Paper 7.9 London April (1970).

43. Johnson, W., 3rd Carbon Conf. Soc. Chem. Ind. Paper 7.6 London April (1970).

44. Johnson, D.J., Nature 226 750 (1970).

45. Allen, S., Cooper G.A., and Mayer, R. M., Nature 224 684 (1969).

46. Robson, D., Assabghy, F.Y.I. and Ingram, D.J.E., Nature 221 51 (1969).

47. Robson, D., Assabghy, F.Y.I. and Ingram, D.J.E., J. Phys. D. Appl Phys. 4 1426 (1971).

48. Robson, D., Assabghy, F.Y.I. and Ingram, D.J.E., J. Phys. D., Appl. Phys., 5 169 (1972).

49. Robson, D., Assabghy, F.Y.I., Cooper, E.G., and Ingram, D.J.E., J. Phys. D: Appl. Phys., 6 1822 (1973).

50. Assabghy, F.Y.I., Thesis "The Structure of Polyacrylonitrile Based Carbon Fibres as studied by Electron Spin Resonance and other Electronic Properties" University of Keele (1970).

51. Mrozowski, S., Phys. Rev., 85 609, 86, 1056 (1952).

52. Loebner, E.E., Phys. Rev., 102 46 (1956).

53. Mrozowski, S., and Chaberski, A., Phys. Rev. 104 74 (1956).

54. Singer, L.S., "Proc. 5th Conf. On Carbon," Pergamon Press London 2 37 (1963).

55. Pastor, R.C., and Hoskins, R.H., J. Chem. Phys. 32 264 (1960).

56. Lewis, I.C., and Edstrom, T., "Proc. 5th Conf. on Carbon," 2 413 (1963).

57. Singer, L.S., and Lewis, I.C., Carbon 2 115 (1964).

58. Lewis, I.C., and Singer, L.S., Carbon 5 373 (1967).

59. Lewis, I.C., and Singer, L.S., Carbon 7 93 (1969).

60. Singer, L.S., Spry, W.J., and Smith, W.H., 3rd Carbon Conf. Pergamon Press p 121 (1959).

61. Hoskins, R.H., and Pastor, R.C., J. Appl. Phys. 31 1506 (1960).

62. Wagoner, G., Proc. 4th Carbon Conf. Pergamon Press p 167 (1960).

63. Dyson, F.J., Phys. Rev., 98 349 (1955).

64. Mrozowski, S., Carbon, 3 305 (1965).

65. Marchand, A., and Delhaes, D., Proc. X11 Cooloque Ampere, North Holland Publishing Co., Amsterdam, 135, (1963).

66. Mrozowski, S., Carbon, 4 227 (1966).

67. Arnold, G.M., Carbon, 5 33 (1967).

68. Arnold, G.M., and Mrozowski, S., Carbon 6 243 (1968).

69. Mrozowski, S., Carbon 6 841 (1968).

70. Delhaes, P., and Carmana, F., Carbon 10 677 (1972).

71. Yamaguchi, T., Carbon 2 95 (1964).

72. Fujita, S., Carbon 6 746 (1968).

73. Johnson, D.J., and Tyson, C.N., J. Phys. D. Appl. Phys. 3 526 (1970).

74. Badami, D.V., New Scientist p 251 5th Feb. (1970).

75. Boas, J.F., Dunhill, R.H., Pilbrow, J.R., Srivastiva, R.C., and Smith, T.D., J. Chem. Soc. A 94 (1969).

76. Hyde, J.S. and Brown, H.W., J. Chem.Phys.37 368 (1962).

77. Ingram, D.J.E., op. cit., ref. 14, p. 213.

78. Jackson, C., and Wynne-Jones, W.F.K., Carbon, 2 227 (1969).

79. Singer, L.S., and Cherry, A.R., Proc. 9th Carbon Conf. p. 49 (1969).

80. Marsh, H., and Wynne-Jones, W.F.K., Carbon 1 269 (1964).

81. Lloyd, J.P. and Pake, G.E., Phys. Rev., 92 1576 (1953).

82. Pake, G.E., Am. J. Phys. 18 478 (1950).

83. Ingram, D.J.E., Proc. 3rd Carbon Conf., Pergamon Press, p.93 (1959).

84. Van Vleck, J.H., Phys. Rev., 57 426 (1940).

85. McConnell, H.M., and Robertson, R.E., J. Phys. Chem. 61 1018 (1959).

86. Mott, N.F., Adv. Phys., 16, 49 (1967).

87. Mott, N.F., Journal of Non-Crystalline Solids, 1 1 (1968).

88. Walley, P.A., and Jonscher, A.K., Thin Solid Fibres, 1, 367, (1968).

89. Mott, N.F., Phil. Mag., 19 835 (1969).

90. Harker, H., Phil. Mag., 16 1193 (1967).

91. Huebener, R.P., Phys. Rev., 135 A 1281 (1964).

92. Adkins, C.J., Freake, S.M. and Hamilton, E.M., Phil. Mag., 22 175 (1970).

93. Morgan, M., Thin Solid Fibres, 7 313 (1971).

94. McConnell, H.M., J. Chem. Phys. 24 764 (1956).

95. Bersohn, R., J. Chem. Phys., 24 1066 (1956).

96. Weissman, S.I., J. Chem. Phys., 25 890 (1956).

97. Jarrett, H.S., J. Chem. Phys. 26 1289 (1956).

98. Ayscough, P.B., "Electron Spin Resonance in Chemistry," Methuen, London (1967).

99. Bresler, S.E., Kazbekov, E.N., and Saminskii, E.M., Polymer Sci, 1 540 (1959)

100. Butyagin, P. Yu., Berlin, A.A., Kalmanson, A.E., and Blumenfeld, L.A., Vysokomolekul, Soedin, 1 865 (1959).

101. Campbell, D., Macromol. Revs., J. Polymer Sci., D 4 91 (1970).

102. Kausch - Blecken von Schmeling, M.H., J. Macromol. Sci., - Revs. Macromol. Chem., C 4 (2) 243 (1970).

103. Miyagawa, I., and Itoh, K., J. Chem. Phys., 36 2157 (1962).

104. Morton, J.R., and Horsfield, A., J. Chem. Phys., 35 1152 (1961).

105. Horsfield, A., Morton, J.R., and Whiffen, D.H., Mol. Phys. 4 425 (1961).

106. Zurkov, S.N., Zakrevskii, V.A, and Tomashevskii, E.E., FTT, 6 1912 (1964); Soviet Phys. - Solid State 6 1508 (1964).

107. Zurkov, S.N., Savostin, A. Ya. and Tomashevskii, E.E., Don SSR 159 303 (1964): Soviet Phys. - Doklady 9 986 (1964).

108. Zurkov, S.N., and Tomashevskii, I.P.P.S. Conf. Series No. 1 Oxford p 200 Sept. 1966.

109. Zurkov, S.N., Tomashevskii, E.E., and Zakrevskii, V.A., Soviet Phys. - Solid State, 3 2074 (1962).

110. Roylance, D.K., Devries, K.L., and Williams, M.L., 2nd International Conf. on Yield and Fracture, Brighton, Paper No. 48 April (1969).

111. Tobalsky, A., and Eyring, H., J. Chem. Phys., 11 125 (1943).

112. Becht, J., and Fischer, H., Kolloid - Z, 229 167 (1969)

113. Becht, J., Devries, K.L. and Kausch, H.H., European Pol. Journal, 7 105 (1971).

114. Becht, J., and Fischer, H., Kolloid Z - Z Polymer 240 766 (1970).

115. Spencer-Smith, J.L., Fibre Science Technology 1 (1) 43 (1968).

116. Fischer, H., Hellwege, K.H., and Neudofl, P., J. Polymer Sci, A, 1 2109 (1963).

117. Hukudo, K., Kusumoto, N., Kawand, I., and Takayangi, M., J. Polymer Sci., B, 3 743 (1965).

118. Dubinskaya, A.M., and Butyagin, P.Y., Vysokomolekul, Soedin, B9 525 (1967).

119. Devries, K.L., Roylance, D.K., and Williams, M.L., Rept. UTEC DO 68-056, College of Engineering, University of Utah, July (1968).

120. Bewers, R.B., White, E.F.T., and Brown, L., Trans. Faraday Soc. 56 1529 (1960).

121. Houtz. J., Text. Res. J., 20 786 (1950).

122. Bresler, S.E., Zurkov, S.N., Kasbekov, E.N., Saminskii, E.M., and Tamashevskii, E.E., Soviet Phys. - Tech. Phys. English Transl. 4 321 (1959).

123. Abraham, R.J., Melville, H.W., Overall, D.W., and Whiffen, D.H. Trans. Faraday Soc., 54 1133 (1958).

124. Graves, C.T., and Ormerod, M.G., Polymer 4 81 (1963).

125. Marquardt, D.W., Bennett, R.G., and Burrell, E.J., J. Mol Spectr. 7 269 (1961).

126. Heuvil, H.M., and Lind, K.C.J.B., J. Polymer Sci, A - 2 8 401 (1970).

127. Marquardt, D.W., J. Soc., Industrial and Applied Maths, 11 431.

128. Peacock, N., and Khan, M.S., Department of Fibre Science University of Strathclyde.

129. Libby, D., Ormerod, M.G., and Charlesby, A., Polymer 1 212 (1960).

130. Kiselev, A.G., Mokulskii, M.A., and Lazurkin, Ya. S., Vysokomolekul Soedin., 2 1678 (1960).

131. Cochron, E.L., Adrian, F.J., and Bowers, V.A., J. Chem. Phys., 36 1938 (1962).

132. Ingram, D.J.E., Symons, M.C.R., and Townsend, M.G., Trans. Faraday Soc., 54 409 (1958).

133. Bamford, C.H., Jenkins, A.D., Symons, M.C.R. and Townsend M.G., J. Polymer Sci., 34 184 (1959).

134. Ohnishi, S.O., Ikeda, Y., Kashiwagi, M., and Nitta. I., Polymer 2 119 (1961).

135. Abraham, R.J., and Whiffen, D.H., Trans. Faraday Soc., 54 1291 (1958).

136. Ohnishi, S. Bull Chem. Soc. Japan, 35 254 (1962).

137. Lawton, E.J., Balwit, J.S., and Powell, R.S., J. Chem. Phys., 33 695 (1960).

138. Loy, B.R., J. Polymer Sci., 44 341 (1960).

139. Ohnishi, S., Ikeda, Y., Sutimoto, S., and Nitta, I., J. Polymer Sci., 47 503 (1960).

140. Lawton, E.J., and Balwit, J.S., J. Phys. Chem. 65 815 (1961).

141. Miller, A.A., J. Chem. Phys. 63 1755 (1959).

142. Rexroad, H.N.,and Gardy, W., J. Chem. Phys. 30 399 (1959).